THE ROLE OF HETEROGENIC SPINAL REFLEXES IN COORDINATING AND STABLIZING A MODEL FELINE HINDLIMB

A Dissertation
Presented to
The Academic Faculty

by

Nathan Eric Bunderson

In Partial Fulfillment
of the Requirements for the Degree
Doctor of Philosophy in the
School of Biomedical Engineering

Georgia Institute of Technology
April 2008

THE ROLE OF HETEROGENIC SPINAL REFLEXES IN COORDINATING AND STABLIZING A MODEL FELINE HINDLIMB

Approved by:

Dr. Thomas J. Burkholder, Advisor
School of Applied Physiology
Georgia Institute of Technology

Dr. Roman O. Griogoriev
School of Physics
Georgia Institute of Technology

Dr. Lena H. Ting
Department of Biomedical Engineering
Georgia Institute of Technology
Emory University

Dr. Shawn Hochman
Department of Physiology
Georgia Institute of Technology
Emory University

Dr. T. Richard Nichols
School of Applied Physiology
Georgia Institute of Technology

Date Approved: March 12, 2008

To my family

ACKNOWLEDGEMENTS

Thank you Claire Honeycutt, Victoria Stahl, and Jinger Gottschall for the tremendous help in conducting the experiments which would've not only been impossible without you but also absolutely no fun. Thank you to the Ting group, my surrogate family: C'iana Barker, Stacie Chvatal, Lucas McKay, Kyla Ross, Seyed Safavynia, Jevin Scrivens, Kartik Sundar, Gelsy Torres-Oviedo, Torrence Welch, and Jasper Yen. I'm grateful for your invaluable insight into my research and even more for your friendship. You all made the whole experience really enjoyable. Thanks Keith van Antwerp for helping me through the tough times, and for the great ideas. Thank you, Roman Grigoriev, Shawn Hochman, Richard Nichols, Lena Ting and Tom Burkholder for being a fantastic committee, available and open to discussions and meetings which were very useful to my progress. Thank you, Richard and Lena, for the incredibly unselfish sharing of resources, time, space, equipment, and advice. Thank you, Tom. I couldn't have hoped for a better learning experience. Thank you for the constructive criticisms, the deadlines, and especially for truly caring about my progress. Thank you to my family back home and new family here for the priceless support only a family can give. Thank you, dear Erin, widowed by grad school. Thank you for letting me do what needs to be done and for patiently reminding me what is most important. I love you. Most of all I am grateful to my Father in Heaven. "My God hath been my support; he hath led me through mine afflictions in the wilderness; and he hath preserved me upon the waters of the great deep."

TABLE OF CONTENTS

LIST OF TABLES

LIST OF FIGURES

SUMMARY

In addition to its intrinsic importance during quiet standing, posture also serves as the background for a wide variety of other critical motor tasks. The hierarchical nature of the motor control system suggests that the different layers may be responsible for different aspects of posture. I tested the hypothesis that spinal reflexes are organized according to optimal principles of stability, control accuracy, and energy. I found that there were no globally stable muscle activation patterns for muscles operating near optimal fiber length, suggesting that the intrinsic viscoelastic properties of muscle are insufficient to provide limb stability. However, for stiffer muscles a stable limb could be created by selectively activating muscles based on their moment-arm joint angle relationships. The optimal organization of length and velocity feedback to control and stabilize the endpoint position of a limb could not be produced from a purely muscle controller, but required neural feedback to improve endpoint performance, reduce energetic cost, and produce greater coordination among joints. I found that while muscles at near optimal fiber length were insufficient to provide limb stability, the length feedback provided by the autogenic stretch reflex was sufficient to stabilize. Length feedback was also sufficient to produce the directional tuning of muscle activity and constrained ground reaction forces as is observed in experiments. These results have implications for controlling powered prosthetic devices, suggesting that subdividing the responsibility for stability among hierarchical control structures will simultaneous improve stability and maneuverability of the devices.

CHAPTER 1

INTRODUCTION

Emerging fields at the intersection of movement biology and engineering have extraordinary potential in assistive technologies such as medical robots and prosthetics. A humbling perspective is gained, however, by comparing the robustness and versatility of the best engineered system with biological solutions. Not only are we unable to reproduce many of the capabilities of biology but our understanding of how the nervous and musculoskeletal systems accomplish these tasks is extremely limited. The goal of basic research in motor control is to develop our understanding of the nervous system. What are the strategies, pathways, mechanisms, networks, bits and pieces of the control of movement?

In 2007 there were over 2 million people living in the US with a limb amputation. Despite dramatic increases in knowledge in the field of robotics and controls over the past half century, there has not been a successful transfer to prosthetic applications. In addition, many neurological and muscular deficiencies affect the ability of patients to perform normal motor functions including balance. A major difficulty in developing natural powered prosthetics and treating balance disorders is that the mechanisms by which the nervous and musculoskeletal systems interact to achieve balance are poorly understood. Improving our understanding of the mechanisms of postural stability would be extremely useful in improving prosthetic design and balance disorder treatments as well as motor control research in general. In addition to its intrinsic importance during quiet standing, postural control also serves as the background for a wide variety of other critical motor tasks. The goal of this dissertation is to provide understanding of how neural feedback and intrinsic musculoskeletal properties are coordinated to achieve efficient postural stability.

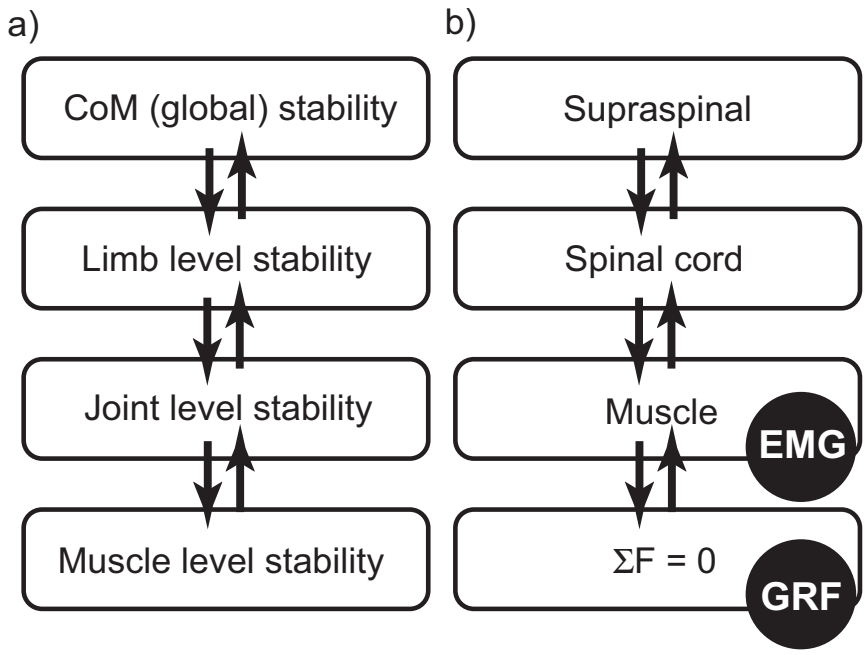

Figure 1.1: Postural control hierarchies. A) Postural control requires stability at multiple levels. In order for the center of mass (CoM) to be stabilized each limb must be stable. In order for a limb to be stable the constituent joints and muscles must be stabilized. B) The motor control hierarchy ranges from the immediate interactions with the environment and intrinsic musculoskeletal properties to neural control through spinal and supraspinal pathways. External forces such as the ground reaction force (GRF) and gravity cause skeletal motion which deforms the tendons and muscles. The deformation of these soft tissues causes changes in their force output which influences skeletal motion and interaction forces with the environment. The external forces, internal muscle forces, and deformations are transduced and communicated to networks in the spinal cord. This information is integrated in spinal networks and fed back to the muscles. It is also communicated higher up through the hierarchy to the brainstem and other higher centers. The neural contributions are reflected in a change in muscle activation (Electromyography EMG).

Background and Motivation

What mechanisms do animals use to achieve efficient and robust postural stability? The introduction is organized to provide an overview of the postural task and what is known about how biological systems accomplish postural stability, as well as an introduction to the gaps in this knowledge. The anatomy and physiology of the specific mechanisms animals may use to stabilize is provided. To measure the performance of the biological system and to choose strategies of motor control, the engineering principles of optimal control and Lyapunov stability are relied upon heavily, and a brief background of these principles is also provided in the introduction.

The Postural Task

There are multiple levels to the postural task during quiet standing (Figure 1.1a). Ultimately, the center of mass (CoM) must be stabilized, or maintained above a base of support (global level). In order for the center of mass to be stabilized the individual limbs must be coordinated to provide appropriate restoring forces at the ground to compensate for any external disturbances. The restoring forces are provided by the transformation of muscle forces through joint torques to a limb endpoint force. The resultant endpoint force is sensitive to the configuration of the limb and so the limb must be stabilized (limb level). For a limb to be stable the joints that comprise the limb must be stabilized (joint level). In addition, multiple muscles may contribute differentially to force generation (Bernstein 1967) and stability (Bunderson et al. 2008, Young et al. 1992) of a given joint and so must be coordinated to provide stability (muscle level). In this way the stability of the whole requires stability and coordination of the constituents at multiple levels.

There are various mechanisms that animals use to accomplish postural stability at the different levels of the task that constitute a motor hierarchy (Figure 1.1b). The hierarchy is comprised of intrinsic mechanical properties of muscle, short latency spinal reflexes, longer latency postural responses, and volitional actions. The respective roles of the various mechanisms in postural control is debated, however, the debates are centered on the global problem of balancing the CoM and generally do not address the subtasks of stabilizing and coordinating the limb and joint responses to perturbation (Hasan 2005, Lyalka et al. 2005, Macpherson and Fung 1999, Morasso and Sanguineti 2002, Peterka 2002). Since stability and coordination of the constituents (muscles, joints, and limbs) is required for stability of the whole (CoM) it is conceivable that the responsibility for stabilizing the constituents is provided by the lower levels of the motor control hierarchy including intrinsic muscle properties and spinal reflex pathways.

Which mechanisms and strategies biological systems employ to accomplish postural control is generally studied using perturbation methods; a destabilizing perturbation is applied to an animal and the strategy used by the animal to achieve postural stability is observed. The cat has served as a classical model of postural control (Liddell and Sherrington 1924, Macpherson 1988) and the postural response to perturbations of the animals has been reported in terms of CoM motion as well as outputs at the other levels (ground reaction forces, joint kinematics, and muscle EMGs) (Lacquaniti and Maioli 1994, Lacquaniti and Maioli 1994, Macpherson 1988, Macpherson 1988). In addition neural outputs have been reported in configurations related to posture (Bosco and Poppele 1997, Bosco et al. 2000).

The response to an external perturbation displays characteristic phases that support the model of hierarchical control. Ground reaction forces change coincident with the applied perturbation, which implies the contribution of elastic, viscous and inertial properties of the limb. No immediate alteration in muscle electrical activity is seen, but EMG changes are observed with latencies characteristic of the monosynaptic stretch reflex, polysynaptic spinal reflexes, and supraspinal reflexes. Forces resulting from these stereotypical muscle activations facilitate recovery from increasingly complex perturbations, requiring increasing levels of sensory integration or increasingly complex internal models.

The net postural correction is the force applied through the limbs to the ground. Independent forelimb and hindlimb control has been demonstrated in the postural response of cats (Deliagina et al. 2006), but a consistent "force constraint strategy" is observed in both forelimbs and hindlimbs (Macpherson 1988). Quietly standing cats subject to horizontal perturbations of the support surface in a variety of directions revealed a "force constraint strategy", where forces are constrained to a preferred direction regardless of the direction of postural perturbation (Macpherson 1988, Macpherson 1994). This strategy has also been demonstrated in the human postural

response (Henry et al. 2001). In cats it has been shown to be dependent on the posture of the animal (Torres-Oviedo et al. 2006) and is not due to limitations in the force-producing capabilities of the limb (McKay et al. 2007). Spinalized animals with poor postural control do not exhibit a force constraint strategy which suggests that the strategy is important for balance (Macpherson and Fung 1999). It has been shown that the ground contact forces are controlled independently from the control of limb geometry (Lacquaniti and Maioli 1994) but it is not clear whether the force constraint is the result of a global strategy to balance the CoM or part of a sub-strategy to stabilize the limb.

Muscle activity is also constrained during the postural response in cats and humans (Macpherson 1988, Torres-Oviedo and Ting 2007). EMG signals were measured from hind and forelimb muscles of cats subject to the horizontal perturbations and muscle activity was found to vary with the direction of the platform perturbations (Macpherson 1988). The magnitude of the tuned responses was reduced in the spinalized cats with reduced balance control and the responses were delayed (Macpherson and Fung 1999). These changes in muscle activity indicate that some level of neural control is important for standing balance.

The changes in EMG responses may be due to a variety of mechanisms including spinal reflexes, longer latency supraspinal responses, and volitional control. The effect of each of these mechanisms on EMG patterns is difficult to separate except that the earliest responses can only be due to spinal reflexes. The spinal reflexes are flexible in that their sensitivity is modulated by supraspinal centers in postural tasks (Hoffer et al. 1990, Schouten et al. 2008, Sinkjaer and Hoffer 1990). In addition, proprioceptive spinal feedback is distributed across a limb (Bonasera and Nichols 1994, Eccles et al. 1957, Jankowska 1992, Nichols 1989), and the outputs of the spinal pathways are correlated with whole-limb variables (Bosco et al. 2000). Taken together, these results suggest that the spinal reflex pathways could play a role in the stabilization and coordination at the limb level (Nichols et al. 1999). However, the contributions of the various levels of the

motor control hierarchy to stabilization of the various levels of the task is not known, and it remains unclear to what extent the observed endpoint forces, kinematics, and muscle activities represent a specific strategy of CoM stabilization or simply emerge from limb and joint stabilization. This dissertation is concerned with addressing the role of proprioceptive spinal reflexes, particularly length feedback, in providing efficiency, stability, and coordination at the limb level.

Mechanisms of Postural Control

A key theme to the work has been the idea of hierarchies in motor control (Figure 1.1b). The various levels of the hierarchy each contribute to postural control to varying degrees (Deliagina et al. 2006, Hasan 2005, Peterka 2002, Ting and McKay 2008). The first response of the body to any outside force comes from the intrinsic musculoskeletal properties. Soft tissues are stretched or unstretched and, due to their inherent viscoelasticity, forces are applied to the skeleton which resist or assist the motion. At the next level of the hierarchy are the spinal reflex pathways. The soft tissues contain sensors such as muscle spindles, Golgi tendon organs, and cutaneous receptors, which sense perturbations and relay that information through feedback loops in the spinal cord to motoneurons that activate muscles throughout the body, further contributing to the response of the body to perturbations. Finally, the sensed information is also carried to higher centers including the brainstem, cerebellum, and motor cortex, where further reflexive and volitional control is accomplished. These higher centers are also involved in the modulation of the sensitivity of the spinal reflex pathways and motoneuron excitability. To what extent each layer is responsible for postural control is an intensely debated topic(Hasan 2005).

Intrinsic Mechanisms of Postural Control

Soft tissues such as muscle, tendon, and ligament are the origin of the intrinsic viscoelastic resistance to perturbation. The viscoelasticity of muscle has proven to be extremely challenging to describe and dependent on multiple parameters (Epstein and Herzog 2003). Part of the difficulty in describing this viscoelasticity is that it arises from molecular interactions in muscle that are not fully understood. The prevailing theory of muscle force generation, the sliding filament theory (Huxley 1957), is that the force generated by a sarcomere is greatest when the thick, myosin filaments exactly overlap the thin, actin filaments. As the sarcomere changes length, the amount of overlap between thick and thin filaments changes, reducing the number of actin binding sites for myosin and reducing the number of attached, force-generating crossbridges, decreasing active tension (Gordon et al. 1966). Other contributions to the elasticity of muscle include short range stiffness, which may arise from the slow cycling rate of actin-myosin crossbridges (Campbell and Lakie 1998, Getz et al. 1998, Huyghues-Despointes et al. 2003, Nichols and Cope 2004, Rack and Westbury 1974). Gasser and Hill (1924) observed that the speed of shortening of a muscle fiber decreased with the inertial load on the muscle, indicating that the muscle was inherently viscous. Although this viscoelasticity is described as an intrinsic property, in reality it is not independent of neural activity; stronger muscle activation results in greater viscoelasticity (Gasser and Hill 1924, Rack and Westbury 1969).

Two common forms of mathematical muscle models have emerged. First described by A.F. Huxley (1957), Huxley models attempt to describe the whole fiber properties of muscle by modeling the action of individual myosin molecules. The properties of an entire fiber and muscle arise from the concatenation of many of these individually-modeled sarcomeres. On the other hand, Hill models (Hill 1938) are based on the length-tension and force-velocity properties of muscle fibers. Instead of modeling the action of individual sarcomeres, Hill models use elastic and force generating elements

that describe the observed properties of whole fibers. The advantage of Hill models over Huxley models is that they are much more computationally efficient. In models which include many kinematic degrees of freedom and muscles, such as the one used in this dissertation, Hill models are used extensively (Epstein and Herzog 1998). In the models of this dissertation I used muscle models of varying levels of complexity for the different studies. Each mathematical muscle model is described in the chapter in which it is used.

The viscoelasticity of muscle is inherently stabilizing at the muscle level but may be destabilizing at the joint level. This is due to the fact that muscle affects joint torques through a line of action at which force is applied to the skeleton by the tendons. This is analogous to the fact that the torque applied to a bolt through a wrench depends on where on the handle the wrench is grasped and the angle at which the force is applied. The muscle force – joint torque relationship (moment arm) varies with joint motion, thereby altering the net effect of the force. A viscoelastic muscle level may be either stabilizing (Young et al. 1992) or destabilizing (Bunderson et al. 2008) at the joint level due to the moment arm contribution.

Although the intrinsic musculoskeletal properties provide instantaneous resistance to perturbations, it has not been established whether they are of sufficient magnitude to stabilize limb posture in a variety of animals and tasks (Edwards 2007, Morasso and Sanguineti 2002, Morasso and Schieppati 1999, Richardson et al. 2005, Winter et al. 1998, Winter et al. 2001). The correlation between the center of pressure (CoP) and CoM was used to argue for intrinsic muscle control of postural sway in humans (Winter et al. 1998, Winter et al. 2001). However, Morasso and coworkers argued that this correlation does not indicate intrinsic control, but rather feedforward neural control of postural sway (Morasso and Sanguineti 2002, Morasso and Schieppati 1999). This debate, however, is in regard to the normal postural sway in unperturbed quiet standing and it is generally held that control of posture in response to perturbations requires neural control (Peterka 2002). Even if the intrinsic musculoskeletal properties are insufficient in cats to stabilize

the center of mass it has not been tested whether they are sufficient for the subtask of stabilizing an individual limb. In this dissertation I have tested whether intrinsic muscle properties are sufficient to stabilize at the limb level of a cat.

Spinal Mechanisms of Postural Control

The next level of the motor control hierarchy is comprised of reflex pathways in the spinal cord which excite or inhibit muscle activity based on information from a variety of sensors in the skin, muscles, tendons, or joints. The proprioceptive sense originates largely from sensors at the muscle level: muscle spindles and Golgi tendon organs. The sensed information is relayed by afferent fibers to the spinal cord by mono- and poly-synaptic networks and fed back to the motoneurons, which constitutes a short latency feedback loop important to posture and locomotion (Windhorst 2007). The fact that proprioceptive spinal feedback is distributed across a limb (Bonasera and Nichols 1994, Eccles et al. 1957, Jankowska 1992, Nichols 1989), and the outputs of the spinal pathways are correlated with whole-limb variables (Bosco et al. 2000) suggest that the spinal reflex pathways could play a role in the stabilization and coordination at the limb level (Nichols et al. 1999).

Golgi tendon organs (GTOs) are sensors in the tendon of muscle that are sensitive to muscle force. Located at the junction of muscle and tendon, the GTO capsules contain the axons of several group Ib afferents. The group Ib's are sensory neurons with cell bodies in the dorsal root ganglia and large-diameter myelinated axons. The axons are intertwined with the collagen of the tendon, allowing the transduction of muscle tension to the axons themselves. Tension within the collagen causes an increase in the firing rate of the GTO and a decrease in the firing rate of adjacent GTOs (Jami 1992). The net firing of a population of these sensors in the tendon of a muscle provides a reasonably accurate estimate of active force generated by the muscle (Crago et al. 1982, Stephens et al. 1975). In the spinal cord the response to the firing of group Ib neurons is generally inhibitory;

that is, an increase in force of a muscle generally causes a decrease in the activation of motoneurons of that muscle (Jami 1992). This inhibitory effect is accomplished through the excitation of Ib inhibitory interneurons, which in turn inhibit the muscles motoneuron. However, there is evidence for positive force feedback in postural tasks (Pratt 1995).

Muscle length and velocity information is sensed by muscle spindles. Interspersed with the force-generating (extrafusal) fibers of a muscle are the sensory intrafusal fibers. Each muscle spindle is comprised of several intrafusal fibers, a single group Ia afferent and multiple group II afferents. The intrafusal fibers have contractile apparatus at the polar regions of the fiber and are innervated with annulospiral endings of large diameter group Ia afferents and smaller group II afferents at the equatorial region of the fiber. In response to stretch, ion channels in the annulospiral endings of the afferents open, resulting in an influx of sodium, thereby increasing the resting potential of the axons. The intrafusal fibers are classified as dynamic nuclear bag fibers, static nuclear bag fibers, and nuclear chain fibers. The dynamic bag fibers respond to fast changes of length, while the static bag fibers and chain fibers respond to static changes in length. These differences between fibers result in specialization of the group Ia and group II afferents. Since the group Ia afferents innervate both bag and chain fibers they are often described as being sensitive to both length and velocity of the intrafusal fibers. Likewise, group II afferents are primarily associated with the chain fibers making them sensitive to the length of the intrafusal fibers. The sensitivity of these afferents to fiber length and velocity can be adjusted by varying the tension of the polar regions of the fiber which are innervated by gamma motoneurons.

The force (Nichols et al. 1999, Pratt 1995), velocity (Houk et al. 1981) and particularly length feedback (Liddell and Sherrington 1924, Lloyd 1946) provided by these proprioceptive sensors have long been believed to play a large role in providing postural stability through spinal reflex mechanisms (Sherrington 1910). Information from each of the sensors is integrated in the spinal cord and sent to higher centers in

addition to being returned to the muscles through spinal reflex pathways. The group Ia and to a lesser extent the group II neurons make direct, monosynaptic contact with motoneurons. The sensory – motor feedback pathway in the spinal cord is also mediated polysynaptically through interneurons. In the latter case, there are excitatory and inhibitory connections and a wide divergence of sensory information. In summary, spinal reflexes include sensory input, information integration with interneurons and motoneurons, and motor output. They are rapid due to being contained completely within the spinal cord without requiring the influence of supraspinal centers. However, supraspinal centers may influence the sensitivity of these reflexes (Miller et al. 1996).

The most direct spinal reflex pathway is the monosynaptic stretch reflex (Eccles and Lundberg 1958, Liddell and Sherrington 1924), whereby group Ia afferents make monosynaptic connections in the spinal cord with alpha motoneurons of the original muscle. Excitation of the Ia afferent therefore results in excitation of the homonymous alpha motoneurons. The group II afferents also make mono-synaptic connections to the alpha motoneurons (Kirkwood and Sears 1975). In addition to the stretch reflex, sensory receptors from a given muscle provide excitatory feedback to synergistic muscles, those of similar action, and inhibitory feedback to antagonist muscles, those of opposing action (Liddell and Sherrington 1924, Lloyd 1946).

The Ia afferent feedback in the cat hindlimb including homonymous excitation and reciprocal inhibition and is non-uniform (feedback gains between different muscles are not of uniform strength) (Eccles 1956, Eccles et al. 1957, Nichols 1989). Force feedback has an even wider limb distribution (Jankowska 1992, Powers and Binder 1985). Stimulation of hindlimb extensor muscles in cats evoked non-uniform excitatory responses that were widely distributed among other hindlimb extensor muscles through force feedback (Pratt 1995) . Both length and force heterogenic feedback can be non-uniform, favoring force generation by one muscle of a pair or at one joint over another (Bonasera and Nichols 1994, Eccles and Lundberg 1958, Nichols et al. 1999, Pratt 1995).

Despite the long history of research into the spinal reflex pathways it has been difficult to relate the neurophysiological results to the functional postural response of animal. Sherrington (1910) described the postural control capabilities of spinal and decerebrate cats and attributed them to homonymous spinal reflex, or length regulation of a single muscle. As the inhibitory action of the reflexes on antagonists became clear (Lloyd 1946) the functional role of the spinal reflex was expanded to include position control of a whole joint (Merton 1953). However, it was shown in human subjects that reflex control of the whole limb does not mimic a servo-like system (Crago et al. 1976) and the stretch reflex may be a better regulator of muscle stiffness than muscle length (Nichols and Houk 1976). These results have led to the view that the spinal reflexes are organized in a manner that coordinates the response at the limb level (Nichols et al. 1999).

Again, the effect of the spinal reflexes on postural control has remained elusive due to the difficulty of separating their effects from those of the intrinsic muscle properties and neural control from supraspinal centers. Spinalization changes the excitabilities of the spinal feedback pathways so this preparation is not ideal for determining the effect of these pathways in addition the effects of these pathways on the stability of the constituent levels (muscles, joints, limbs) has not been tested. In this dissertation I have tested whether energetically optimal limb control can be constructed from the intrinsic viscoelasticity of muscles, from simple autogenic length feedback, or complex interjoint feedback. In addition I have tested whether length feedback through spinal reflex pathways is sufficient to stabilize at the limb level of a cat.

Supraspinal Mechanisms of Postural Control

Processed information from the spinal cord is transmitted to the brainstem and cerebellum where further sensory integration is accomplished. The brainstem has been shown to participate in postural adjustments during a voluntary task (Schepens and Drew

2004). Higher centers provide the potential for voluntary control, yet response latencies may be significantly longer. Higher centers are also the locale for multiple sensory modality integration (e.g. vestibular, visual, neck afferents) resulting in an overall representation and interpretation of the body in space. In addition to the long latency reflexive networks, an important role of the higher centers is the modulation of excitability of the spinal networks through a primarily inhibitory pathway (lateral reticulospinal tract) and a primarily excitatory pathway (medial reticulospinal tract).

While visual and vestibular information integrated in the brainstem and cerebellum are certainly used for postural control to varying degrees in different contexts, experiments with labyrinthectomized cats in a darkened room have demonstrated that neither vestibular nor visual information is required for the force constraint strategy or the directional tuning of EMG patterns (Inglis and Macpherson 1995). Although this information is not necessary to generate the postural response it has also been argued that the latency of the onset of the EMG response is appropriate for proprioceptive and cutaneous sensory integration at the level of brainstem and cerebellum (Horak and Macpherson 1996). The role of the brainstem and cerebellum with respect to the spinal reflexes has been tested in spinalized animal preparations. Spinalized cats could be trained to stand (De Leon et al. 1998, Fung and Macpherson 1999), but could balance only for short periods of time (Macpherson and Fung 1999). In the spinalized cats with reduced balance control, the directional tuning of EMG remains intact although delayed and with reduced magnitude. This would seem to suggest that the long latency response is necessary for postural control. However, in addition to directing the long latency response the higher centers control spinal reflex excitability (Miller et al. 1996). The inability of the spinalized cats to generate a postural response may be due one or both of these effects.

Evidence that the excitability control rather than the long latency response from higher centers is necessary for the postural response was shown in rabbits subject to

spinal hemisection (Lyalka et al. 2005). Rabbits subject to ventral hemi-section of the spinal cord lost and did not regain the postural response, while rabbits subject to dorsal or lateral hemisection quickly regained the postural response (Lyalka et al. 2005). The authors contend that since both dorsal and lateral hemisections substantially interfere with the feedback loops of the higher centers the most plausible explanation is that the excitability of the spinal networks is maintained in these preparations and not in the ventral hemi-section. They conclude that the spinal networks play a large role in generating the postural response.

The pyramidal tract neurons (PTNs) (neurons of the corticospinal tract) were recorded in cats subject to a periodically tilting of the platform on which they stood. The fact that the activity of these neurons correlated with tilt of the platform was taken as evidence that the motor cortex is directly involved in postural corrections (Beloozerova et al. 2005). Further it was found that individual PTNs for a specific limb were directly dependent upon the proprioceptive information from the contralateral limb, indicating a role in the postural controller (Karayannidou et al. 2008). There is also evidence in humans that longer latency postural responses involve direct corticospinal projections onto motoneurons (Taube et al. 2006). In spite of these results, however, it has been shown that premammilary decerebrate cats generate a postural response to perturbations (Bard and Macht 1958). Although the higher centers especially brainstem may be important for the global task of balancing the center of mass this level of stability and level of neural control was not tested. This thesis is built on the hypothesis that apparently complex neural control and ostensibly high degree of sensory integration can be an emergent property of anatomical structure and simple length feedback.

Hierarchical Postural Control

The hierarchical structure of the motor control system may be reflected in the motor task itself. In balance control during quiet standing ultimately the center of mass

(CoM) must be stabilized, which, again, requires the coordination and stability of multiple levels (limbs, joints, muscles). The stability of the whole therefore requires stability and coordination of the constituents. The hierarchical nature of both task and controller suggest that different levels of the motor control system are responsible for different levels of the task.

Postural control debates regarding the relative roles of intrinsic muscle and neural mechanisms, as well as spinal and supraspinal contributions are centered on the global problem of balancing the CoM and do not address the subtasks of stabilizing and coordinating the limb and joint responses to perturbation (Lyalka et al. 2005, Macpherson and Fung 1999, Morasso and Sanguineti 2002, Peterka 2002). Although it is generally agreed that the intrinsic properties of muscle are insufficient to balance the CoM in humans (Morasso and Sanguineti 2002, Peterka 2002) it is unknown whether they are sufficient for the sub-task of providing limb stability. The role of spinal reflexes in postural control has also been debated, again, in the context of balancing the CoM (Lyalka et al. 2005, Macpherson and Fung 1999). Since stability and coordination of the constituents (muscles, joints, and limbs) is necessary to balance the CoM it is conceivable that the responsibility for stabilizing the constituents is provided by the lower levels of the motor control hierarchy including intrinsic muscle properties and spinal reflex pathways. In particular muscle stiffness and length feedback both provide a positional sensor for the configuration of the limb and could be used to stabilize at the level of muscle, joint, and limb. I hypothesized that the lowest levels of the motor control system, the intrinsic properties of muscles are insufficient to stabilize a whole cat hindlimb and that muscle length feedback provided by spinal reflex mechanisms is sufficient to stabilize the cat hindlimb. I test this by demonstrating that an anatomically accurate model of the cat hindlimb is mathematically unstable under all patterns of muscle activation unless the intrinsic stiffness of muscles was augmented by length feedback. In addition I hypothesized that the observed postural response in terms of

tuned muscle activation and constrained ground reaction forces would be observed in the limb stabilized by length feedback, and test this by demonstrating that application of measured and approximated gains of length feedback to the perturbed hindlimb results in constrained ground reaction forces and tuned muscle activation patterns.

Ultimately stability could be provided by very stiff muscles or by strong length feedback gains at the cost of increased energetic expenditure. Based on the assumption that the biological system seeks to minimize energy expenditure I also hypothesized that the stabilizing spinal reflexes are organized according to optimal principles of control accuracy and energy. I tested this by designing an optimal asymmetric heterogenic feedback controller for a three-link hindlimb model measuring the effectiveness of the controller in maintaining postural endpoint control of a multi-link system. I show that for a postural endpoint task, asymmetric control allows improved endpoint performance, reduced energetic cost, and greater coordination among joints (Bunderson et al. 2007).

The hypotheses were tested using a mathematical model of a cat hindlimb. The benefit of using a mathematical model was that the intrinsic muscle properties and spinal reflex pathways could be applied independently and optimal control theory could be used to determine optimal reflex gains. First, I determined the optimal length and velocity feedback gains for maintaining postural control of a planar three-link limb model. This optimization was also applied to determine the optimal feedback between the joints of a three-dimensional seven degree-of-freedom (DoF) model and these optimal gains were compared to the length and velocity feedback provided by known spinal reflex pathways. The second study directly tested whether the intrinsic muscle properties are sufficient to provide limb stability. Here the problem of musculoskeletal redundancy was addressed by evaluating limb stability across a wide variety of functionally equivalent patterns of muscle activation. The third study tested whether length feedback in addition to the intrinsic muscle properties were sufficient to provide limb stability. In this study the response of the limb under postural perturbations was compared with the response of

intact cats (Macpherson and Fung 1999) specifically in terms of muscle activity (electromyography, EMG) and ground reaction forces (GRF). Finally, the limb perturbations were applied to a decerebrate cat and the GRF and kinematics of the limb were compared with modeling results.

Investigative Approach

Engineering Principles of Control

By using a mathematical model to evaluate the postural control problem, different levels of intrinsic mechanical and neural control can be independently and systematically investigated. For example, the effects of each level of control on system outputs (e.g. EMG, GRF, and kinematics) can be estimated through dynamic simulation and contrasted. In addition, the mathematical approach allows both rigorous determination of how the stability of the system depends on the different levels of control, and the application of optimal control theory to predict and test candidate strategies of neural control. In the first study an optimal control formulation – the linear quadratic regulator – was used to determine the organization of length and velocity feedback that optimally controls a simplified model of a limb. In the second and third studies, the detailed hindlimb model was linearized about an equilibrium posture and the stability of the limb (with and without length feedback, respectively) was quantified using Lyapunov stability theory. Additionally in the third study, the responses of the full, nonlinear hindlimb model with length feedback during forward dynamic simulations were compared to those of intact cats. Finally, in the fourth study, the responses of the hindlimb model during forward dynamic simulations were compared to those of a decerebrate cat. Linearization of non-linear systems, Lyapunov stability, and optimal control are introduced here briefly.

A requirement for the linear quadratic regulator formulation is that the system must be linear. Although the muscle models and rigid body equations of motion (f(x)) are inherently nonlinear, the postural task being evaluated is near static equilibrium. The equations of motion may therefore be linearized about this equilibrium point using a Taylor series approximation

$$\Delta\dot{\vec{x}} = \left.\frac{\partial f}{\partial \vec{x}}\right|_{\vec{x}=0} \frac{\Delta\vec{x}}{1!} + \left.\frac{\partial^2 f}{\partial \vec{x}^2}\right|_{\vec{x}=0} \frac{\Delta\vec{x}^2}{2!} + \ldots \quad . \tag{1}$$

If the disturbances are small, the higher order terms are much smaller than the first order term and the system can be approximated as

$$\Delta\dot{\vec{x}} = A\Delta\vec{x} \tag{2}$$

Where,

$$A = \left.\frac{\partial f}{\partial \vec{x}}\right|_{\vec{x}=0} . \tag{3}$$

This approximation of the system is used to evaluate the stability of the model and to predict patterns of length and velocity feedback.

Lyapunov stability theory establishes rigorous mathematical definitions of and tests for “stability”. The solution to equation (2) is an exponential that decays to the equilibrium if the matrix A is negative definite or, in other words, if all eigenvalues are less than zero. Thus, according to Lyapunov stability theory, if the linear system (Equation 1) is perturbed slightly from equilibrium ($\Delta\dot{\vec{x}} = \vec{0}$) and subsequently returns to equilibrium then it is said to be asymptotically Lyapunov stable.

Optimal control theory can be applied to the linearized equations of motion in order to predict patterns of length and velocity feedback. Optimal control theory is based on mathematical constructs that minimize a theoretical cost function associated with a system. In biomechanical systems, such "costs" can include measures of energy and accuracy. Mathematical models and optimal control are being used increasingly in

evaluating postural control (He et al. 1991, Kuo 1995, Kuo 2005, Todorov 2004, Todorov and Jordan 2002). The great benefit of optimal control theory is that in addition to being descriptive the models have the potential to be predictive of neural connectivity. Models of human balance control have been used to explain physiologically observed properties such as the hip and ankle strategies of postural control in terms of the sensory weighting (Kuo 1995). In addition, optimal state estimation and control have been used to predict the effect of the deterioration of various sensory modalities (vision, vestibular, joint proprioception) on the ability to balance (Kuo 2005). He et al. (1991) applied linear optimal control theory to a planar cat hindlimb model to predict length and force feedback between muscles. The ability to identify the trade-offs the nervous system makes between energetic and accuracy goals is a key feature of these applications. Liu and Todorov demonstrate that many specific features of motor tasks, such as late corrections during in reaching tasks, are attributable to this type of trade-off (Liu and Todorov 2007). In this dissertation, a specific optimal control formulation called the linear quadratic regulator is used to predict patterns of length and velocity feedback. The linear quadratic regulator formulation is described in detail in chapter 2.

Muscle, Joint and Extrinsic Space

Analyzing motor tasks from the perspective of these three spaces: extrinsic space, joint space, and muscle space, provides valuable insight into how the nervous system may coordinate control at one end to achieve results at the other end (Valero-Cuevas 2006) (Figure 1.2). Motor tasks are often considered in terms of extrinsic, Cartesian space, such as maintaining the center of mass above a base of support. However, to actually accomplish this goal many joints must be coordinated, and exactly how the CoM is maintained above the base of support could be more specifically defined in terms of the joint motions in joint space. Further, the joints of the limb are controlled not directly, but through the activation of muscles that cross the joints. Finally, in most cases, any given

joint is crossed by multiple muscles, some of which in turn cross other joints. The task of balance then requires coordination of all the muscles in muscle space to achieve the desired result in extrinsic space.

It is interesting that the chiasmatic structure seen in the hierarchies of motor control is reflected here in the dimensional mapping between these three spaces. In the motor control hierarchy a perturbation sensed in extrinsic (cutaneous), joint (joint proprioceptors) or muscle (spindles, GTO) space is processed and an appropriate response is returned back through the muscles (muscle space) to joint motion (joint space) resulting in ground reaction forces and center of mass movement (extrinsic space). The parallel mathematical mappings between the spaces are described here briefly along with their intuitive interpretation. To begin with, imagine an animal standing on a movable platform. As the platform begins to move, the displacement of the toe ($\Delta\vec{x}_{TOE}$)

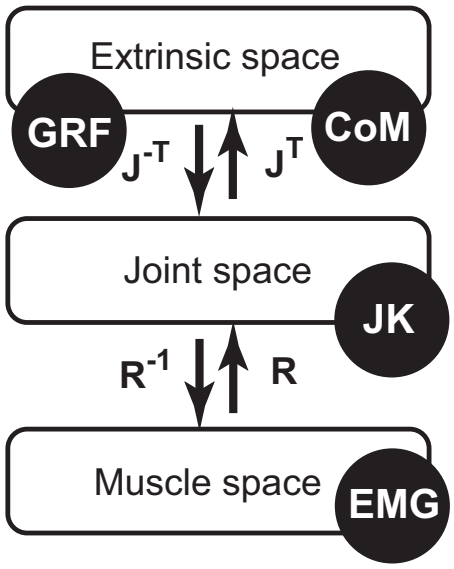

Figure 1.2: Multiple coordinate transformations are required in integrating sensory information and generating an appropriate motor response. The transformations from extrinsic (Cartesian) space to joint space are accomplished through the endpoint Jacobian (**J**). The transformations from joint space to muscle space are accomplished through the muscle moment arm matrix (**R**). The postural response can be measured in muscle space (EMG), joint space (joint kinematics JK), and extrinsic space (GRF and CoM motion).

in contact with the platform is explicitly related to the displacement of all the joints ($\Delta\vec{\theta}$). Mathematically this relationship is defined by the endpoint Jacobian which is simply the change endpoint position with the change in joint angles,

$$\mathbf{J} = \frac{\partial \vec{x}_{TOE}}{\partial \vec{\theta}} . \tag{4}$$

In other words, the endpoint Jacobian J is the mapping between the extrinsic and joint spaces. This joint motion will cause a lengthening or shortening of each musculotendon unit and the relationship between the joint displacement and musculotendon length change ($\Delta\vec{L}_{MT}$) is,

$$\mathbf{R} = \frac{\partial \vec{L}_{MT}}{\partial \vec{\theta}} . \tag{5}$$

The matrix R is the mapping between joint and muscle space. Next, suppose that the nervous system senses the lengthening of each muscle and so generates a response appropriate to the perturbation. Each muscle will be activated appropriately to produce a force and the combination of these muscle forces will result in torques applied to all the joints crossed by the activated muscles. The torque caused by the muscle forces is related to the muscle forces by,

$$\vec{T}_M = \mathbf{R}^T \Delta\vec{F}_M . \tag{6}$$

This relationship demonstrates the mapping between joint and muscle space with the same matrix in terms of kinetics as opposed to kinematics (Eq. 5). Finally, in order to resist the applied endpoint force and restore equilibrium the joint torque induced by the muscles must be related to the endpoint force applied by,

$$\vec{T}_M = \mathbf{J}^T \Delta\vec{F}_{TOE} . \tag{7}$$

This relationship demonstrates kinetically the mapping between joint and extrinsic spaces.

The control of any given motor task necessarily involves multiple physical transformations that can be described both biologically and mathematically. In the motor tasks considered in this work, this cascade involves the following transformations: from external or internal perturbation to sensory signal, from sensory signal to muscle activation, from muscle activation to muscle force, from muscle force to joint torques, and finally from joint torques to kinematics and endpoint forces. These mappings are instrumental in describing and analyzing the biological principles of postural control in mathematical form and biomechanical models are a powerful tool in implementing these translations.

Summary

In balance control during quiet standing ultimately the center of mass must be stabilized which requires the coordination and stability of constituent levels (limbs, joints, muscles). In addition the neuromusculoskeletal system is arranged in a hierarchy of control structures. The hierarchical nature of both task and controller suggest that different levels of the motor control system are responsible for different levels of the task.

I hypothesized that spinal reflexes are organized according to optimal principles of control accuracy and energy for stabilizing an animal at the limb level. In the first study of the thesis I determined the optimal organization of joint length and velocity feedback to stabilize a simplified model of a limb (Bunderson et al. 2007). I have compared this organization of feedback with the known spinal reflex pathways of the cat hindlimb.

I further hypothesized that the lowest level of the motor control system, the intrinsic properties of muscles are insufficient to stabilize a cat hindlimb, that muscle length feedback is sufficient to stabilize the cat hindlimb, and that the limb stabilized with length feedback will result in a force constraint strategy and tuned muscle activation. In the second study I tested whether the intrinsic muscle properties are sufficient to

provide limb stability (Bunderson et al. 2008). The problem of motor redundancy was addressed and the stability criterion was tested with a wide variety of functionally equivalent patterns of muscle activation. The third study tested whether the known homonymous spinal length feedback pathways are sufficient to provide limb stability. Also the response of the limb under postural perturbations was compared with the response of intact cats (Macpherson and Fung 1999) in terms of EMG and ground reaction forces (GRF). In the fourth study, limb perturbations were applied to a decerebrate cat and the GRF and kinematics of the limb were compared with modeling results.

CHAPTER 2

ASYMMETRIC INTERJOINT FEEDBACK CONTRIBUTES TO POSTURAL CONTROL OF REDUNDANT MULTI-LINK SYSTEMS

Introduction

Postural control has proven to be a daunting engineering problem, but one that animals solve as a matter of course. Control of multi-link systems is mathematically complicated by dynamic coupling among segments, which introduce torques at the remote joints in response to motion of any segment (Lacquaniti and Soechting 1986, Sage et al. 1999). For kinematically redundant multi-link systems, maintaining the position of the endpoint does not fully constrain the configuration of the joints and this absence of a one-to-one relationship between the control goal of endpoint position and the system state variables further complicates the control problem (Patel and Shadpey 2005). Despite the computational complexities, biological systems derive striking postural stability and control accuracy from the properties of muscles and proprioceptive reflexes (Kargo and Giszter 2000, Sinkjaer 1997).

Biological systems use a complex network of inter- and intra-joint feedback along with intrinsic musculotendon properties to achieve endpoint control. The intrinsic properties of individual muscles provide instantaneous stiffness, viscosity, and interjoint coupling (Hamill and Knutzen 2003). These mechanisms are amplified by a carefully structured hierarchy of neural feedback mechanisms. At the lowest level, the stretch reflex (Sherrington 1898) has been considered to provide spring-like or servo-like control of an individual muscle (Merton 1953, Nichols and Houk 1976). Feedback from individual muscle spindles was subsequently shown to excite motorneurons of synergistic muscles and to inhibit motorneurons of antagonists (Liddell and Sherrington 1925, Lloyd 1946), giving rise to the concept of a myotatic unit comprised of both agonists and

antagonists to provide servo-like control of individual joints (Merton 1953). In human subjects, reflex control does not mimic a servo-like system (Crago et al. 1976), and the variation in intermuscular feedback gains measured *in vivo* varies among muscles crossing a single joint (Nichols 1989). Short latency spindle reflexes modulate activity of many heteronymous muscles (Eccles 1956, Eccles et al. 1957, Nichols 1989), and it seems that reflex mechanisms can provide an integrated control system, spanning and coordinating multiple joints (Nichols et al. 1999). This heterogenic feedback can be asymmetric, favoring force generation by one muscle of a pair or at one joint over another (Bonasera and Nichols 1994, Eccles and Lundberg 1958, Nichols et al. 1999, Pratt 1995).

Asymmetry in heterogenic feedback results in an asymmetric, or non-conservative, system (Hogan 1985). Hogan raised this point to argue that symmetric or spring-like systems simplify control by allowing higher centers to specify endpoint position in terms of a potential function, the gradient of which defines the relationship between endpoint displacement and the restoring force. The idea that the human arm functions as a symmetric system was tested during constrained planar motion in humans and found to hold for only two of the four subjects tested (Mussa-Ivaldi et al. 1985). On average, 6.5% of the forces could not be accounted for under a symmetric assumption, and it is not clear whether this is an important fraction or not. Even though substantial asymmetries are present at the muscle level, synergistic muscles form a highly redundant network around limited mechanical degrees of freedom, which may minimize the mechanical effect of the asymmetries. However, substantial asymmetries in heterogenic feedback have been predicted using linear musculoskeletal models (Barin 1989, He et al. 1991, Park et al. 2004). He and coworkers (He et al. 1991) used linear optimal control theory to predict length and force feedback between muscles of the feline hindlimb and found the heterogenic feedback gains to be asymmetric. Considering higher levels of joint and interjoint feedback, asymmetric controllers were required to match human

postural responses modeled using two- (Park et al. 2004) and three- (Barin 1989) link inverted pendulum models. Asymmetric joint-level stiffnesses have also been predicted (Stroeve 1999) and measured (Mussa-Ivaldi et al. 1985) in human arm models. Asymmetric controllers therefore appear to have performance advantages, despite the added complexity. But, experimental observations supporting the importance of asymmetric reflexes have been equivocal, and it may be that the benefit provided by asymmetric interjoint feedback is relatively small and does not influence neural organization.

Optimal controllers are mathematical constructs that minimize a theoretical cost function associated with a system. In biomechanical systems, "costs" can include measures of energy and accuracy. The linear quadratic regulator (Bryson and Ho 1975) is ideally suited to this class of problems and has frequently been used to test hypothetical cost functions to probe the organizing principles of the central nervous system (He et al. 1991, Kuo 1995, Kuo 2005). One of the strongest advantages of the LQR approach is that it provides a unique, analytical solution, but previous work has not evaluated the change in cost associated with deviations from the optimal analytical solution, by, for example eliminating the asymmetric components of the feedback controller.

The aim of this paper is to determine whether asymmetric interjoint feedback improves the performance of postural tasks for a generic redundant limb model. We hypothesize that an asymmetric multi-joint control strategy results in lower energetic cost of recovery and reduced endpoint displacement due to perturbations. We use optimal control theory to design specifically structured controllers and measure the effectiveness of each in maintaining postural endpoint control of a multi-link system. We show that the benefits of asymmetric feedback are task-dependent. Asymmetric feedback provides no benefit in a system tasked to maintain a specific joint configuration, but the system tasked to maintain joint configuration provides relatively poor endpoint stability. For a postural endpoint task, asymmetric control allows improved endpoint performance,

reduced energetic cost, and greater coordination among joints. These advantages of the optimal asymmetric controller could influence the structure of a biological controller, and is consistent with the limited experimental data in the literature.

Methods

The analytical methods of the paper follow the format of Table 2.1. First, we define a kinematically redundant multi-link model. Second, two postural tasks (a joint control task and endpoint control task), are specified for the model. Third, three structures corresponding to a diagonal controller (single-joint control, homonymous feedback), a symmetric controller (multi-joint symmetric feedback), and an unconstrained controller (multi-joint asymmetric feedback) are designed for each postural task resulting in a total of 6 optimal controllers. The endpoint stiffness and viscosity characteristics, and dynamic response of the model are reported. To test the hypothesis that asymmetric multi-link strategies improve efficiency and control, the model is subjected to impulse perturbations at the endpoint, and kinematic and kinetic performance metrics are reported.

Table 2.1: Analytical Methods

A. Model:	Planar, 3-link, lumped parameter model		
B. Kinematic task specification:	Joint Control, minimize: d_J^2	Endpoint Control, minimize: $0.9d_{EP}^2 + 0.1d_J^2$	
C. Controller constraint ($\mathbf{k_R}$,$\mathbf{k_B}$):	Diagonal (JD, ED) $\begin{bmatrix} d_1 & 0 & 0 \\ 0 & d_2 & 0 \\ 0 & 0 & d_3 \end{bmatrix}$	Symmetric (JS,ES) $\begin{bmatrix} s_1 & s_4 & s_5 \\ s_4 & s_2 & s_6 \\ s_5 & s_6 & s_3 \end{bmatrix}$	Unconstrained (JU, EU) $\begin{bmatrix} u_1 & u_4 - u_7 & u_5 - u_8 \\ u_4 + u_7 & u_2 & u_6 - u_9 \\ u_5 + u_8 & u_6 + u_9 & u_3 \end{bmatrix}$
D. Performance evaluation:	Endpoint viscoelastic properties	Dynamic response (ξ)	$d_J^{\max}, d_{EP}^{\max}, C_e = \int_0^\infty \left(\vec{u}^T \mathbf{R} \vec{u}\right) dt$

Model

The model simulates a system of three identical links joined by single degree of freedom rotational joints (Figure 2.1a). Each link of the model is a thin rod of length *L* and mass *m*. The nominal joint configuration for simulations was chosen to mimic feline stance posture (θ_1 = -51°, θ_2 = -86°, θ_3 = 35°) based on experimental data (Torres-Oviedo et al. 2006). Additional simulations were performed with tree shrew posture (θ_1 = -150°, θ_2 = 120°, θ_3 = -117°) (Schilling 2005), which is more compact. The equations of motion for the system, expressed in the generalized coordinate system, $\vec{\theta} = [\theta_1, \theta_2, \theta_3]^T$, are

$$\mathbf{M}\ddot{\vec{\theta}} = -\vec{v}(\vec{\theta}, \dot{\vec{\theta}}) + \vec{T}(\vec{\theta}, \dot{\vec{\theta}}) + \mathbf{J}(\vec{\theta})^T \vec{F}_{END}. \quad (1)$$

where **M** is the inertia matrix, $\vec{v}$ is the centrifugal and Coriolis forces, $\vec{T}$ is the control joint torques, **J** is the Jacobian, and $\vec{F}_{END}$ is an applied force at the endpoint. The equations for **M,** $\vec{v}$ and **J** were derived in Autolev (Online Dynamics, Sunnyvale, CA).

These equations were derived in non-dimensional units $\hat{L}$, $\hat{m}$, and $\hat{t}$ with the characteristic length *L,* mass *m*, and force σ. The characteristic time τ is derived from *L*, *m*, and the characteristic force or "effort" of the system (σ),

$$\tau = \sqrt{\frac{Lm}{\sigma}}.$$

The effort of the system can be thought of as the ratio of accuracy to energy; for greater effort, accuracy of the system is increased with decreased energetic efficiency.

The control torque applied to each joint element is determined by a lumped parameter, viscoelastic model,

$$\vec{T}\left(\vec{\theta}, \dot{\vec{\theta}}\right) = -\mathbf{k_R}\left(\Delta\vec{\theta}\right) - \mathbf{k_B}\dot{\vec{\theta}},$$

where, $\mathbf{k_R}$ is the dimensionless 3x3 joint stiffness matrix and $\mathbf{k_B}$ the dimensionless 3x3 joint viscosity matrix.

The system described in Eq. 1 was linearized by Taylor series expansion of the model around its nominal configuration with no applied endpoint force. At the zero

velocity equilibrium point Coriolis forces are zero, and the governing equations in state space representation become

$$\dot{\vec{z}} = \begin{bmatrix} \mathbf{0}_{3x3} & \mathbf{I}_{3x3} \\ -\mathbf{M}^{-1}\Big|_{\substack{\dot{\vec{\theta}}=\dot{\vec{\theta}}_0 \\ \vec{\theta}=\vec{\theta}_0}} \mathbf{k_R} & -\mathbf{M}^{-1}\Big|_{\substack{\dot{\vec{\theta}}=\dot{\vec{\theta}}_0 \\ \vec{\theta}=\vec{\theta}_0}} \mathbf{k_B} \end{bmatrix} \vec{z}\,, \tag{2}$$

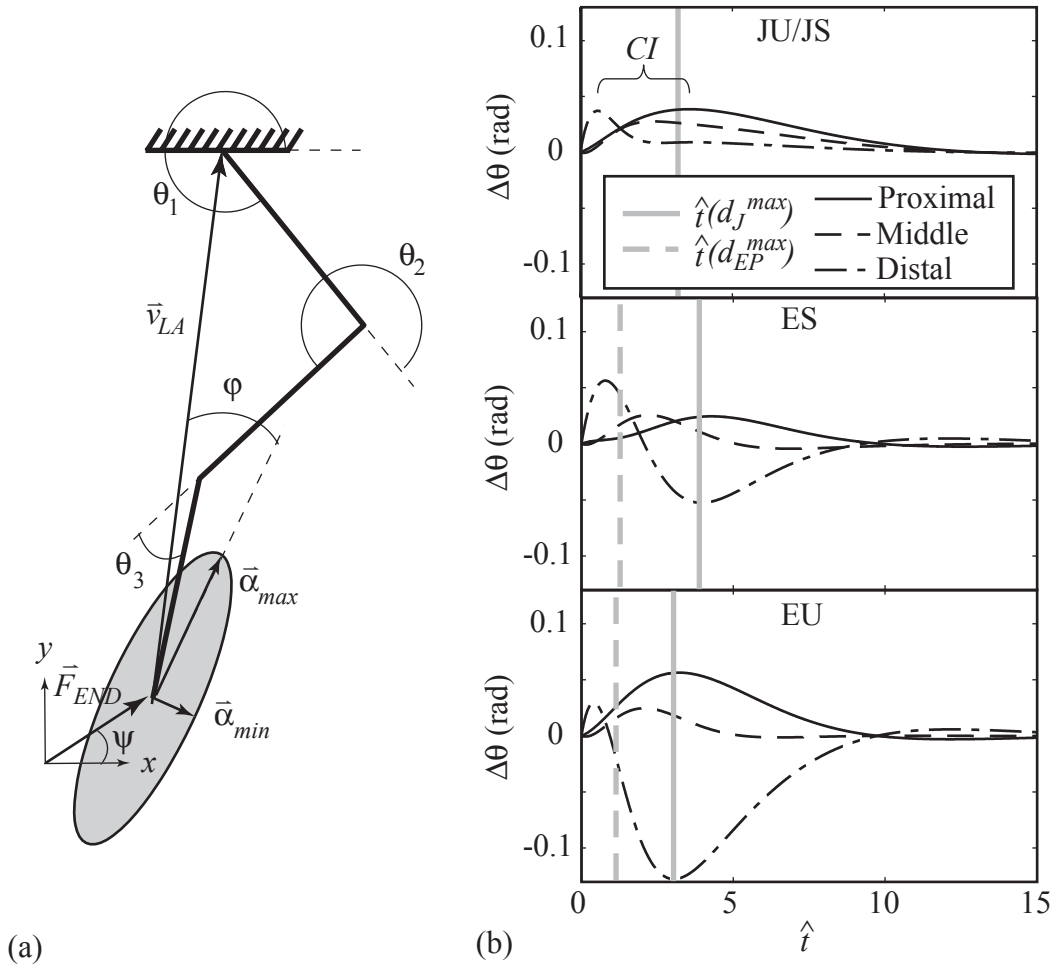

Figure 2.1: Model diagram with example endpoint ellipse. (A) Three-link model (heavy black lines) with generalized coordinate system ($\vec{\theta} = [\theta_1, \theta_2, \theta_3]^T$). The limb axis, $\vec{v}_{LA}$, is directed from the endpoint to the proximal joint. The endpoint stiffness (k_{R_END}) and viscosity (k_{B_END}) ellipses are characterized by the angle φ between the limb axis and direction of maximum stiffness, $\vec{\alpha}_{MAX}$. The direction of minimum stiffness is $\vec{\alpha}_{MIN}$. Endpoint position perturbations (B) of equal magnitude are applied in all directions and the Jacobian pseudo-inverse used to compute the limb configuration for each endpoint position. Model responses (B) (top: JU/JS, middle: ES, bottom: EU) are shown for a perturbation applied in the *x* direction ($\psi = 0°$). The time of maximum endpoint (dashed gray line) and maximum total joint (solid gray line) displacements are indicated.

where $\vec{z} = [\vec{\theta} - \vec{\theta}_0, \dot{\vec{\theta}}]^T$. Rearranging terms and defining the state matrix (**A**), input matrix (**B**), and state feedback matrix (**k**) as

$$\mathbf{A} = \begin{bmatrix} \mathbf{0}_{3x3} & \mathbf{I}_{3x3} \\ \mathbf{0}_{3x3} & \mathbf{0}_{3x3} \end{bmatrix}, \ \mathbf{B} = \begin{bmatrix} \mathbf{0}_{3x3} \\ \mathbf{M}^{-1}\Big|_{\substack{\dot{\vec{\theta}}=\dot{\vec{\theta}}_0 \\ \vec{\theta}=\vec{\theta}_0}} \end{bmatrix}, \ \mathbf{k} = \begin{bmatrix} \mathbf{k}_\mathbf{R} & \mathbf{k}_\mathbf{B} \end{bmatrix}, \tag{3}$$

allows Eq. (2) to be written in the form, $\dot{\vec{z}} = (\mathbf{A} - \mathbf{Bk})\vec{z}$.

Task Specification and Optimization

The steady-state linear quadratic regulator (LQR) formulation (Bryson and Ho 1975) was used to uniquely determine the components of the optimal state feedback matrix **k**. The matrix minimizes a cost function (C_t) of the form

$$C_t = C_k + C_e = \int_0^\infty (\vec{z}^T \mathbf{Q} \vec{z}) dt + \int_0^\infty (\vec{u}^T \mathbf{R} \vec{u}) dt = \int_0^\infty (\vec{z}^T \mathbf{Q} \vec{z} + \vec{u}^T \mathbf{R} \vec{u}) dt . \tag{4}$$

The first term of this expression, $\vec{z}^T \mathbf{Q} \vec{z}$, is a weighted sum of squares of state errors, and defines the kinematic cost C_k. Two control tasks were defined to specify the kinematic cost. A joint control matrix ($\mathbf{Q_J}$) represents the task of holding the limb at its nominal configuration, quantified by simple sum of squares of link displacement,

$$d_J^2 = \sum_{i=1}^{n} \left(\hat{L} \Delta\theta_i\right)^2 = \vec{z}^T \mathbf{Q}_\mathbf{J} \vec{z} , \quad \mathbf{Q}_\mathbf{J} = \hat{L}^2 \begin{bmatrix} \mathbf{I}_{3x3} & \mathbf{0}_{3x3} \\ \mathbf{0}_{3x3} & \mathbf{0}_{3x3} \end{bmatrix}, \tag{5}$$

where n is the number of joints. The accuracy matrix ($\mathbf{Q_{EP}}$) was chosen to represent the task of maintaining endpoint position in Cartesian space, and incorporates an internal model in the form of the Jacobian,

$$d_{EP}^2 = dx^2 + dy^2 = \vec{z}^T \mathbf{Q}_\mathbf{EP} \vec{z} , \quad \mathbf{Q}_\mathbf{EP} = \begin{bmatrix} \mathbf{J}^T \mathbf{I}_{2x2} \mathbf{J} & \mathbf{0}_{3x3} \\ \mathbf{0}_{3x3} & \mathbf{0}_{3x3} \end{bmatrix}. \tag{5}$$

This control matrix assumes a constant Jacobian evaluated at the model's nominal state and is therefore valid only for joint configurations close to this state. Since $\mathbf{Q_{EP}}$ is not positive semi-definite, a requirement for LQR optimization, the endpoint task is

determined by a weighted sum of joint and endpoint control ($\vec{z}^T \mathbf{Q_E} \vec{z} = 0.1 d_J^2 + 0.9 d_{EP}^2$). The accuracy matrix $\mathbf{Q_E}$ for the endpoint task is

$$\mathbf{Q}_{\mathrm{E}} = 0.1\mathbf{Q_J} + 0.9\mathbf{Q_{EP}}.$$

The second term, $\vec{u}^T \mathbf{R} \vec{u}$, is a weighted sum of squares of the torques. The effort weighting matrix, $\mathbf{R} = \mathbf{I}_{3x3}$, was chosen to equally weight torque production at each joint and results in the sum of the squares of the joint torques, defining an energetic cost (C_e).

The minimum solution of the cost function defined in Eq. (4) for a system of the form $\dot{\vec{z}} = \mathbf{A}\vec{z} + \mathbf{B}\vec{u}$ and control law, $\vec{\mathrm{u}} = -\mathbf{k}\vec{z}$, is

$$C_{t,\min} = \min_{\vec{u}(t)} \left[\int_0^\infty \left(\vec{z}^T \mathbf{Q} \vec{z} + \vec{u}^T \mathbf{R} \vec{u} \right) dt \right] = \vec{z}_0^T \mathbf{S} \vec{z}_0 .$$

The matrix **S** is the constant, analytical solution of the matrix algebraic Riccati equation,

$$\mathbf{0} = \mathbf{A}^T\mathbf{S} + \mathbf{S}\mathbf{A} + \mathbf{Q} - \mathbf{S}\mathbf{B}\mathbf{R}^{-1}\mathbf{B}^T\mathbf{S}, \tag{7}$$

and the optimal state feedback matrix is

$$\mathbf{k} = \mathbf{R}^{-1}\mathbf{B}^T\mathbf{S}. \tag{8}$$

Controller Constraints

To determine the consequences of structural changes in model stiffness ($\mathbf{k_R}$) and viscosity ($\mathbf{k_B}$), two matrix constraints were used. First, a constrained controller with diagonal $\mathbf{k_R}$ and $\mathbf{k_B}$ produces torque at each joint due to motion of that joint only, representing single joint control. The equivalent biological system would be comprised of only uniarticular muscles without heterogenic feedback across joints, and is similar to a myotatic unit. Second, a constrained controller with symmetric off-diagonal terms causes the torque at a joint to be influenced by motion of remote joints, representing symmetric multi-joint control. The biological equivalent would include biarticular muscles, but is constrained so that net heterogenic feedback is symmetric across joints.

Constrained controllers ($\tilde{\mathbf{k}}$) are not guaranteed to produce the absolute minimum **S**. Optimal constrained controllers are obtained by nonlinear minimization of the Frobenius norm of the difference between the absolute minimum (**S**) and $\tilde{\mathbf{S}}$,

$$f = \left\| \mathbf{S} - \tilde{\mathbf{S}} \right\|_F = \sqrt{\sum_{i=1}^{2n} \sum_{j=1}^{2n} \left| \mathbf{S}_{ij} - \tilde{\mathbf{S}}_{ij} \right|^2},$$

where $\tilde{\mathbf{S}}$ is derived from application of the constrained controller ($\tilde{\mathbf{k}}$) to Eq. (4). Controllers for both the joint and endpoint tasks were determined subject to no constraints (JU, EU) and to the constraints of diagonal (JD, ED) and symmetric (JS, ES) stiffness and viscosity matrices.

Analytical Methods

To quantify the global viscoelastic properties of each controller model, endpoint stiffness ($\mathbf{k_{R\_END}}$) and viscosity ($\mathbf{k_{B\_END}}$) (Figure 2.1a) were determined from stiffness and viscosity matrices. The endpoint stiffness is defined by,

$$\mathbf{k}_{\mathbf{R\_END}} = \left(\mathbf{J} \mathbf{k}_{\mathbf{R}}^{-1} \mathbf{J}^T \right)^{-1},$$

for the multi-link model with no background force applied to the endpoint. Endpoint viscosity ($\mathbf{k_{B\_END}}$) and endpoint inertia ($\mathbf{M_{END}}$) matrices are determined by the same transformation of joint viscosity ($\mathbf{k_B}$) and inertia (**M**).

Ellipse eccentricities ($s = 1 - \alpha_{MIN} / \alpha_{MAX}$), areas ($A$), and the deviation ($\varphi$) of the direction of maximum stiffness of the ellipse ($\vec{\alpha}_{MAX}$) from the vector from the endpoint to the proximal joint center ($\vec{v}_{LA}$) are reported (Figure 2.1a).

The degree of asymmetry of the endpoint stiffness was measured with the quantity $Z_{mean\_\mathbf{R}}$ (Mussa-Ivaldi et al. 1985). $Z_{mean\_\mathbf{R}}$ is the ratio of asymmetric endpoint stiffness to symmetric endpoint stiffness,

$$Z_{mean\_\mathbf{R}} = \sqrt{\frac{\det\left(\mathbf{k}_{\mathbf{R\_END}} - \mathbf{k}_{\mathbf{R\_END}}^T \right)}{\det\left(\mathbf{k}_{\mathbf{R\_END}} + \mathbf{k}_{\mathbf{R\_END}}^T \right)}}.$$

The degree of asymmetry of the joint viscosity was measured from the joint viscosity $\mathbf{k_{B\_END}}$ with the quantity $Z_{mean\_\mathbf{B}}$ calculated in the same way as $Z_{mean\_\mathbf{R}}$,.

Dynamic properties of each model were quantified by the time to maximum endpoint displacement $\hat{t}\left(d_{EP}^{\max}\right)$, coordination index (*CI*) and damping ratios (ξ_i) of the three primary modes. The coordination index is the maximum time between individual peak joint displacements (Figure 2.1b). Damping ratio represents the ratio of actual damping to critical damping of the system. The damping ratios (ξ_i) are determined according to the method of Inman (1984) as the eigenvalues (ξ_i) of the matrix $\boldsymbol{\xi}$,

$$\boldsymbol{\xi} = \mathbf{k}_{\mathbf{B}cr}^{-1/2}\mathbf{k}_{\mathbf{B}}\mathbf{k}_{\mathbf{B}cr}^{-1/2},$$

where the critical damping matrix ($\mathbf{k}_{\mathbf{B}cr}$) is defined as

$$\mathbf{k}_{\mathbf{B}cr} = 2\mathbf{M}^{1/2}\left(\mathbf{M}^{-1/2}\mathbf{k}_{\mathbf{R}}\mathbf{M}^{-1/2}\right)^{1/2}\mathbf{M}^{1/2}.$$

The exponent ½ represents the unique positive-definite square root of a positive-definite matrix. The solution of the Riccati equation (7) is a system with $\mathbf{k_B}$ equal to $1/\sqrt{2}$ $\mathbf{k}_{\mathbf{B}cr}$ (see Appendix), resulting in damping ratios of $1/\sqrt{2}$ for all modes of the unconstrained controllers JU and EU.

To determine the success of the various controllers in optimizing joint and endpoint control, impulse force perturbations of equal magnitude were applied in all directions (ψ) to the endpoint of the model (Figure 4.1b). The linear system response to an impulse endpoint force perturbation, assuming a constant Jacobian, is given by

$$\vec{z}\left(\hat{t}\right) = \exp\left(\left(\mathbf{A} - \mathbf{BK}\right)\hat{t}\right)\begin{bmatrix}\mathbf{0}\\ \mathbf{M}^{-1}\mathbf{J}^{T}\vec{F}_{END}\end{bmatrix}.$$

Performance of each controller is quantified by the maximum joint ($d_J^{\max}$) (Eq. 5) and endpoint ($d_{EP}^{\max}$)(Eq. 6) displacements experienced by the model and by the energy expenditure of the controller (C_e) (Eq. 4), for a perturbation in a given direction, ψ. Three sample responses (JU/JS, ES, EU) are shown in Figure 2.1b for a perturbation

applied in the x direction ($\psi = 0°$). The time of maximum endpoint and joint displacements are shown in Figure 2.1b. Note that depending on the controller, the maximum endpoint and joint displacements may occur at different times. The endpoint position perturbation magnitude ($\left|\bar{F}_{END}\right| = 0.1$) was chosen so that no component of the matrix $\mathbf{J}(\theta)^{\mathrm{T}}\mathbf{J}(\theta)$ differed by more than 10% from the value at the nominal posture during the perturbation. To evaluate the global performance of the control models, $d_J^{\max}$, $d_{EP}^{\max}$, and C_e were averaged ($\overline{d_J^{\max}}$, $\overline{d_{EP}^{\max}}$, $\overline{C_e}$) across perturbation direction, ψ.

Results

Controller Structure

The optimal unconstrained control structure minimizing joint displacement (JU) contains only diagonal elements for $\mathbf{k_R}$, and only symmetric components for $\mathbf{k_B}$ (Table 2.2) and is therefore identical to JS. The joint control task, therefore, does not benefit from asymmetry in interjoint feedback. The distal joint of the diagonal constrained joint controller (JD) is 45% more stiff and 47% less viscous than the proximal joint, reflecting the lower system inertia below the distal joint.

In contrast, the optimal unconstrained control structure minimizing endpoint displacement (EU) is dramatically asymmetric, with off-diagonal stiffness terms ranging from 0.54-1.63, compared with diagonal stiffness terms of 0.93-1.31. Upper off-diagonal terms are smaller than the lower off-diagonal terms meaning that the torque generated at distal joints due to motion at proximal joints is greater than torque generated at proximal joints due to distal joint motion. For EU, the asymmetry in endpoint stiffness and viscosity is $Z_{mean\_\mathbf{R}} = 11.5\%$, and $Z_{mean\_\mathbf{B}} = 1.5\%$, respectively. For ED, diagonal joint stiffness terms vary more than for JD, increasing by 300% from proximal to distal while viscosity increases by 46% across joints (Table 2.2). Addition of symmetric terms inverts this relationship, dramatically decreasing stiffness and viscosity at distal joints.

Single joint stiffnesses are decreased by an average of 46%, and viscosities by an average of 62% when symmetric terms are introduced.

Endpoint Characteristics

The endpoint stiffness and viscosity ellipses incorporate both controller characteristics and system geometry and provide an integrated measure of the performance of the kinematically redundant system. These ellipses are characterized by their eccentricity, which indicates directional sensitivity, and their area, which indicates overall system stiffness. The endpoint stiffness ellipses of the joint control models (Figure 2.2b) are highly eccentric (JD: $s = 0.967$; JU/JS: $s = 0.967$) (Table 2.3), with the direction of greatest resistance near the axis of the limb (JD: $\varphi = -7.4°$; JU/JS: $\varphi = -7.9°$). In general the direction of maximum stiffness for all controller models is aligned closely with the limb axis (within 9°). The joint control models contain no internal model of the endpoint position, so the eccentricity of the endpoint ellipses reflects geometrical characteristics of the system.

Table 2.2: Model inertia matrix and stiffness (k_R) and viscosity (k_B) components.

	JD			JU/JS			**M**		
	1.03	0	0	1.00	0	0	6.41	3.41	1.31
k_R	0	1.15	0	0	1.00	0	3.41	2.99	0.99
	0	0	1.49	0	0	1.00	1.31	0.99	0.58
	4.09	0	0	3.33	1.22	0.49			
k_B	0	3.27	0	1.22	2.06	0.48			
	0	0	2.15	0.49	0.48	0.84			
	ED			ES			EU		
	2.29	0	0	2.75	1.26	1.23	1.17	0.39	0.19
k_R	0	4.94	0	1.26	1.70	0.59	0.93	1.31	0.33
	0	0	9.14	1.23	0.59	0.69	1.82	1.23	0.93
	6.50	0	0	4.76	1.84	1.47	3.95	1.85	0.74
k_B	0	7.37	0	1.84	2.49	0.86	2.53	2.71	0.82
	0	0	9.49	1.47	0.86	0.68	2.03	1.46	1.00

Table 2.3: Endpoint inertial, stiffness and viscosity ellipse characteristics

$\mathbf{K_{R\_END}}$	φ (°)	s	A	$\mathbf{K_{B\_END}}$	φ (°)	s	A
JD	-7.4	0.967	1.09	JD	-8.7	0.967	10.96
JU/JS	-7.9	0.967	0.89	JU/JS	-8.6	0.897	4.34
ED	-4.6	0.975	10.91	ED	-7.4	0.968	44.21
ES	-8.9	0.839	2.63	ES	-11.9	0.868	7.62
EU	-8.6	0.808	2.12	EU	-9.1	0.748	6.68
$\mathbf{M_{END}}$	-5.7	0.727	3.84				

When subject to the diagonal constraint, the endpoint control model (ED) also results in a highly eccentric (s = 0.975) stiffness ellipse (Figure 2.2b, Table 2.3). Relaxing the diagonal constraint to permit symmetric interjoint stiffness (ES) reduces the eccentricity of the stiffness ellipse (s = 0.839). The reduction in stiffness eccentricity is primarily due to decreased stiffness in the direction of maximum stiffness (ED: α_{max} = 11.8, ES: α_{max} = 2.3), resulting in larger displacements in that direction, while the minimum stiffness increases only slightly (ED: α_{min} = 0.29, ES: α_{min} = 0.36). Releasing all constraints on the control model (EU) further reduces endpoint stiffness eccentricity (s = 0.808). The area of the stiffness ellipse decreases dramatically with the addition of symmetric off-diagonal terms (ED: A = 10.91; ES: A = 2.63), and decreases further with the addition of asymmetric off-diagonal terms (EU: A = 2.12).

The endpoint viscosity ellipses demonstrate the same trends (Figure 2.2c, Table 2.3); there is a sharp decrease in eccentricity and area with the addition of symmetric terms for both the joint and endpoint controllers (JD: s = 0.967, A = 10.96; JU/JS: s = 0.897, A = 4.34; ED: s = 0.968, A = 44.21; ES: s = 0.868, A = 7.62, EU: s = 0.748, A = 6.68). The orientation of the endpoint viscosity ellipses is within 12° of the limb axis.

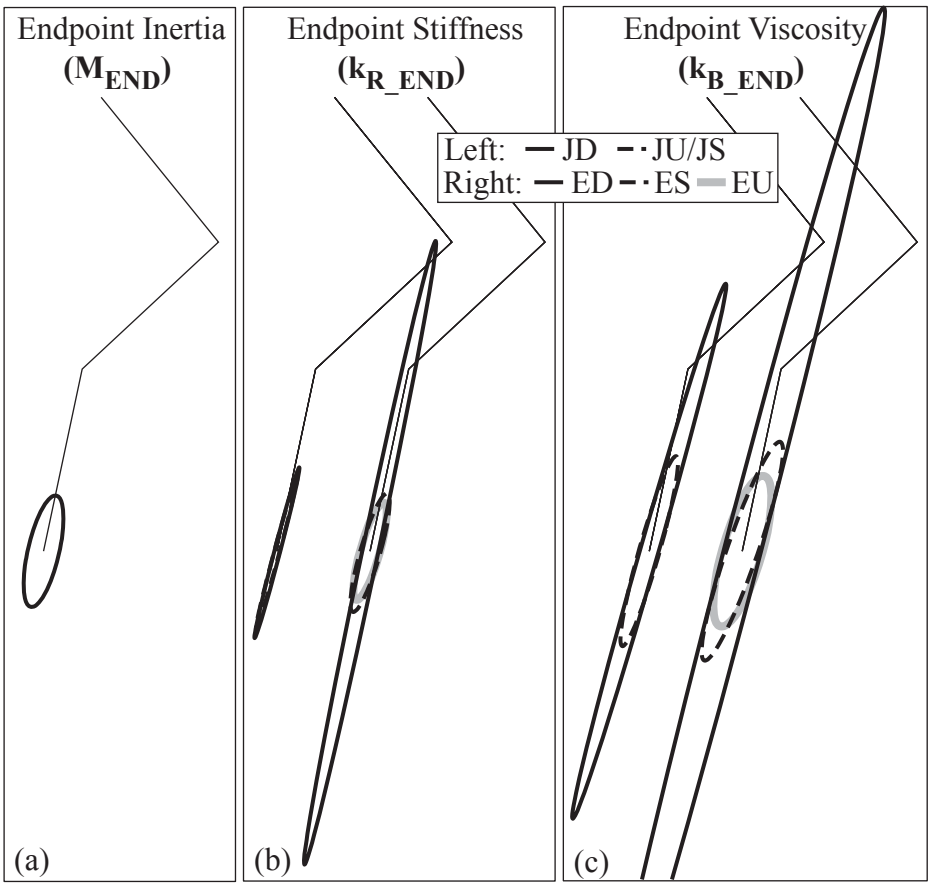

Figure 2.2: Endpoint ellipses for the six models. Ellipses represent the endpoint inertia (A), stiffness (B), and viscosity (C) of the optimal joint (left in B and C), and endpoint (right in B and C) controllers. The stiffness matrix of the JD, and JU/JS model is diagonal resulting in highly eccentric endpoint stiffness ellipses (B), while the addition of symmetric terms to the viscosity matrix for the joint controller JU/JS results in a dramatically less eccentric endpoint viscosity ellipse (C). The addition of symmetric terms to k_R and k_B in the endpoint controllers ES and EU also result in dramatically less eccentric and smaller endpoint ellipses (B,C). All ellipses are of approximately the same orientation.

Dynamic Response

To characterize the ability of each controller to maintain endpoint position, we analyzed the response of the system to a force impulse perturbation applied at the endpoint. The dynamic response of JU/JS, ES, and EU models (Figure 4.1b) demonstrate the different strategies employed to achieve joint and endpoint control. In all responses the distal joint experiences the greatest and most rapid initial displacement in response to the perturbation.

Motion of the JU/JS controller model is dominated by inertia, and joints follow a progressive displacement pattern with individual joints reaching peak displacement successively. Peak endpoint displacement is 0.15, occuring at $\hat{t} = 3.3$, and geometric recovery does not begin until substantially after the distal joint has completed its recovery. Maximal joint displacements follow a successive distal-to-proximal pattern (Figure 2.1b, upper panel) and occur over a dimensionless time of 3.0 (*CI*).

The endpoint controllers (ED,ES,EU), each of which contains an internal model of endpoint position, all display much better endpoint performance than the joint controllers (JD, JU/JS). The maximal ED controller displacement was 0.09, 43% less than the best joint controller (JU/JS), and geometric recovery began at $\hat{t} = 1.9$. For the ES controller, interjoint coupling links the rapid motion of the distal segment to amplified torque generation at the proximal joints. The symmetry of this coupling causes slower displacement of the more proximal joints that poduces a sustained torque generation at the distal joint, which is sufficient to reverse the direction of motion of the distal joint (Figure 4.1b, middle and lower panels). Interjoint coupling increases the apparent stiffness of proximal joints early in the perturbation, but reverses the apparent stiffness of the distal joint later in the perturbation. This result is due to coupling of the inertially retarded motion of proximal and middle joints to torque generation at the distal joint. The reversal of the distal joint counteracts the continuing motion of the proximal and middle joints to maintain the *x*-*y* location of the endpoint. The time to peak endpoint displacement is faster for the ES controller at 1.3, but maximal joint displacements still follow a successive pattern as in the JU/JS controller model and occur within a dimensionless time of 3.5 (*CI*).

This compensating effect of the distal joint is amplified for the EU controller, where torque generation is coupled asymmetrically. The asymmetry of interjoint coupling permits the distal joint to undergo exaggerated extension without substantially altering proximal joint torque production. Although there is an initial yield as the

perturbing force is applied, interjoint elastic coupling results in large distal joint torque generation as the proximal joint begins to yield, and subsequent motion of the distal joint is largely synchronous with the proximal joint (Figure 4.1b, lower panel). Maximal individual joint displacements do not follow a successive pattern and the coordination index is 1.2, in contrast with 3.0 for the JU/JS model and 3.5 for the ES model. Maximal endpoint displacement of 0.07 occurs at $\hat{t} = 1.1$, substantially before any single joint displacement maximum, and geometric recovery begins quickly after cessation of perturbation. Table 2.4 shows the time to maximum endpoint displacement and coordination index averaged over perturbation direction $\left(\overline{\hat{t}(d_{EP}^{\max})}, \overline{CI}\right)$. The average values follow the trends described for the response to a perturbation in the *x*-direction (ψ = 0º) with a 7% decrease in $\overline{\hat{t}(d_{EP}^{\max})}$ and 40% decrease in $\overline{CI}$ from ES to EU.

The global dynamic response of multi-link systems can be quantified with damping ratio (Table 2.4). The damping ratio of diagonal controller models vary widely including underdamped (JD: ξ = 0.59, ED: ξ = 0.67) and overdamped (JD: ξ = 2.08, ED: ξ = 3.33) modes. Symmetry allows for a more uniform response for ES for which all modes are underdamped (0.41, 0.57, 0.97). The analytical solution to the matrix algebraic Riccati equation dictates that the damping ratio of EU and JU/JS be 1/√2.

Table 2.4: Dynamic properties. Averaging is done across perturbation direction (ψ)

	JD	JU/JS	ED	ES	EA
$\overline{\hat{t}(d_{EP}^{\max})}$	3.08	3.01	1.83	1.25	1.16
$\overline{CI}$	2.59	2.61	1.65	2.90	1.75
ξ_i	0.59	0.71	0.67	0.41	0.71
	1.64	0.71	1.85	0.57	0.71
	2.08	0.71	3.33	0.97	0.71

Cost

Costs associated with endpoint impulse force perturbations are presented in Figure 2.3. The tradeoff in kinematic and energetic cost can be seen for the joint control model (Figure 2.3a-c). The maximum joint displacement averaged over perturbation direction ($\overline{d_J^{\max}}$) is 12% higher for the JU/JS controller model than the restricted JD (Figure 2.3a, Table 2.5), while the average energetic cost ($\overline{C_e}$) is 15% lower for JU/JS than JD (Figure 2.3a, Table 2.5). This means that the symmetric interjoint coupling through the viscosity matrix for JU/JS serves to coordinate joint motions so that the total energetic cost is minimized at the expense of slightly larger joint displacements ($\overline{d_J^{\max}}$) compared with JD. The average maximum endpoint displacement ($\overline{d_{EP}^{\max}}$) is 4% lower for JU/JS than JD.

The kinematic-kinetic tradeoff is also seen for the endpoint controllers (Figure 2.3d-f, Table 2.5). The addition of symmetric off-diagonal terms (ES) results in an 11% increase in $\overline{d_{EP}^{\max}}$, but a 28% decrease in $\overline{C_e}$ compared with ED. The addition of asymmetric interjoint coupling, however, results in a decrease in both kinematic ($\overline{d_{EP}^{\max}}$ decreased by 16% over ES) and kinetic ($\overline{C_e}$ decreased by 21% over ES) quantities. The improvements in endpoint control are achieved by exaggerated joint displacement; $\overline{d_J^{\max}}$ is 140% (ES) and 400% (EU) greater for the coupled controllers than ED.

Table 2.5: The average maximum displacements and energetic cost. Averaging is done across perturbation direction (ψ)

	JD	JU/JS	ED	ES	EU
$\overline{d_J^{\max}}$	0.034	0.039	0.019	0.046	0.096
$\overline{d_{EP}^{\max}}$	0.106	0.101	0.057	0.063	0.053
$\overline{C_e}$	0.026	0.022	0.055	0.040	0.031

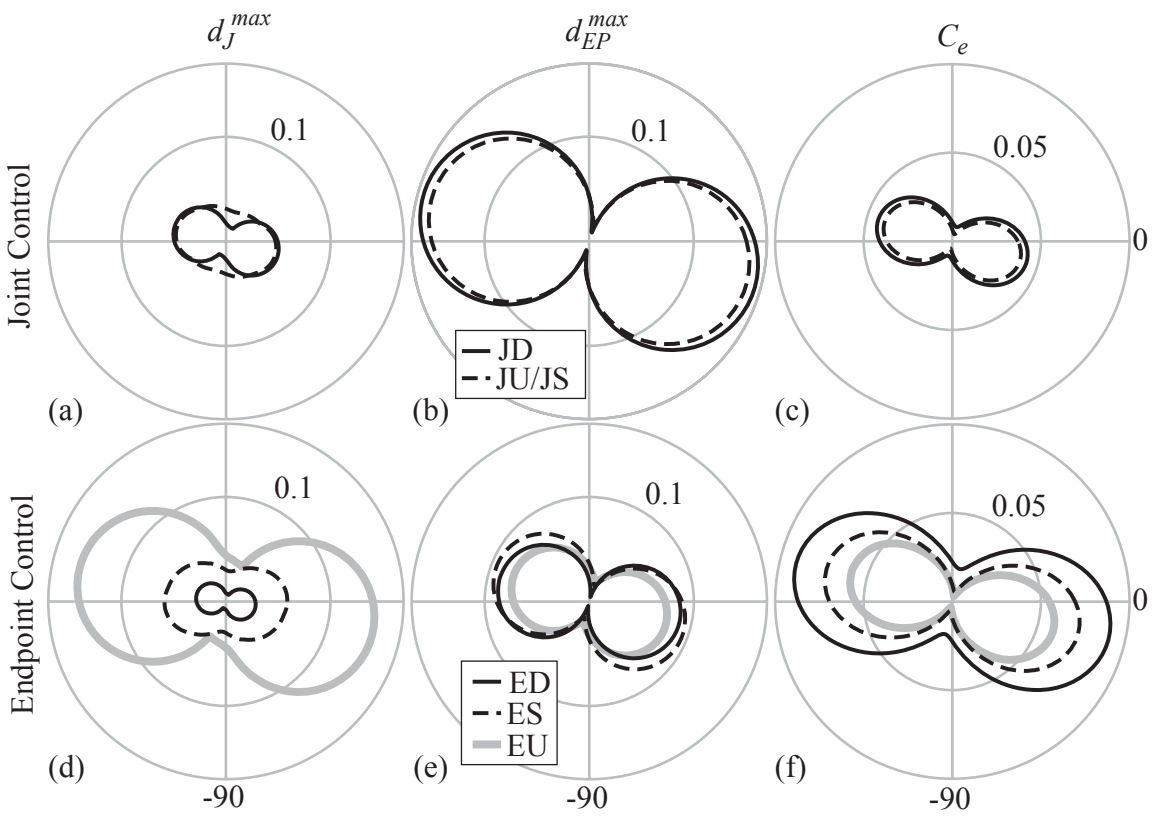

Figure 2.3: Measures of kinematic and kinetic performance. (A,D) The maximum joint displacement ($d_J^{\max}$) (Eq. 5), (B,E) maximum endpoint displacement ($d_{EP}^{\max}$) (Eq. 6), and (C,F) energetic cost (C_e) (Eq. 4) for the optimized models (JD, JU/JS, ED, ES, EU) for impulse perturbations of equal magnitude across perturbation direction (ψ).

The average displacement magnitudes ($\overline{d_J^{\max}}$, $\overline{d_{EP}^{\max}}$) for the two unconstrained optimal controllers (JU/JS and EU) reflect the tasks for which each was optimized. JU/JS has 60% lower $\overline{d_J^{\max}}$ than EU, while EU has 47% lower $\overline{d_{EP}^{\max}}$ than JU/JS.

The optimization was performed for an additional posture (θ_1 = -150°, θ_2 = 120°, θ_3 = -117°) based on the stance phase of locomotion of the tree shrew *Tuapaia glis* (Schilling 2005). The asymmetric structure of endpoint stiffness and viscosity was maintained for this posture ($Z_{mean\_\mathbf{R}}$ = 20.5%, $Z_{mean\_\mathbf{B}}$ = 9.9%), but the resulting kinematic and energetic cost improvement ($\overline{d_{EP}^{\max}}$ decreased by 5% from ES to EU; $\overline{C_e}$ decreased by 11% from ES to EU), and homogenization of endpoint stiffness (ES: s =

0.648, A = 2.16, EU: s = 0.684, A = 2.23), viscosity (ES: s = 0.560, A = 4.62, EU: s = 0.575, A = 5.54), and damping ratios (ES: 0.58, 0.64, 0.77; EU: 0.71) were smaller than seen in the extended posture, indicating that the benefits of asymmetry are limb configuration dependent.

Discussion

The goal of this project was to determine whether asymmetric interjoint feedback improved the performance of postural tasks as evaluated by energetic cost and maintenance of endpoint position. The optimal controller for maintaining endpoint position contained substantial asymmetry in the off-diagonal terms, supporting the hypothesis that this structure contributes to endpoint control, and in agreement with similar models (Barin 1989, He et al. 1991, Park et al. 2004). The results are coherent and testable with uncontrolled manifold (UCM) hypothesis (Scholz and Schoner 1999, Todorov and Jordan 2002): EU achieves much greater endpoint control than JU/JS, at the expense of variability in the state. For the cat-like posture, the asymmetry provided an improvement (40% $\overline{CI}$, 16% $\overline{d_{EP}^{\max}}$) in the recovery from perturbation and a reduction (21%) in energetic cost. These gains were more dramatic when the system was in an extended, cat-like posture than in a compressed, rodent-like posture. The energetic benefit is substantial and likely to contribute to the development of neural control strategies, at least in some areas of the workspace. The same analysis performed on a two degree of freedom model produced optimal asymmetric controllers (EU) that were only slightly better than the symmetric controllers (ES) for both an extended ($\overline{C_e}$: 5%, $\overline{d_{EP}^{\max}}$: 4%) and flexed ($\overline{C_e}$: 3%, $\overline{d_{EP}^{\max}}$: 2%) posture, suggesting that the improvement in control due to asymmetry is specific to kinematically redundant systems (unpublished observations).

The degree of asymmetry for the optimal endpoint controller is consistent with experimentally determined magnitudes. Mussa-Ivaldi and coworkers (Mussa-Ivaldi et al. 1985) measured elastic $Z_{mean\_\mathbf{R}}$ values for human arm ranging from 0.4% to 20.9% with a mean of 6.5% across four subjects and five arm configurations, which is similar to the EU controller $Z_{mean\_\mathbf{R}}$ of 11.5% in the feline posture and $Z_{mean\_\mathbf{R}}$ of 20.5% in the shrew-like posture.

Interjoint coupling provides substantial improvement in endpoint control, and both symmetric and asymmetric multi-joint control strategies result in greater homogeneity of endpoint properties and dynamic response. The endpoint stiffness ellipse eccentricities of the ES and EU controllers are reduced by 6.4 and 7.7 fold, respectively, over the ED controller. Viscosity endpoint ellipses are reduced 4.1 (ES) and 7.8 (EU) fold. Lower eccentricity means greater similarity in response across perturbations. The dynamic response characteristics also become more uniform with the addition of asymmetric terms for the endpoint model. Damping ratios are all $1/\sqrt{2}$ for EU and vary from 0.41 to 0.97 for ES as opposed to ED where damping ratios vary from 0.67 to 3.33.

The homogeneity of damping ratio permitted by asymmetric feedback has a dramatic effect on the coordination of the limb. For ES, maximal joint displacements follow a successive pattern, with an average coordination index of 2.9 while maximal joint displacements follow a more coordinated pattern for EU model for the same perturbation, with a $\overline{CI}$ of 1.8 (Table 2.4). The time course of middle joint displacement varies little between the ES and EU models, and the principal effect of the asymmetry is to impose the kinematics of the proximal joint response on the distal joint.

Two postural tasks were specified to examine two potential mechanisms the central nervous system (CNS) uses to accomplish a stable endpoint posture. The joint control task seeks to minimize the deviation of each specific joint. The optimal controller for this task predicts a myotatic unit-like stiffness component, with no off-diagonal terms, and all interjoint coupling achieved by viscosity. Physiologically, the static response is

dominated by individual joint or muscle displacements, encoded in the Group I & II spindle response (Matthews and Stein 1969). The dynamic response, including all of the predicted interjoint coupling, is strongly influenced by velocity, which is encoded in the Group I spindle afferent (Matthews 1963). The appearance of interjoint coupling only within the viscosity matrix generates torques at remote joints that counteract inertial coupling. This coupling could not be provided by biarticular muscles since they would contribute to both joint viscosity and joint stiffness. This controller, however, presents relatively poor endpoint performance characteristics because of the lack of an internal model. The displacement of the endpoint in response to a perturbation is highly dependent on perturbation orientation. The system presents excellent resistance along the limb axis, which would provide sound weight support, but poorly resists perpendicular perturbations, and would require a stronger and faster response from higher centers to correct for any non-vertical perturbation. The response of the system to perturbation is also uncoordinated. Individual joints return to their initial configuration as quickly as possible, which would result in lower inertia segments responding extremely rapidly and a system that responds with time characteristic of the largest assembly. In a biological system, in which the distal segments are systematically lighter than proximal segments, the joint control model would predict nearly rigid distal joints and a system response dominated by the hip or shoulder.

The endpoint control task seeks to minimize the deviation of the endpoint from a specified position, regardless of the joint angles necessary to produce that endpoint position. In the endpoint control model, $\mathbf{Q_E}$ contains an internal model of the Jacobian, and the optimal $\mathbf{k_R}$ depends directly on posture through the Jacobian, and optimal $\mathbf{k_B}$ depends on posture through both $\mathbf{k_R}$ and $\mathbf{M}$. The shrew-like posture is a more flexed posture and while the degree of asymmetry is increased, the benefits of that asymmetry decrease, indicating that the quantitative benefits of asymmetry are posture dependent. In either of the test postures, the highly extended feline posture or the much more compact

shrew posture, the mean energetic cost of recovering from an impulse perturbation was smaller for the EU than ES (11% shrew-like, 21% cat-like).

Regardless of posture, the optimal controller was asymmetric in the sense that displacement of the proximal joint resulted in powerful torque production at the distal joint, while displacement of the distal joint induced relatively small torques at the proximal joint. The existence or strength of reflex feedback between hip and ankle muscles in cats is largely unknown, due to the technical difficulties of working with hip muscles (Loeb and Duysens 1979). Stretch of the hip flexor iliopsoas, representative of a negative θ_1 perturbation, has been reported to reduce ankle extensor activity during gait (Hiebert et al. 1996), equivalent to a positive torque at the distal joint as predicted by the optimal controller. Group I feedback from vasti to soleus, which would contribute to $\mathbf{k_B}(3,2)$, has been measured (Eccles et al. 1957), although feedback from vasti to gastrocnemius (contributing to both $\mathbf{k_{R,B}}(3,2)$ and $\mathbf{k_{R,B}}(2,2)$) is inhibitory (Wilmink and Nichols 2003). Length changes in soleus have little or no effect on vastus force generation ($\mathbf{k_{R,B}}(2,3)$, (Wilmink and Nichols 2003), which suggests that, in the cat, $\mathbf{k_R}(3,2)$ would be greater than $\mathbf{k_R}(2,3)$, as predicted by the optimal control model. EU also contains a strongly asymmetric relationship between proximal and distal joints. For small proximal joint motion the distal joint remains relatively compliant, suitable for rejection of small endpoint perturbations. For large proximal joint motion the asymmetry contributes to greater impedance at the distal joint. This strategy is consistent with an observed role for the ankle in relationship to the hip in human pedaling (Fregly and Zajac 1996).

The measure of energetic cost used in this analysis is the integrated, squared torque produced during the recovery from perturbation. This differs from work done or absorbed, and it does not account for co-contraction nor energetic savings associated with biarticular muscles. As a biological cost function, it also neglects the higher muscle mass available to the proximal joints, although this may be compensated by structuring the

model with uniform segmental inertias, where the moment of inertia of distal segments is generally lower than proximal segments. A cat foot, for example, is roughly 12% of the mass of the thigh. The model also departs from biological systems by not considering delays associated with reflex feedback, but these simplifications are not expected to alter the fundamental asymmetric structure of the feedback gains.

To determine whether predicted magnitudes of joint stiffness and viscosity are of appropriate physiological magnitude, $\mathbf{k_R}$ and $\mathbf{k_B}$ of EU were redimensionalized for average cat (m = 84 g, L = 9.5 cm) and tree shrew (m = 4 g, L = 3 cm) limb dimensions for comparison to measured values. The scaling parameter, σ, was chosen for the cat (σ = 4.0 N) so that the limb restores equilibrium on the same order as that measured experimentally (~400 ms) (Macpherson 1988). Since no data is available for the postural response of a shrew, σ is approximately scaled with muscle force (P_0), σ_{SHREW} = 0.4 N. Dimensional values of $\mathbf{k_B}/\mathbf{k_R}$ range from 0.05 to 0.21 s for the cat, and from 0.02 to 0.05 s for the shrew. The viscosity of mammalian muscle increases with animal size,and the prediction that shrew $\mathbf{k_B}/\mathbf{k_R}$ is 50-80% smaller than cat is consistent with this scaling. Intrinsic viscosity results from the force velocity relation, and varies from 0.1-2 $(P_0\ s)/L_0$, depending on fiber type and species (Close 1972). The apparent intrinsic stiffness of muscle depends strongly on the length range being considered. The range most relevant to postural perturbations is likely the short range stiffness, resulting from crossbridge elasticity, of 20-100 P_0/L_0. (Huxley and Simmons 1971), yielding viscosity to stiffness ratio in the range of 0.001-0.1 s, which is consistent with the model prediction. Over longer length ranges, stiffness described by the isometric length tension relationship is approximately 0.4 P_0/L_0. This suggests viscosity to stiffness ratios in the range of 0.25-5 s, which is only slightly higher than the model prediction.

It is worth while to consider the implications of scaling an optimal solution with effort, σ. As pointed out by Kuo (Kuo 1995), σ has various interpretations, including a measure of the relative cost of kinematic penalty, the speed of system response, and the

gain of intrinsic and reflexive impedance properties. The structure of optimal $\mathbf{k_R}$ and $\mathbf{k_B}$ matrices are constant for the given parameters. However, to obtain dimensional stiffness and viscosity $\mathbf{k_R}$ is proportional to σ and $\mathbf{k_B}$ is proportional to $\sqrt{\sigma}$. Thus, the dimensional endpoint ellipses would have the same shape and orientation with the size scaling with σ for stiffness and $\sqrt{\sigma}$ for viscosity. The scaling also maintains a constant damping ratio across σ. These traits are consistent with observed characteristics of human arms. Mussa-Ivaldi and coworkers (Mussa-Ivaldi et al. 1985) found that adaptive changes in postural stiffness in response to a force in a single direction were accomplished by varying the size rather than the shape or orientation of the ellipses. This is consistent with the idea that the "optimal" solution has the same shape and orientation but different magnitude for varying levels of effort. Perrault and coworkers (Perreault et al. 2004) found that endpoint arm elasticity increased linearly with voluntary force generation while viscosity increased nonlinearly, consistent with σ scaling. In addition, they found that relative scaling of stiffness and viscosity resulted in two underdamped modes that are consistent across all subjects and conditions tested. The consistency of damping ratios across subjects and effort level is also in agreement with σ scaling.

Since the magnitude of the optimal controllers scale not only with the physical size of the model (mass and length) but with a voluntary force or effort, both intrinsic and reflex properties of the limb must also scale with effort. The force of a reflex can vary even with a constant stimulus. Descending neurons from higher centers make synaptic connections at the alpha motor neurons, interneurons and presynaptic terminals of the afferent fibers, changing the tonic activity of the cell to modulate the sensitivity of reflex response. Alpha-gamma coactivation may be responsible for coordinated increases of intrinsic and reflexive components of muscle impedance; in general gamma motor neurons are set at higher levels as the speed of movement increases (Hulliger et al. 1989). Prochazka and coworkers (Prochazka 1989) describe significant changes in

monosynaptic reflex pathways (tendon and H-reflex) in anticipation of co-activation, so that the reflex and intrinsic magnitudes may scale together.

Acknowledgement

This work was supported by NIH grant HD46922 to LHT.

Appendix

Using LQR theory to determine optimal stiffness and viscosity matrices results in an optimal viscosity matrix that is $1/\sqrt{2}$ times the critical damping matrix. This appendix contains the derivation of this result from the matrix algebraic Riccati equation (7) and the optimal state feedback matrix Eq. (8). Matrices **R**, **Q**, **M** and **S** are symmetric. Applying Eq. (8) to Eq. (7) yields

$$\mathbf{0} = \mathbf{A}^T\mathbf{S} + \mathbf{S}\mathbf{A} + \mathbf{Q} - \mathbf{S}^T\mathbf{B}\left(\mathbf{R}^{-T}\mathbf{R}\right)\mathbf{R}^{-1}\mathbf{B}^T\mathbf{S} = \mathbf{A}^T\mathbf{S} + \mathbf{S}\mathbf{A} + \mathbf{Q} - \mathbf{k}^T\mathbf{R}\mathbf{k}\,.$$

Matrix **S** is symmetric and divided into components,

$$\mathbf{S} = \begin{bmatrix} \mathbf{S_A} & \mathbf{S_B} \\ \mathbf{S_B} & \mathbf{S_C} \end{bmatrix}.$$

Substituting the definitions of **S**, as well as **A**, **k**, and **Q**, Eqs. (3-5),

$$\mathbf{0} = \begin{bmatrix} \mathbf{0} & \mathbf{0} \\ \mathbf{I} & \mathbf{0} \end{bmatrix}\begin{bmatrix} \mathbf{S_A} & \mathbf{S_B} \\ \mathbf{S_B} & \mathbf{S_C} \end{bmatrix} + \begin{bmatrix} \mathbf{S_A} & \mathbf{S_B} \\ \mathbf{S_B} & \mathbf{S_C} \end{bmatrix}\begin{bmatrix} \mathbf{0} & \mathbf{I} \\ \mathbf{0} & \mathbf{0} \end{bmatrix} + \begin{bmatrix} \mathbf{Q}_1 & \mathbf{0} \\ \mathbf{0} & \mathbf{0} \end{bmatrix} - \begin{bmatrix} \mathbf{k}_\mathbf{R}^T \\ \mathbf{k}_\mathbf{B}^T \end{bmatrix}\mathbf{R}\begin{bmatrix} \mathbf{k_R} & \mathbf{k_B} \end{bmatrix},$$

and simplifying, yields

$$\begin{bmatrix} \mathbf{k}_\mathbf{R}^T\mathbf{R}\mathbf{k_R} & \mathbf{k}_\mathbf{R}^T\mathbf{R}\mathbf{k_B} \\ \mathbf{k}_\mathbf{B}^T\mathbf{R}\mathbf{k_R} & \mathbf{k}_\mathbf{B}^T\mathbf{R}\mathbf{k_B} \end{bmatrix} = \begin{bmatrix} \mathbf{Q}_1 & \mathbf{S_A} \\ \mathbf{S_A} & 2\mathbf{S_B} \end{bmatrix}. \tag{9}$$

Equation (8) can be written as

$$\begin{bmatrix} \mathbf{k_R} & \mathbf{k_B} \end{bmatrix} = \begin{bmatrix} \mathbf{R}^{-1}\mathbf{M}^{-1}\mathbf{S_B} & \mathbf{R}^{-1}\mathbf{M}^{-1}\mathbf{S_C} \end{bmatrix}, \tag{10}$$

Solving the left hand side of the matrix equality in Eq. (10) for $\mathbf{S_B}$ and applying to the lower left hand matrix equality of Eq. (9),

$$\mathbf{k}_\mathbf{B}^T\mathbf{R}\mathbf{k_B} = 2\mathbf{M}\mathbf{R}\mathbf{k_R}\,, \tag{10}$$

Pre-multiplying both sides by $\mathbf{k}_\mathbf{B}^T\mathbf{M}^{-1}$ and simplifying

$$\mathbf{k}_\mathbf{B}^T\mathbf{M}^{-1}\mathbf{k}_\mathbf{B}^T\mathbf{R}\mathbf{k}_\mathbf{B} = 2\mathbf{k}_\mathbf{B}^T\mathbf{R}\mathbf{k}_\mathbf{R}. \tag{11}$$

Which is symmetric, by the relationships in Eq. (9). Taking the transpose of the left side

$$\mathbf{k}_\mathbf{B}^T\mathbf{R}\mathbf{k}_\mathbf{B}\mathbf{M}^{-1}\mathbf{k}_\mathbf{B} = 2\mathbf{k}_\mathbf{B}^T\mathbf{R}\mathbf{k}_\mathbf{R}. \tag{12}$$

Pre-multiplying both sides of Eq. (12) by $\mathbf{R}^{-1}\mathbf{k}_\mathbf{B}^{-T}$

$$\mathbf{k}_\mathbf{B}\mathbf{M}^{-1}\mathbf{k}_\mathbf{B} = 2\mathbf{k}_\mathbf{R}. \tag{13}$$

Pre- and post-multiply Eq. (13) by the unique positive definite square root ($\mathbf{M}^{-1/2}$) of positive definite matrix $\mathbf{M}^{-1}$,

$$\mathbf{M}^{-1/2}\mathbf{k}_\mathbf{B}\left(\mathbf{M}^{-1/2}\mathbf{M}^{-1/2}\right)\mathbf{k}_\mathbf{B}\mathbf{M}^{-1/2} = 2\mathbf{M}^{-1/2}\mathbf{k}_\mathbf{R}\mathbf{M}^{-1/2}. \tag{14}$$

If $\mathbf{k}_\mathbf{R}$ and $\mathbf{k}_\mathbf{B}$ are positive definite, then

$$\mathbf{M}^{-1/2}\mathbf{k}_\mathbf{B}\mathbf{M}^{-1/2} = \sqrt{2}\left(\mathbf{M}^{-1/2}\mathbf{k}_\mathbf{R}\mathbf{M}^{-1/2}\right)^{1/2}. \tag{15}$$

Solve for $\mathbf{k}_\mathbf{B}$.

$$\mathbf{k}_\mathbf{B} = \sqrt{2}\mathbf{M}^{1/2}\left(\mathbf{M}^{-1/2}\mathbf{k}_\mathbf{R}\mathbf{M}^{-1/2}\right)^{1/2}\mathbf{M}^{1/2} = \frac{1}{\sqrt{2}}\mathbf{k}_{\mathbf{B}cr}$$

CHAPTER 3

REDUCTION OF NEUROMUSCULAR REDUNDANCY FOR POSTURAL FORCE GENERATION USING AN INTRINSIC STABILITY CRITERION

Introduction

Maintaining standing balance is an important motor function where the overall task is to stabilize the body center of mass (CoM) by generating the appropriate forces in each limb. However, each limb has multiple muscles acting at many joints – more degrees of freedom than the joint torques specified by the task – suggesting a wide range of muscular coordination strategies is possible (Bernstein 1967), even within a single limb.

The stability of the limb configuration is part of the postural task that could resolve this neuromuscular redundancy. Muscle activity in response to a perturbation occurs after 50 ms in a cat, and electromechanical delays of the musculoskeletal system add another 50 ms delay before stabilizing forces are produced (Horak and Macpherson 1996). A feedforward neural strategy of choosing an intrinsically stabilizing muscle activation pattern would potentially reduce the necessity for active neural feedback as well as decrease the number of candidate muscle activation patterns for performing the postural task.

Several mechanisms in the musculoskeletal system can provide instantaneous mechanical stability as a function of muscle activation patterns. The length-tension (Gordon et al. 1966, Rack and Westbury 1974), and force-velocity (Gasser and Hill 1924) relationships of muscle are inherently stabilizing and depend monotonically on muscle activation; stronger activation results in greater viscoelasticity (Rack and Westbury 1969). Muscle moment arms also change with joint motion, altering the net torque

produced at a joint, and can contribute to either joint stability or instability (Young et al. 1992). Although these intrinsic musculoskeletal properties provide instantaneous feedback in response to perturbations, it has not been established whether they are sufficient to stabilize limb posture in a variety of animals and tasks (Edwards 2007, Morasso and Sanguineti 2002, Morasso and Schieppati 1999, Richardson et al. 2005, Winter et al. 1998, Winter et al. 2001).

In this study, we hypothesized that the muscular redundancy in postural control is reduced when muscle activation patterns are chosen with respect to both intrinsic musculoskeletal stability and endpoint force production. We evaluated our hypothesis using Lyapunov stability theory applied to the linearized mathematical model of the feline hindlimb (Burkholder and Nichols 2004) activated with a large set of muscle activation patterns that produced identical endpoint forces. We found that a reduced set of stabilizing muscle activation patterns exists, but that the relationship between individual muscle characteristics and whole-limb stability is not straightforward.

Methods

Methods Overview

We used a computational model to analyze the relationship of whole-limb mechanical stability of the cat hindlimb to individual muscle properties. The model is three-dimensional, has physiologically relevant degrees of freedom, and experimentally determined muscle properties (Burkholder and Nichols 2000, Burkholder and Nichols 2004, Roy et al. 1997, Sacks and Roy 1982). We generated a set of muscle activation patterns that produced the identical postural endpoint force and examined the model response to small disturbances to the limb for each muscle activation pattern. Using linear system-analysis tools (Alexandrov et al. 2005, Szidarovszky and Bahill 1992), we quantified the patterns of limb motion (limb modes) in response to disturbances, and the rate (eigenvalues) at which the whole-limb configuration returned to or moved away from

the initial position. To determine individual muscle contributions to whole limb stability we compared the local (joint-level) stiffness of muscles to the stability of the limb modes. Finally, we constructed muscle activation patterns based on the local stiffness of muscles and compared the whole-limb stability of these patterns to the randomly generated patterns.

Musculoskeletal Model

The model had three degrees of freedom at the hip, and two each at the knee and ankle (Burkholder and Nichols 2004, McKay et al. 2007, van Antwerp et al. 2007). The pelvis was fixed and the foot was connected to the ground through a pin joint at the metatarsophalangeal joint (MTP) leaving 4 degrees of freedom. The equations of motion for the model were expressed in the generalized coordinate system, $\vec{\theta} = [\theta_{HF}, \theta_{HA}, \theta_{HR}, \theta_{KE}, \theta_{KA}, \theta_{AE}, \theta_{AA}]^T$, where the subscripts denote the positive direction of joint movement: hip flexion (HF), hip adduction (HA), hip external rotation (HR), knee extension (KE), knee adduction (KA), ankle extension (AE), and ankle adduction (AA). Limb motion was described by the equations of motion:

$$\ddot{\vec{\theta}} = \mathbf{M}^{-1}\left[-\vec{V}(\vec{\theta},\dot{\vec{\theta}}) - \vec{G}(\vec{\theta}) + \mathbf{R}(\vec{\theta})\mathbf{F_{MAX}}(\vec{\theta},\dot{\vec{\theta}})\vec{\varepsilon} - \mathbf{J}(\vec{\theta})^T \vec{F}_{MTP}(\vec{\theta},\dot{\vec{\theta}})\right], \qquad (1)$$

where **M** is the inertia matrix, $\vec{V}$ is the vector of centrifugal and Coriolis torques, $\vec{G}$ is the vector of gravitational torques, **R** is the moment arm matrix, $\mathbf{F_{MAX}}$ is a diagonal matrix whose components are the maximum individual muscle forces corrected for pennation angle, $\vec{\varepsilon}$ is the vector of muscle activation levels ($\vec{0} \le \vec{\varepsilon} \le \vec{1}$), $\mathbf{J}^T$ is the transpose Jacobian mapping of external force at the MTP to joint torques, $\vec{F}_{MTP}$ is the resultant force at the MTP which is calculated using the constraint that translational acceleration of the MTP be zero. 31 muscles were modeled using an adaptation of the Hill muscle model (Zajac 1989) using architectural parameters taken from the literature (Roy et al. 1997, Sacks and Roy 1982). The stiffness of each muscle was set to 3

F_{MAX}/L^0_F where F_{MAX} is the maximal force of the muscle and L^0_F is optimal fiber length. This value is near maximal stiffness described by the length-tension curve (Gordon et al. 1966) and the analysis was repeated for varying levels of stiffness.

Selection of Muscle Activation Patterns

Postural muscle activation patterns ($\vec{\varepsilon}$) were chosen to produce the endpoint force vector measured experimentally in standing cats, $\vec{F}^0_{MTP}$, when the model was placed in an initial posture matched to kinematic data (Torres-Oviedo et al. 2006):

$$\mathbf{RF_{MAX}}\vec{\varepsilon} = \vec{G} + \mathbf{J}^T\vec{F}^0_{MTP} \tag{4}$$

Equation (4) is redundant and has a 24 dimensional solution space (null space). To span the $\vec{\varepsilon}$ solution space, activation sets were chosen by projecting a random activation vector, $\vec{0} \le \vec{\varepsilon}_0 \le \vec{1}$ into the solution space using the quadratic cost function,

$$c = (\vec{\varepsilon} - \vec{\varepsilon}_0)^T(\vec{\varepsilon} - \vec{\varepsilon}_0) \tag{5}$$

and constraints,

$$\mathbf{RF_{MAX}}(\vec{\varepsilon} - \vec{\varepsilon}_0) = \vec{G} + \mathbf{J}^T\vec{F}^0_{MTP} - \mathbf{RF_{MAX}}\vec{\varepsilon}_0 \tag{6}$$

$$\vec{0} - \vec{\varepsilon}_0 \le (\vec{\varepsilon} - \vec{\varepsilon}_0) \le \vec{1} - \vec{\varepsilon}_0 \tag{7}$$

The optimization yields an activation set $\vec{\varepsilon}$ which produces the desired endpoint force, has all muscle activations between 0 and 1, and minimizes the distance to $\vec{\varepsilon}_0$. The test population consisted of 10,000 activation sets, which was large enough for the mean and covariance of activation level of 23 of the 31 modeled muscles to converge (Valero-Cuevas et al. 2003). Five of eight nonconvergent muscles had knee-flexor moment arms, and thus were not expected to be highly active in standing. Increasing the sample size 12-fold resulted in convergence of only 3 additional muscles, and orders of magnitude more samples were required for the remaining muscles to converge.

Whole-Limb Stability of Muscle Activation Patterns

To determine whether a given muscle activation pattern $\vec{\varepsilon}$ produced a stable limb configuration, equation 1 was linearized by Taylor-series expansion about the initial posture at rest, and Lyapunov stability theory was applied to resulting linear, time-invariant state matrix. If all of the eigenvalues of the state matrix are negative, then the system is asymptotically stable such the limb will always return to the equilibrium posture under small perturbations (Szidarovszky and Bahill 1992). The derivation of the dynamic equations of motion including the muscle model equations, and the linearization were performed using custom Matlab (Mathworks, Inc. Natick, MA) routines (www.neuromechanic.com).

For each muscle activation pattern, the eigenvectors of the state matrix (limb modes), represent coordinated movements of joints and define a basis spanning all possible limb motion for the linearized system (Alexandrov et al. 2005). To compare across muscle activation patterns, the limb modes were grouped by hierarchical cluster analysis. Distance between eigenvectors was computed using the Euclidean distance between vectors and the cluster hierarchy was created using Ward's linkages (Ramsay and Silverman 2005). The number of clusters was determined by the greatest average link height with inconsistent with lower linkages. In order to have a physically interpretable metric of stability, the real component of the eigenvalue was converted to the perturbation halving time:

$$t_{50} \equiv \frac{\ln(0.5)}{\mathrm{Re}(\lambda)}, \tag{7}$$

where λ is the eigenvalue corresponding to the limb mode. A restatement of the Lyapunov criteria for asymptotic stability is that a given muscle activation pattern $\vec{\varepsilon}$ produces a stable limb configuration if t_{50} for all limb modes is positive. Negative values of t_{50} ($\lambda > 0$) represent the perturbation doubling time in an unstable limb.

To determine whether a limb stability criterion could reduce the redundancy of muscle activation patterns, we compared the total muscle activation set to the subset of stable muscle activation patterns. We compared the range of activation for each muscle and the number of principal components required to account for 95% of the variability in each set.

Stability Contribution of Individual Muscles

To determine whether specific muscles were associated with whole-limb stability, we calculated correlation coefficients between limb mode eigenvalues and muscle activation levels. We used a threshold of $|r| > 0.4$ to determine substantial correlation for 31 degrees of freedom (all $p<10^{-35}$).

We also determined whether individual muscle contributions to joint stiffnesses were predictive of whole-limb stability across the set of muscle activation patterns. Each muscle crosses more than one degree of freedom (e.g. knee flexion/extension and knee ab/adduction) and therefore contributes to multiple joint stiffnesses when activated. Because the stiffness of the muscle across the joints are not independent, we quantified the contributions of each muscle to the joint stiffness by computing the eigenvalues of the stiffness matrix for each muscle (e.g. the Jacobian of muscle torque with respect to all of the degrees of freedom crossed by that muscle). As a metric of stability, we defined the terms *maximum local positive stiffness* (κ_i^+), *maximum local negative stiffness* (κ_i^-), and *mean local* ($\bar{\kappa}_i$) *stiffness* for each muscle such that:

$$\kappa_i^+ = \max\left[eig\left(\frac{\partial\left(\vec{R}_i F_{M,i}\right)}{\partial\theta} \right) > 0 \right]$$

$$\kappa_i^- = \min\left[eig\left(\frac{\partial\left(\vec{R}_i F_{M,i}\right)}{\partial\theta} \right) < 0 \right],$$

$$\bar{\kappa}_i = mean\left[eig\left(\frac{\partial\left(\vec{R}_i F_{M,i}\right)}{\partial\theta} \right) \right].$$

Prediction of Stable Muscle Activation Patterns

To determine whether local muscle stiffness could be used to restrict the set of muscle activation patterns for standing posture, we replaced the cost function (5), with one weighted by each muscle's mean local stiffness ($\bar{\kappa}_i$):

$$c = (1-\mu)(\vec{\varepsilon} - \vec{\varepsilon}_0)^T(\vec{\varepsilon} - \vec{\varepsilon}_0) - \mu\bar{\bar{\kappa}}_i^T(\vec{\varepsilon} - \vec{\varepsilon}_0) \quad (8)$$

We then evaluated whole-limb stability of muscle activation patterns generated as a function of μ. A value of $\mu = 1$ resulted in a single unique activation set regardless of the random activation guess $\vec{\varepsilon}_0$.

Finally, to verify the robustness of results to a weight-bearing configuration, the entire analyses were recomputed with the fixed pelvis constraint relaxed to allow a single translational degree of freedom in the vertical direction. To satisfy equilibrium, the weight of the pelvis was set to a value of about ¼ the weight of a cat, such that the combined weight of the pelvis and limb was equal to the vertical component of the ground reaction force.

Results

Mechanical Modes

Whole-limb motion was characterized by four limb-mode clusters (graphical representations in Figure 3.1). The first mode can be approximately described as ankle motion in the sagittal plane (AS) (Figure 3.1A). The remaining three modes can be described primarily as frontal plane motion of the ankle (AF), hip (HF), and knee (KF) (Figure 3.1B-D). Limb modes with t_{50} faster than 7 msec were not examined, as they were all unconditionally stable, and faster than physiological timescales relevant to

postural control. The included angle between the means of the four clusters ranged from a maximum of 102º between AS and AF to a minimum of 69º between AS and HF with an average inter-cluster distance of 88º and an average intra-cluster distance of 13º.

Stability of All Muscle Activation Patterns

Only 35% of the muscle activation patterns were stable in all limb modes (Table 3.1). Two modes (KF and HF, Figure 3.2) were stable for greater than 99.5% of muscle activation patterns (Table 3.1). The remaining two were stable for 88% (AF) and 37% (AS) of activation patterns, respectively (Figure 3.2, Table 3.1). KF was the fastest mode with $|t_{50}|$ between 7-36 ms, while all other modes were slower than 62 ms (Table 3.1).

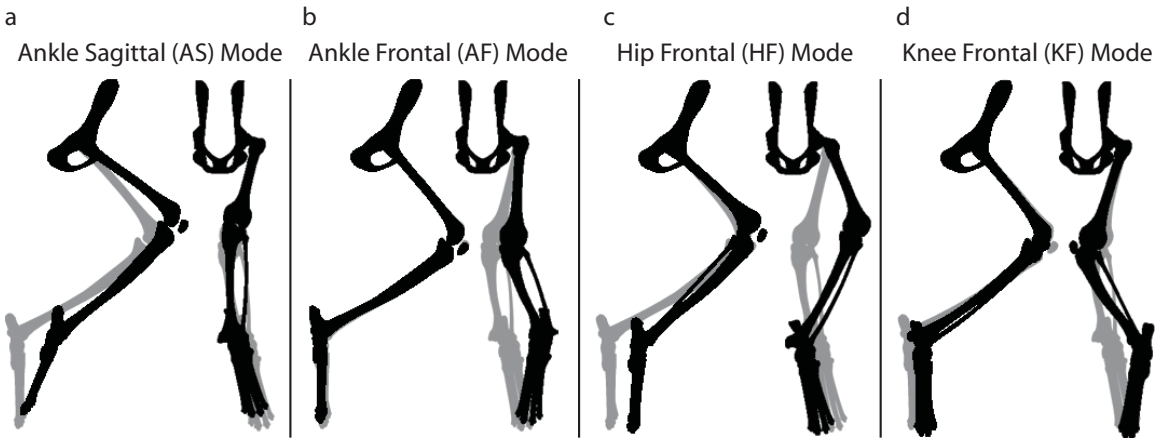

Figure 3.1: Mechanical modes of the limb. Four limb modes characterized the whole-limb motion following perturbations. A) The ankle sagittal (AS) mode is dominated by flexion and extension of the ankle, but includes motion at all joints. B,C,D) The remaining three modes are dominated by motions in the frontal plane. The gray limb represents the nominal limb posture. The black limb represents the limb displacement associated with each of the four modes describing limb motion. Note that this appears to displace the toe from its endpoint constraint in some cases because the eigenvectors are scaled for illustrative purposes. The modes are a feature of the linearized model and are valid only for small angle displacements.

Table 3.1: Stability characterization of each limb mode

	AS	AF	HF	KF	ALL
% stable	37	88	99.5	100	35
t_{50} (sec) stable modes	0.224 – 68	0.125 – 60	0.228 – 45	.007–.036	
t_{50} (sec) unstable modes	0.062 – 67	0.065 – 67	0.088 - 35		
Mean t_{50} (sec) stable	0.683	0.270	0.387	0.020	
Mean t_{50} (sec) unstable	-0.305	-0.436	-0.359		

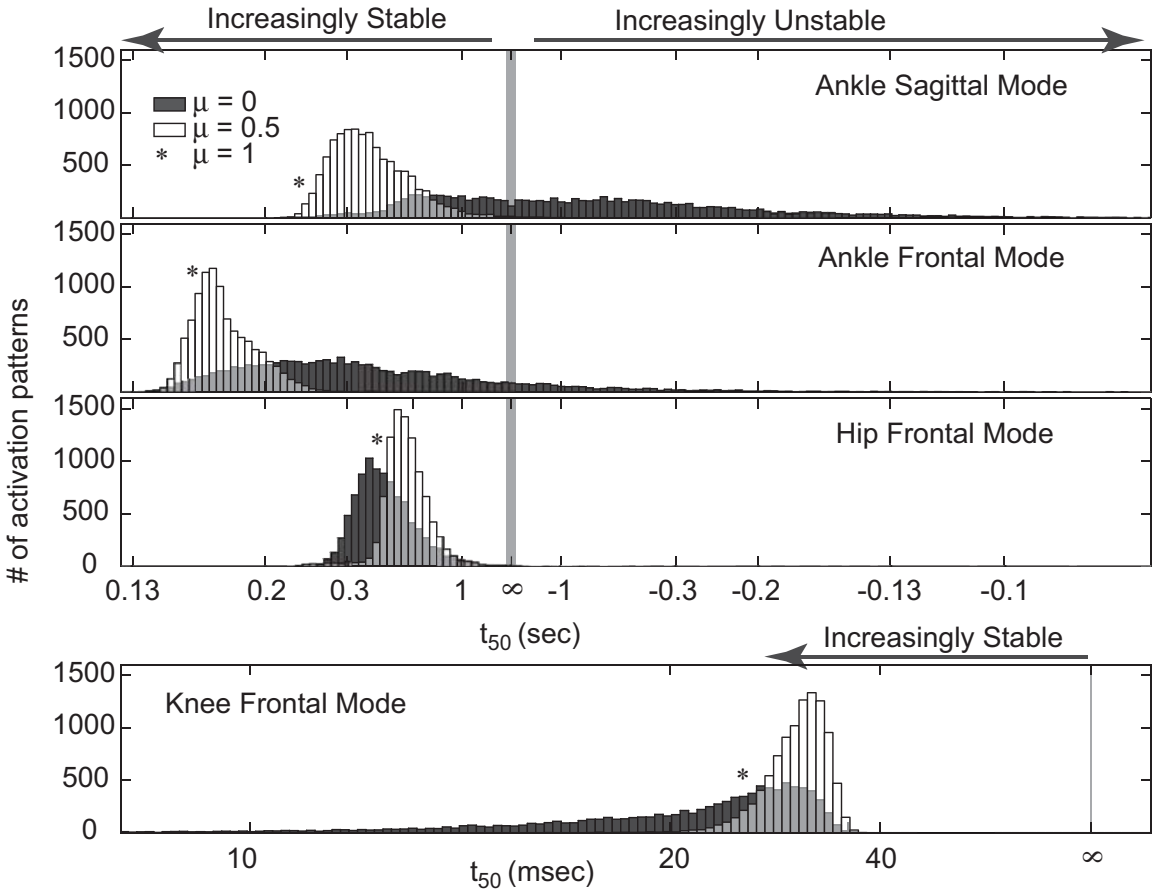

Figure 3.2: Histogram of limb stability for each mode across all muscle activation patterns. Histograms show the number of activation sets for each binned eigenvalue range for each limb mode. Limb modes with positive finite t_{50} (eigenvalues less than 0) are stable and limb modes with negative finite t_{50} (eigenvalues greater than 0) are unstable. The gray band centered at neutral stability ($t_{50} = \infty$) spans all limb modes with doubling time magnitude greater than 10 seconds. The dark gray histogram shows the distribution of stability of each mode for the set of random activation patterns ($\mu = 0$), for which A) The AS mode was stable for 37% of muscle activation patterns, B) the AF mode was stable for 88%, C) the HF was stable for 99.5%, and D) the KF mode was stable for 100% of muscle activation patterns. The white histogram shows the distribution of the stability of the limb when the selection of muscle activation patterns was biased toward locally stiff muscles ($\mu = 0.5$). The asterisk represents the t_{50} value for the unique muscle activation pattern that maximized the activation of locally stiff muscles ($\mu = 1$). 35% of the patterns resulted in a limb with negative eigenvalues (stable) in all modes.

Stability Contribution of Individual Muscles

The range of activation levels within each muscle were similar in the stable and unstable sets, with only a 4% average decrease in the range of muscle activation levels between the two sets; only Gluteus Medius (GMED) decreased in range of activation by more than 10%. Fifteen principal components were required to account for 95% of the variability in both stable and total sets.

Few correlations were found between individual muscle activation levels and limb mode stability (Figure 3.3a). HF and KF stability were most strongly correlated with inactivation of Biceps Femoris, posterior compartment (BFP) and Rectus Femoris (RF) (r=0.52, and r=0.57, respectively for HF; r=0.83, and r=0.72, respectively for KF) (Figure 3.3a, 3rd and 4th column, asterisks). AF stability was most strongly correlated with activation of Tibialis Posterior (TP) and Peroneus Brevis (PB) (r=-0.45, and r=-0.68, respectively), and deactivation of Flexor Hallucis Longus (FHL, r=0.51) (Figure 3.3a, 1st column, asterisks). AS stability was most strongly correlated with activation of Medial Gastrocnemius (MG, r=-0.78), VL (r=-0.52), and EDL (r=-0.40), and deactivation of FHL (r=0.60) (Figure 3.3a, 2nd column, asterisks).

No consistent relationships between local stiffness of activated muscles and whole-limb stability were found (Figure 3.3a and 3b). Most muscles had stronger positive than negative local stiffness (i.e. the magnitude of κ_i^+ (Figure 3.3a, black bars) was greater than the magnitude of κ_i^- (Figure 3.3b, white bars)). In AS, stability was strongly correlated with MG, VL, and EDL activation, but only MG had greater than average local positive stiffness (Figure 3.3b). The activation of these four muscles was highly correlated because they are mutually advantageous when standing up against gravity (data not shown). KF stability was negatively correlated with activation of BFP, the muscle with the greatest positive local stiffness. Although BFP had the large maximum local stiffness, it also had substantial negative local stiffness values as well,

highlighting the difficulty of assigning responsibility of whole-limb stability to the characteristics of a particular muscle.

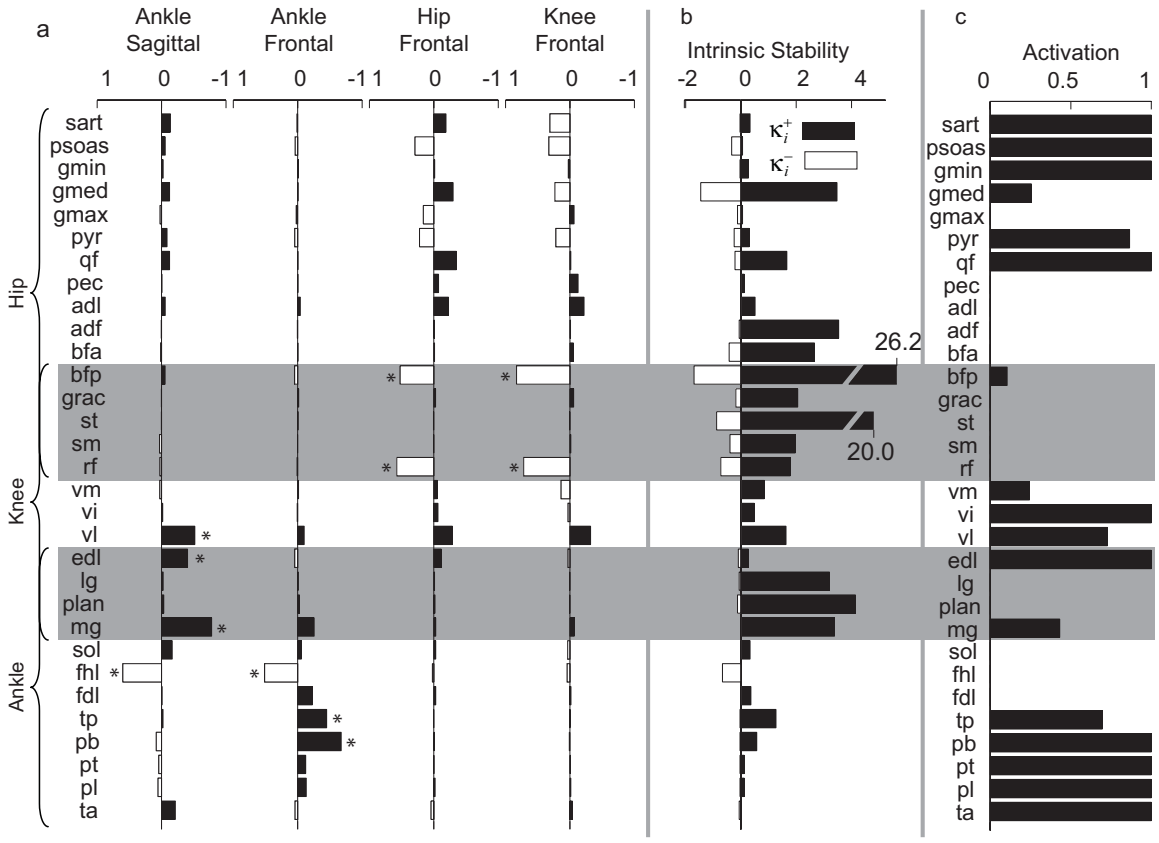

Figure 3.3: Relationship between overall limb stability, individual muscle activation levels, and joint-level stiffness of individual muscles. Gray bars indicate biarticular muscles. A) Correlation coefficients of individual muscle activation with eigenvalues of each mode. Negative correlation coefficients indicate that activation of the muscle correlates with increased modal stability (decreased eigenvalue). Muscles with statistically significant correlation coefficient magnitudes of greater than 0.4 are indicated by an asterisk (*). In general, hip and knee muscles are correlated with HF and KF stability and knee and ankle muscles are correlated with AS and AF stability. B) The maximum local positive (black bars, κ_i^+) and negative (white bars, κ_i^-) stiffness for each muscle. C) The muscle activation pattern generated when using a cost function maximizing activation of muscles with high local stiffness ($\mu = 1$, Eq. 8) results in a unique activation pattern with strong coactivation of hip and ankle uniarticular muscles.

Prediction of a Stable Set of Muscle Activation Patterns

An increasingly stable set of muscle activation patterns was found when muscles with large mean local stiffness were preferentially selected (*i.e.* weighting factor μ, Equation 8, was increased) (Figure 3.4a). For $\mu > 0.5$, all muscle activation patterns were

stable in all modes (Figure 3.2, Figure 3.4). The number of principal components decreased monotonically with μ (Figure 3.4a); a value of $\mu = 1$ resulted in a unique activation pattern (Figure 3.3c). This activation pattern was in the 99.96 percentile of stability in mode AS, and the 96, 59, and 42 percentile of stability in modes AF, HF, and KF, respectively (Figure 3.2, asterisks).

In contrast, as intrinsic stiffness of individual muscles was increased from the nominal value of 3 F_{MAX}/L^0_F, the number of stable muscle activation patterns increased monotonically, but the number of principal components to describe 95% of data variability remained at 15 (Figure 3.4b). At stiffness values of 0.3 F_{MAX}/L^0_F, corresponding to the stiffness of the length-tension curve at 95% optimal fiber length, no stable muscle activation patterns were found. To generate a set with 97% stable muscle activation patterns, intrinsic stiffness had to be increased to 8, which cannot be achieved from the length-tension property of muscle alone, but is less than the short-range stiffness of muscle (Rack and Westbury 1974).

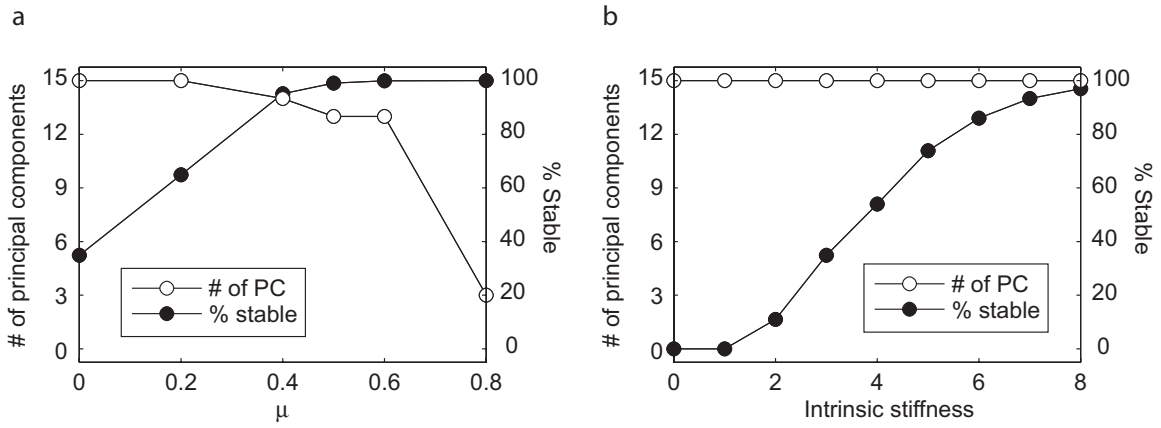

Figure 3.4: Changes in activation set dimensionality and stability due to biasing of the activation sets to locally stiff muscles and to varying magnitudes of intrinsic muscle stiffness. Randomized set of muscle activity were generated for different values of μ, weighting the cost function in favor of locally stabilizing muscles, and at different stiffness values for the muscles. A) As the weighting toward locally stable muscle increases, the percentage of stable muscle activation patterns within each randomized set increases, and the number of principal components accounting for 95% variability of the set decreases. B) As intrinsic stiffness (normalized to the maximum force generating capability of the muscle times the optimal fiber length) increases, the percentage of stable muscle activation patterns increases without decreasing the number of principal components describing 95% variability of the set.

Allowing the pelvis to move vertically did not substantially change the results. In addition to AS, AF, HF, and KF modes, a fifth mode, comprised mostly of hip and knee flexion/extension, was created that was stable for 99% of the activation patterns. The proportion of total stable muscle activation patterns decreased by 3% to 31%, and the correlation of local muscle stability to whole-limb stability was unaffected.

Discussion

Within the large set of activation patterns that satisfy the force requirement for posture, a reduced subset of the same dimensional complexity produced mechanical limb stability, and few strong correlations between specific muscles and stability were found. This suggests that the stability criterion restricts the size of the muscle activation solution space without restricting the muscle activation strategy.

Based on intrinsic musculoskeletal properties, muscle activation patterns may be chosen by the nervous system to set the relative mechanical stability or maneuverability of the limb in addition to meeting the kinetic constraints of a task. It has been suggested that muscles operate near optimum length, where muscle stiffness due to the length-tension relationship is close to zero. There were no globally stable muscle activation patterns for muscle stiffnesses in this range (<1), although KF and HF modes were stable. In contrast, essentially no unstable activation patterns were found for muscle stiffnesses greater than 8. At its maximum slope, the length-tension relationship has a stiffness of 4, which may be increased as much as four-fold by the autogenic stretch reflex (Nichols and Houk 1976), suggesting, along with short-range stiffness contributions (Epstein and Herzog 2003), that these mechanisms alone may be adequate to ensure limb stability. Supporting this idea, cats with spinal cord transection are able to stand independently and resist small perturbations (De Leon et al. 1998, Pratt et al. 1994), but do not generate direction-specific postural responses (Macpherson and Fung 1999). Our model demonstrated that even when the limb is unstable, the perturbation doubling-time was

greater than 100 ms, approximately the latency of active force-generation in postural responses (50 ms muscle activation latency plus 50 ms electromechanical delay) (Macpherson 1988). The viscous force-velocity relationship of muscle contributes significantly to prolonging the perturbation doubling-time, illustrating its importance to postural control.

Neural control may be dedicated more towards sagittal plane control and ankle control, consistent with the primary joint motions of the limb in both locomotion and posture. The high stability of non-sagittal modes in our analysis suggests that frontal plane control of these joints does not require substantial neural control and reflects inherently stabilizing non-sagittal moment arms (Young et al. 1992). The relative instability of ankle flexion/extension and ad/abduction modes is consistent with the important role of the ankle in directing the actions of more proximal muscles (Fregly and Zajac 1996, Ting et al. 1999, van Antwerp et al. 2007, Zajac 2002), which may be particularly important during perturbations (Daley et al. 2007).

Our analysis highlights two strategies by which postural stability may be increased. For novel environments, it may be advantageous to increase limb stability through co-contraction (Osu et al. 2002) or by increasing neural feedback gains (Bonasera and Nichols 1996, Nichols and Houk 1976). In contrast, biasing selection of muscle activation patterns to locally stiff muscles, due to moment-arm properties can also result in whole limb stability without need for co-contraction. These two different strategies may explain our prior data demonstrating different muscle activation patterns across individuals during quiet standing (Torres-Oviedo et al. 2006, Torres-Oviedo and Ting 2007). Similarly, some subjects maintain trunk rotational stiffness through feedforward activation of muscles, whereas others modulate muscle activation in response to trunk motion (Gurfinkel et al. 2006). Our results demonstrate the vast number of possible muscle activation patterns that could stabilize the limb. We propose that individual variations in the selection of a muscle activation pattern may result from

differential tradeoffs between stability, energetic efficiency, and other factors (Welch and Ting 2008).

It may be possible to increase stability of musculoskeletal simulations for a range of dynamics tasks by considering muscle stiffness and moment-arm properties in optimizations of muscle activation patterns. While activation of locally stabilizing muscles did not guarantee whole-limb stability in our analysis, it was possible to increase probability of whole limb stability preferentially selecting muscles with greater local joint stiffness. Our approach may be extendible to more dynamic simulations of locomotion (Higginson et al. 2006, Neptune et al. 2001), and be used to choose muscle activation patterns that increase the stability of the simulations, helping to maintain the body on a particular cyclic trajectory (Holmes et al. 2006).

Acknowledgements

Supported by NIH grant HD46922. The NIH had no role in the design, performance, or interpretation of the study.

CHAPTER 4

LENGTH FEEDBACK IN POSTURAL CONTROL OF A CAT HINDLIMB: A MODELING STUDY AND STABILITY ANALYSIS

Introduction

Postural control is a fundamental task of the neuromusculoskeletal system. In addition to its intrinsic importance during quiet standing, posture also serves as the background for a variety of many other critical motor tasks. The biological mechanisms responsible for postural control have been intensely debated, primarily in the context of a hierarchical neuromusculoskeletal system. Some (Winter et al. 1998) have argued that the lowest level of the hierarchy, the intrinsic viscoelastic properties of the muscles, are sufficient to stabilize quiet standing in a human. On the other hand, others (Hasan 2005) claim that the highest level of the hierarchy, voluntary nervous control, is required for balance control. Many others have argued that the various levels of the intermediate reflex pathways are the most critical in maintaining balance (Lyalka et al. 2005, Macpherson et al. 1997). Even among these there are differences over which pathways are the most important (Deliagina et al. 2008).

When subjected to a perturbation, the system must generate a net restoring force that returns the center of mass to the base of support. The restoring ground reaction forces for cats subjected to horizontal plane perturbations has been described as a passive phase characterized by restoring forces directly countering the perturbation followed by a reflexive response characterized by a "force constraint strategy." Under force constraint, the forces produced by each limb are constrained to a preferred direction regardless of the direction of postural perturbation , and the net response is a directionally tuned change in support force (Macpherson 1988, Macpherson 1994). This constraint has also been demonstrated in the human postural response (Henry et al. 2001). The activation of

individual muscles, as indicated by EMG responses, are directionally tuned (Macpherson 1988); each muscle responds only across a certain range of perturbation directions. The directional tuning of individual muscles parallels the directionally tuned change in support force, so the endpoint force constraint seems to emerge from the directional tuning of individual muscle responses.

The relative amount of spinal and supraspinal control necessary to explain the features of the postural response is still debated. Experimentally, Macpherson (Macpherson 1988) measured the activity in the muscles of the hindlimb of cats subject to horizontal platform displacements and found that a postural response was initiated at latencies consistent with a reflex loop through supraspinal centers. Experiments with labyrinthectomized cats have demonstrated that neither vestibular nor visual information is required for the force constraint strategy or the directional tuning of EMG patterns(Inglis and Macpherson 1995) suggesting that an appropriate postural response requires integration of only proprioceptive and cutaneous sensory information. In contrast, spinalized cats can be trained to stand (De Leon et al. 1998, Fung and Macpherson 1999) and still exhibit directional tuning of the EMG, although delayed and with reduced magnitude. However, rabbits subject to ventral hemi-section of the spinal cord at T12 level experienced dramatically reduced postural response in terms of kinematics and EMG, while rabbits subject to dorsal or lateral hemisection quickly regained the postural response(Lyalka et al. 2005). Lyalka et al. contend that since both dorsal and lateral hemisections substantially interfere with the supraspinal feedback loops, these longer latency reflex loops do not contribute greatly to the postural response in the intact, or dorsal and lateral hemisected animals. On the other hand, the descending tracts that are destroyed in the ventral hemisection interfere with the natural tone of the spinal reflexes therefore reducing the postural response.

The overall function of the postural response is to stabilize the limb and length feedback may provide this stability. Although some have argued that the intrinsic

viscoelastic properties of muscle are sufficient to stabilize posture (Winter et al. 2001) it is generally held that some level of nervous control is necessary in humans(Morasso and Sanguineti 2002) and cats (Macpherson et al. 1997). We have previously shown that at near optimal fiber lengths (95%) (Burkholder and Lieber 2001) the intrinsic stiffness of the hindlimb muscles is insufficient to stabilize the limb (Bunderson et al. 2008). As previously discussed it remains unclear whether the spinal reflex pathways under the appropriate tone are sufficient to stabilize posture, but the preservation of the directional tuning of EMG responses in the spinalized cat is consistent with proprioceptive length feedback. We test the hypothesis that homonymous fiber length feedback is sufficient to provide limb stability by comparing the Lyapunov stability of a model limb with and without fiber length feedback.

One potential explanation for the observed directional tuning of muscle activity and force constraint strategy is the stretch reflex of the muscle. Muscle length and velocity feedback is provided by muscle spindles, groups of intrafusal fibers innervated by large-diameter (group Ia) fibers and smaller group II afferents. The firing rate of these afferents increases with stretching of the spindle and decreases with shortening of the spindle (Houk et al. 1981). These Ia afferents make monosynaptic connections in the spinal cord with homonymous alpha motor neurons, so that excitation of the Ia afferent results in excitation of the homonymous alpha motor neurons. The directional tuning of muscle activity may simply reflect the perturbation directions of maximal muscle lengthening and therefore maximal stretch response. This direction specific stretch response may also be responsible for the force constraint strategy observed in the postural response. An alternative possibility is that the directional tuning of a particular muscle is triggered by an integrated signal from a set of muscle and/or cutaneous afferents and therefore does not reflect the length change of the muscle. Support for this has been shown in voluntary postural tasks with monkeys where the activity of muscles differ from their anatomical action (Fagg et al. 2002, Kurtzer et al. 2006). We test the hypothesis that

the directional tuning of EMG in the postural response is due to homonymous length feedback by comparing experimental muscle tuning curves to tuning curves resulting from length feedback in a model of a cat hindlimb.

We found that the directional tuning of the muscles in response to postural perturbations was similar for 3 of the 6 muscles compared with experiments. The force response was similar for the dynamic portion but diverged as stiffness became dominant. The limb was unstable for all muscle activation patterns without length feedback and became stable for all muscle activation patterns when homonymous length feedback was included.

Methods

Summary

We used a biomechanical model to evaluate the effect of homonymous fiber length feedback on the stability, muscle activity, and ground reaction forces of the limb in response to postural perturbations. A large set of muscle activation patterns were selected that produce the same endpoint force and satisfy the equilibrium constraints of the model. To determine the endpoint perturbation directions that maximally lengthen the muscle the equations of motion for the model were linearized for each muscle activation pattern. Postural perturbations based on those that have been applied experimentally (Macpherson and Fung 1999) were applied to a biomechanical model of a cat hindlimb with and without homonymous length feedback, and the spatial tuning of muscle activation was measured for the limb with fiber length feedback. The ground reaction force was recorded for perturbations in a variety of directions and at different times after perturbation onset. Lyapunov stability of the limb was also evaluated using the linearized state equations for all activation patterns in the limb with and without length feedback.

Anatomical Model

The model had seven kinematic degrees of freedom consisting of hip flexion (HF), hip adduction (HA), hip external rotation (HR), knee extension (KE), knee adduction (KA), ankle extension (AE), and ankle adduction (AA) (Burkholder and Nichols 2004, McKay et al. 2007, van Antwerp et al. 2007). The pelvis was welded to ground (zero degrees of freedom) and the foot was connected to the ground through a pin joint at the MTP (three degrees of freedom reduction), leaving 4 total degrees of freedom. The equations of motion for the system were expressed in the generalized coordinate system, $\vec{\theta} = [\theta_{HF}, \theta_{HA}, \theta_{HR}, \theta_{KE}, \theta_{KA}, \theta_{AE}, \theta_{AA}]^T$, where the subscripts denote the positive direction of joint movement. Limb motion was described by the vector equation,

$$\ddot{\vec{\theta}} = \vec{f}_{\ddot{\theta}} = \mathbf{M}\left(\vec{\theta}\right)^{-1}\left[-\vec{v}\left(\vec{\theta}, \dot{\vec{\theta}}\right) - \vec{G}\left(\vec{\theta}\right) + \mathbf{R}\left(\vec{\theta}\right)\vec{F}_M\left(\vec{\theta}, L_F, a\right) - \mathbf{J}\left(\vec{\theta}\right)^T \vec{F}_{END}\left(\vec{\theta}, L_F, a\right)\right]. \quad (1)$$

where **M** is the inertia matrix, $\vec{v}$ is the centrifugal and Coriolis torques, $\vec{G}$ is the gravitational torques, **R** is the moment arm matrix, **J** is the Jacobian mapping joint velocities to the translational velocity of the MTP, $\vec{F}_M$ is the vector of muscle forces, $\vec{F}_{END}$ is the resultant force at the MTP joint. For clarity, the state dependence of the variables is omitted in future references. These equations of motion were subject to the endpoint acceleration constraint,

$$\vec{F}_{END} = \left(\mathbf{J}\mathbf{M}^{-1}\mathbf{J}^T\right)^{-1}\left[\mathbf{J}\mathbf{M}^{-1}\left(-\vec{v} - \vec{G} + \mathbf{R}\vec{F}_M\right) + \dot{\mathbf{J}}\dot{\vec{\theta}} + \ddot{x}\right], \quad (2)$$

where $\ddot{x}$ is the acceleration of the toe, which is defined by the perturbation.

Muscle Model

31 muscles were modeled using a Zajac adaptation of the Hill muscle model (Zajac 1989). The force of an individual muscle *i* ($F_{M,i}$) was described by,

$$\hat{F}_{M,i} = tfl\left(\delta_i\right), \quad (3)$$

$$F_{M,i} = \hat{F}_{M,i} F_{MAX,i}, \tag{4}$$

where the function *tfl* is a spline relationship of tendon strain (δ_i) to normalized tendon force ($\hat{F}_{M,i}$) and $F_{MAX,i}$ is the maximum isometric force of the muscle. The tendon strain is obtained from the fiber length ($L_{F,i}$), pennation angle (α_i), and musculotendon length of the muscle.

Fiber length dynamics were obtained by solving the state equation,

$$\begin{aligned} &if \quad \left(\frac{\hat{F}_{M,i} - pfl\left(\frac{L_{F,i}}{L^0_{F,i}}\right)}{\cos(\alpha_i)} < a_i afl\left(\frac{L_{F,i}}{L^0_{F,i}}\right) \right) \quad \Rightarrow \quad \frac{\hat{F}_{M,i} - pfl\left(\frac{L_{F,i}}{L^0_{F,i}}\right)}{\cos(\alpha_i)} = a_i afl\left(\frac{L_{F,i}}{L^0_{F,i}}\right)\left(\frac{1+\frac{\dot{L}_{F,i}}{v_{\max,i}}}{1-\frac{\dot{L}_{F,i}}{v_{\max,i} k_{v,i}}}\right) + \frac{\eta_i \dot{L}_{i,F}}{F_{MAX,i}} \\ &else \quad \Rightarrow \quad \frac{\hat{F}_{M,i} - pfl\left(\frac{L_{F,i}}{L^0_{F,i}}\right)}{\cos(\alpha_i)} = a_i afl\left(\frac{L_{F,i}}{L^0_{F,i}}\right)\left(\frac{f_{\max,i} - 1}{\left(\frac{k_{v,i} k_{s,i} v_{\max,i}}{\dot{L}_{F,i}(k_{v,i}+1)}\right)+1} + 1\right) + \frac{\eta_i \dot{L}_{i,F}}{F_{MAX,i}} \end{aligned}, \tag{5}$$

for muscle fiber velocity ($\dot{L}_F$). The functions *pfl* and *afl* relate the ratio of fiber length to optimal fiber length, $L_{F,i} / L^0_{F,i}$, to the normalized isometric force of the muscle and normalized passive force of the muscle respectively. The variables $k_{v,i}$, $k_{s,i}$, and $f_{\max,i}$ are hill equation parameters, $v_{\max,i}$ is the maximum shortening velocity, and η_i is the passive damping of the muscle. The activity level of the muscle (a_i) is governed by the activation dynamics,

$$\dot{a}_i = f_{\dot{a},i} = \begin{cases} (\varepsilon_i - a_i)(k_{a1,i}\varepsilon_i + k_{a2,i}) v_{\max,i} / L^0_{F,i} & if \quad \varepsilon_i \geq a_i \\ (\varepsilon_i - a_i) k_{a2,i} v_{\max,i} / L^0_{F,i} & else \end{cases}, \tag{6}$$

where ε_i is the excitation, $k_{a1,i}$, and $k_{a2,i}$ are activation constants.

Selection of Activation Sets

The initial states of the system were chosen such that all state equations were in equilibrium. Muscle force vectors ($\vec{F}_M$) were chosen such that the muscle torques balance the gravitational and endpoint torques,

$$\mathbf{R}\vec{F}_M = \vec{G} + \mathbf{J}^T \vec{F}^0_{END} . \tag{7}$$

The activation pattern produces a force at the toe ($\vec{F}^0_{END}$) that is derived from experiments(Torres-Oviedo et al. 2006). Since $\mathbf{R}\vec{F}_M$ has dimensions 7 x 31, equation 4 is redundant and there are an infinite number of solutions. To span the $\vec{F}_M$ solution space, activation sets were chosen by projecting a random force vector ($\vec{F}_{M,0}$), into the solution space of equation 7 by quadratic programming with the cost function

$$c = \left(\vec{F}_M - \vec{F}_{M,0}\right)^T \left(\vec{F}_M - \vec{F}_{M,0}\right), \tag{8}$$

and constraints,

$$\mathbf{R}\left(\vec{F}_M - \vec{F}_{M,0}\right) = \vec{G} + \mathbf{J}^T \vec{F}^0_{MTP} - \mathbf{R}\vec{F}_{M,0} , \tag{9}$$

$$\vec{F}_{M,\min} - \vec{F}_{M,0} \le \left(\vec{F}_M - \vec{F}_{M,0}\right) \le \vec{F}_{M,\max} - \vec{F}_{M,0} . \tag{10}$$

To allow changes in activation without saturation, a maximum ($\vec{F}_{M,\max}$) and minimum ($\vec{F}_{M,\min}$) bound to the muscle force vector was chosen so that $\vec{F}_{M,\max}$ was 10% below the maximum force and that $\vec{F}_{M,\min}$ was 1% greater than the minimum force that could be generated by each muscle at a particular posture. The method of choosing activation patterns differs from our previous work (Bunderson et al. 2008) in that the muscle force rather than muscle activation pattern is solved for directly. This is necessitated by the inclusion of a tendon in the muscle model. Ten thousand random muscle force vectors were projected into the solution space. This number was previously found to be sufficient for convergence of the mean activation level of 23 of the 31 modeled muscles (Bunderson et al. 2008, Valero-Cuevas et al. 2003). For each unique

muscle force vector there is a unique fiber length vector and activation pattern that satisfies equilibrium for muscle fiber dynamics.

Reflexes

The reflex model is a direct linear feedback of the deviation of fiber length from the equilibrium fiber length. The excitation for muscle *i* is,

$$\varepsilon_i = \varepsilon_{0,i} + G_i \frac{(L_{F,i} - L_{F0,i})}{L^0_{F,i}} \tag{11}$$

The muscle excitation depends on the current ($L_{F,i}$), initial ($L_{i,F0}$), and optimal ($L^0_{F,i}$) fiber lengths, the initial muscle excitation ($\varepsilon_{i,0}$), and the length feedback gain (G_i). The forward simulations were run without length feedback ($G = 0$) and with length feedback gains approximated from experiments ($G = G_A$). The approximated gains $G_{A,i}$ for the 31 muscles are shown in Table 4.1.

Linearized Equations of Motion

To determine whether a given muscle activation pattern produces a stable limb, equation 1 was linearized by Taylor series expansion about the initial posture. The equations of motion can be linearized to the form of

$$\begin{bmatrix} \Delta\dot{\vec{\theta}} \\ \Delta\ddot{\vec{\theta}} \\ \Delta\dot{\vec{a}} \\ \Delta\dot{\vec{L}}_F \end{bmatrix} = \mathbf{A} \begin{bmatrix} \Delta\vec{\theta} \\ \Delta\dot{\vec{\theta}} \\ \Delta\vec{a} \\ \Delta\vec{L}_F \end{bmatrix}, \tag{12}$$

where **A** is the state matrix defined by,

$$\mathbf{A} \equiv \begin{bmatrix} \mathbf{0} & 1 & \mathbf{0} & \mathbf{0} \\ \dfrac{\partial \vec{f}_{\ddot{\theta}}}{\partial \vec{\theta}} & \mathbf{0} & \mathbf{0} & \dfrac{\partial \vec{f}_{\ddot{\theta}}}{\partial \vec{L}_F} \\ \mathbf{0} & \mathbf{0} & \dfrac{\partial \vec{f}_{\dot{a}}}{\partial \vec{a}} & \dfrac{\partial \vec{f}_{\dot{a}}}{\partial \vec{L}_F} \\ \dfrac{\partial \vec{f}_{\dot{L}_F}}{\partial \vec{\theta}} & \mathbf{0} & \dfrac{\partial \vec{f}_{\dot{L}_F}}{\partial \vec{a}} & \dfrac{\partial \vec{f}_{\dot{L}_F}}{\partial \vec{L}_F} \end{bmatrix}. \tag{13}$$

The linearized state equations were used to determine the endpoint perturbation direction associated with the maximum change in musculotendon length for a given muscle *i*, $\vec{x}_{MTL,i}^{\max}$. This direction will be called the **lengthening direction**. For small displacement perturbations assuming no initial change in fiber length,

$$\vec{x}_{MTL,i}^{\max} = \vec{R}_i \mathbf{K}_\mathbf{J}^{-1} \mathbf{J}^T \left(\mathbf{J} \mathbf{K}_\mathbf{J}^{-1} \mathbf{J}^T \right)^{-1}, \tag{14}$$

where joint stiffness ($\mathbf{K_J}$) is,

$$\mathbf{K_J} = \frac{\partial \vec{G}}{\partial \vec{\theta}} + \frac{\partial \mathbf{R}}{\partial \vec{\theta}} \vec{F}_M + \mathbf{R} \frac{\partial \vec{F}_M}{\partial \vec{\theta}} + \frac{\partial \mathbf{J}^T}{\partial \vec{\theta}} \vec{F}_{END}, \tag{15}$$

and $\vec{R}_i$ is the moment arm vector for muscle *i*. Since this relationship is dependent on muscle force it varies with activation pattern. We report the mean lengthening direction ($\bar{\vec{x}}_{MTL,i}^{\max}$) for all 10,000 activation patterns as well as the angle corresponding to the standard deviation of the patterns from this mean lengthening direction.

The linearized equations of motion were also used to determine the stability of the limb for each activation pattern. Lyapunov stability theory states that if all eigenvalues of the state matrix, **A**, are negative the system is asymptotically stable, that is, under small perturbations the limb will always return to the equilibrium posture. Because of the large number of states we report only the largest eigenvalue. If the largest eigenvalue is less than zero all other eigenvalues will be negative and the system will be stable. The state matrix is activation pattern dependent and we report the largest eigenvalue of the state matrix for all activation patterns for both the reflexive and non-reflexive model. In

order to have a physically interpretable metric of stability, the largest real component of the eigenvalues was converted to the perturbation halving time:

$$t_{50} \equiv \frac{\ln(0.5)}{\mathrm{Re}(\lambda_{\max})}, \tag{16}$$

Simulations

To assess the effect of length feedback on the postural response of the limb, forward dynamic simulations were performed from the initial equilibrium state. The activation pattern for these simulations was based on minimization of the magnitude of the muscle force vector obtained by quadratic programming (equations 8-10) with the random muscle force vector set to zero ($\vec{F}_{M,0} = 0$), similar to a minimization of muscle noise cost function (Crowninshield and Brand 1981).

Perturbations were applied by constraining endpoint acceleration to be,

$$\ddot{\vec{x}} = 3.2\left(e^{-0.5\left(\frac{t-0.2}{0.022}\right)^2} - e^{-0.5\left(\frac{t-0.485}{0.022}\right)^2} \right)\vec{x}_{dir}\,\frac{m}{\mathrm{sec}^2} \tag{17}$$

The acceleration profile consisted of Gaussian pulses at 0.2, and 0.485 sec resulting in a ramp and hold endpoint position perturbation, with a maximum endpoint displacement of 5 cm (Figure 4.1), and a maximum velocity of 18 cm/sec. The directions of perturbations ($\vec{x}_{dir}$) were spaced evenly in the horizontal plane at elevation angles of ±90° (2 perturbations), ±60° (16 perturbations), ±30° (24 perturbations) and 0° (16 perturbations), for a total of 58 perturbations (Figure 4.1).

To determine the directional tuning of the changes in activation for the muscles, the baseline muscle activity level was subtracted from the mean muscle activity level for 0.15 sec after the onset of perturbation. Onset was determined as the time at which the acceleration reached ~25% of maximum (t = 0.165 sec). This mean change in activity was measured for each perturbation direction for the reflexive muscle.

Three-dimensional endpoint force were also computed for both the reflexive and non-reflexive model at the time of maximum acceleration of the first pulse (t = 0.2 sec), when the velocity had reached its maximum (t = 0.25 sec), and during the hold period when the velocity had settled to less than 0.1% of maximum (t = 0.55 sec).

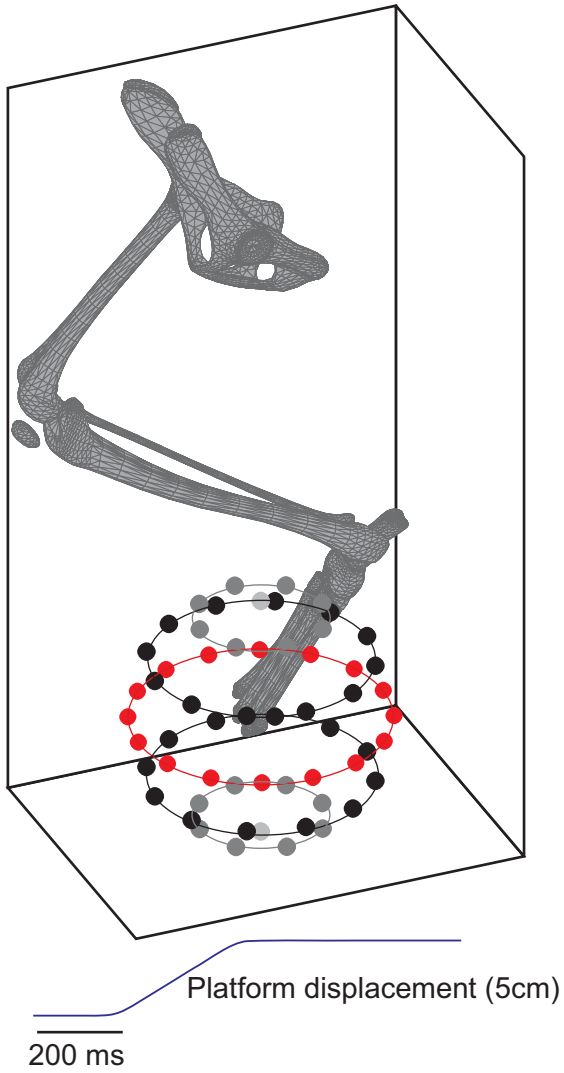

Figure 4.1: Forward simulations with ramp and hold endpoint displacements were performed in 58 directions. The perturbation directions were spaced evenly in the horizontal plane at elevation angles of ±90° (2 perturbations), ±60° (16 perturbations), ±30° (24 perturbations) and 0° (16 perturbations), for a total of 58 perturbations. The endpoint ramp and hold perturbations had peak accelerations of 3.2m/s^2, peak velocity of 18 cm/s and total displacement of 5 cm.

Sensitivity

To determine sensitivity of limb stability to the effective stiffness of muscles both feedback gains and operating fiber length were varied. The stability of the limb was tested at uniform feedback gains of $G = 0.10$, $G = 0.25$, and $G = 0.5$, to determine the sensitivity of stability to length feedback gain. The operating length of the fibers was changed from 95% of optimal length, which minimizes the intrinsic stiffness, to 65% of optimal fiber length, near maximal stiffness of the length tension curve, to determine the stability of the limb with near maximal intrinsic muscle stiffness.

Results

The mean lengthening directions ($\bar{\bar{x}}_{MTL}^{\max}$) reflect the mechanical coupling of the joints as approximated by the linearization. These directions reinforce the joint-action description of muscles, such as the knee extensors (RF, VM, VL, and VI), which all lengthen maximally in response to endpoint dislpacement nearly vertical. Conversely, shortening of these muscles would be expected to produce nearly vertical extension of the limb. Hamstrings, the biarticular hip extensors/knee flexors (GRAC, ST, SM, BFP), are lengthened by perturbations exactly opposite the knee extensors, reinforcing the view that these groups are functional antagonists at both the joint and limb level. Likewise, the ankle dorsiflexors (TA, EDL) and ankle plantarflexors (FHL, SOL, MG, LG, PLAN) had lengthening directions nearly opposing each other. The uni-articular hip-extensors (ADL, ADF, BFA, PEC) were grouped close to the ankle plantarflexors, suggesting functional synergy between these groups (Figure 4.2). The hip extensor Iliopsoas aligned with the bi-articular hip extensor/knee flexors. The only muscles with significant response outside of the sagittal plane were the ankle everters (PB,PL, PT) and ankle inverters (FDL, TP), supporting the view that these muscles primarily provide lateral support for the ankle and the limb.

Table 4.1: Muscle activation pattern (ε) and length feedback gains (G_A) for the forward simulations. The angular difference between lengthening direction (linear approximation) and the direction of maximum averaged muscle activity under the forward simulations is shown for the three dimensional vectors (3D) and projected into the horizontal plane (Horiz)

	ε	G_A	3D	Horiz
ADF	0.01	0.16	16	0
ADL	0.01	0.34	4	15
BFA	0.01	0.26	21	10
BFP	0.01	0.25	7	6
EDL	0.01	0.29	20	28
FDL	0.01	0.54	53	13
FHL	0.03	0.33	20	25
GMAX	0.01	0.41	31	20
GMED	**0.01**	**0.52**	**7**	**21**
GMIN	0.01	0.73	7	21
GRAC	**0.01**	**0.14**	**9**	**18**
LG	0.01	0.39	14	3
MG	0.07	2.96	20	39
PB	0.16	16.16	54	27
PEC	0.01	0.43	5	3
PL	0.33	11.91	79	16
PLAN	0.01	0.58	12	19
ILPS	**0.01**	**0.48**	**70**	**155**
PT	0.21	9.20	81	17
PYR	0.02	1.46	38	33
QF	0.05	4.31	12	23
RF	**0.09**	**4.37**	**20**	**42**
SART	**0.23**	**1.97**	**26**	**10**
SM	0.01	0.12	57	3
SOL	0.60	12.98	23	22
ST	0.01	0.31	8	2
TA	0.01	0.16	25	30
TP	0.01	1.61	51	4
VI	**0.42**	**16.93**	**14**	**127**
VL	0.15	5.02	13	101
VM	0.04	1.49	20	176
MEAN			28	35

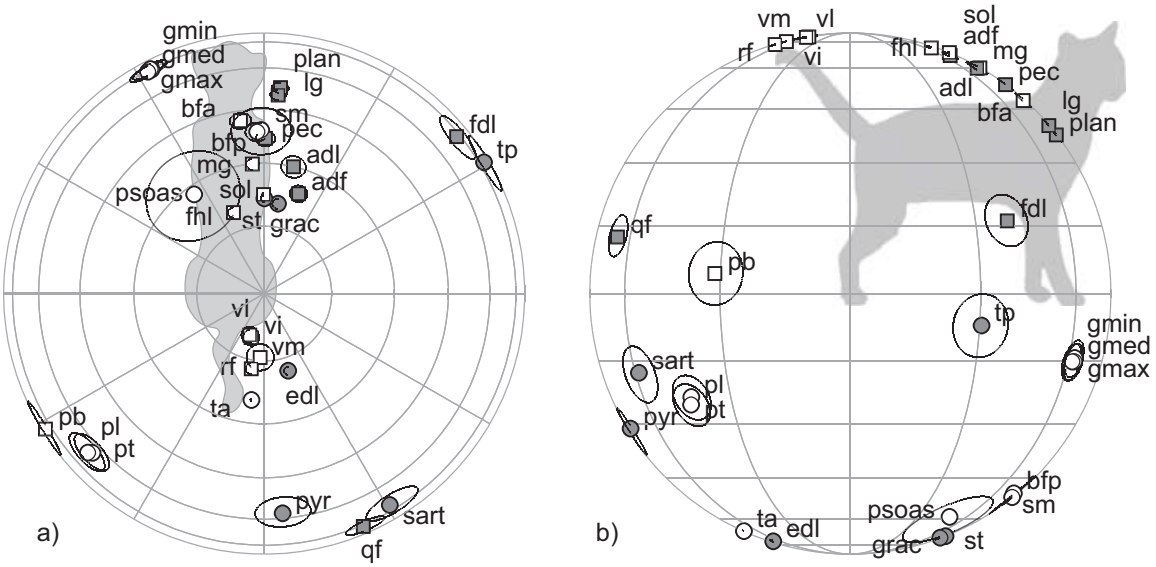

Figure 4.2: The lengthening directions for each muscle were calculated from the linearized state equations for the model. The mean lengthening directions ($\bar{\bar{x}}_{MTL}^{\max}$) across all 10,000 activation patterns is shown in the horizontal (a) and sagittal (b) planes. The hemisphere of the lengthening direction is indicated by the symbol (circle, downward; square, upward; gray, rightward; white, leftward). The angular standard deviation of each muscle for the 10,000 patterns is represented by circles around each muscle.

The mean lengthening directions for each muscle were conserved across activation patterns (Figure 4.2). The standard deviation of the angles of lengthening direction for each activation pattern from the mean lengthening direction for each muscle was on average 3.5°. The standard deviation for Iliopsoas (ILPS) was 11°, all other muscles had a standard deviation of less than 7°. With the exceptions of the ankle stabilizers, the mean muscle lengthening direction of all 10,000 activation patterns lay within a region of ±32° of the rostral-caudal direction in the sagittal plane (Figure 4.2a).

The linearized model of the limb was unstable for all activation patterns without fiber length feedback and stable for all activation patterns with fiber length feedback (Figure 4.3a). The largest real component of the eigenvalues for all activation patterns for the limb without fiber length feedback was greater than zero and less than zero for the limb with fiber length feedback for the same activation patterns, resulting in an asymptotically stable limb for all activation patterns. In terms of perturbation halving

time, the most stable activation pattern reduced perturbations by 50% every 100 ms. On the other hand, the perturbations doubled every 100 ms for the limb operating under the most unstable activation pattern.

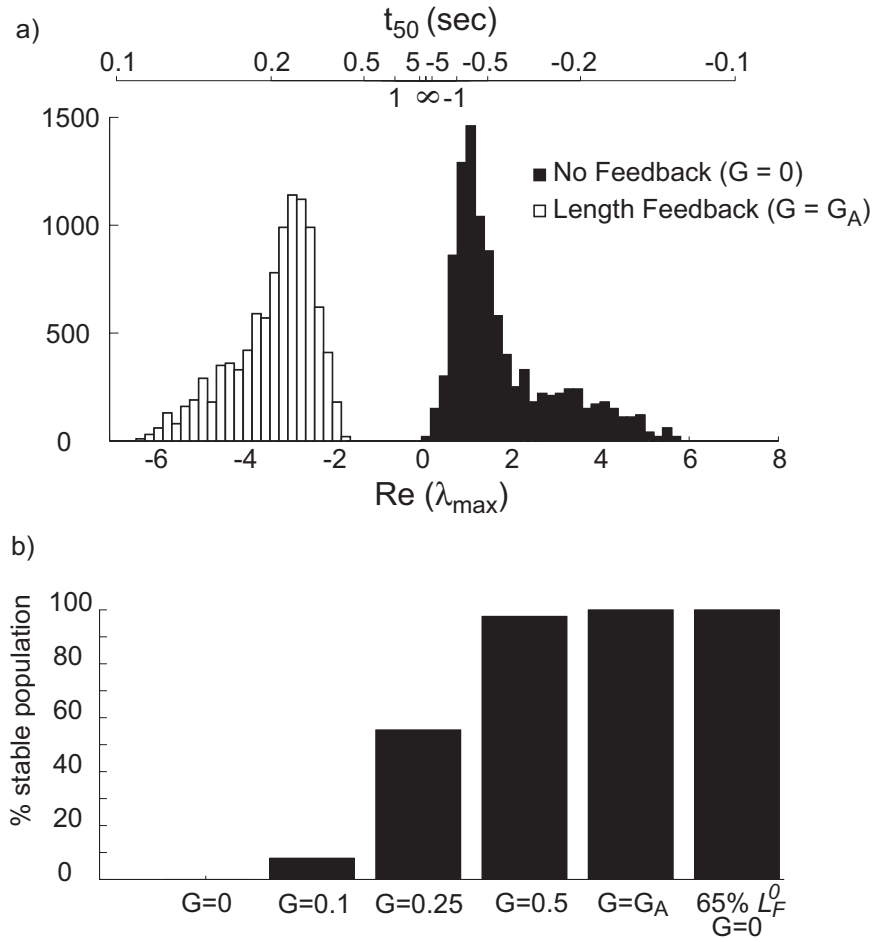

Figure 4.3: The Lyapunov stability of the model depends on length feedback gains. A) The distribution of the largest real component of the eigenvalues (λ_{max}) of the linearized equations of motion is shown across 10,000 activation patterns. The value of λ_{max} is greater than zero for all 10,000 activation patterns in the model without length feedback (a, black square) and less than zero for all 10,000 activation patterns in the model with length feedback (a, white square). Also shown is the perturbation halving time (t_{50}) or the time it takes for a perturbation to be reduced by 50%. B) The percentage of activation sets that are Lyapunov stable ($\lambda_{max} < 0$) is shown for the length feedback gains used in the simulations (G_A) and without length feedback (G=0) and for equal gains across all muscles (G = 0.1, 0.25, 0.5). The stability of the limb without feedback but with all muscles set to near maximal stiffness of the length-tension curve (LF = 65% LF0) is also shown.

Length feedback gain was a strong determinant of stability (Figure 4.3b). The observed reflex gains (G_A) were replaced with various uniform gains (G) applied to all muscles. Increasing G caused the population eigenvalues to migrate towards stable, negative values, increasing the fraction of activation patterns that met the Lyuapunov stability criterion (Figure 4.3b). A gain of 0.5 produced stability in 98% of the muscle activation patterns and decreased to 56% ($G = 0.25$) and 8% ($G = 0.1$). At an operating length of 65% optimal fiber length and no length feedback ($G = 0$) the limb was stable under all activation patterns.

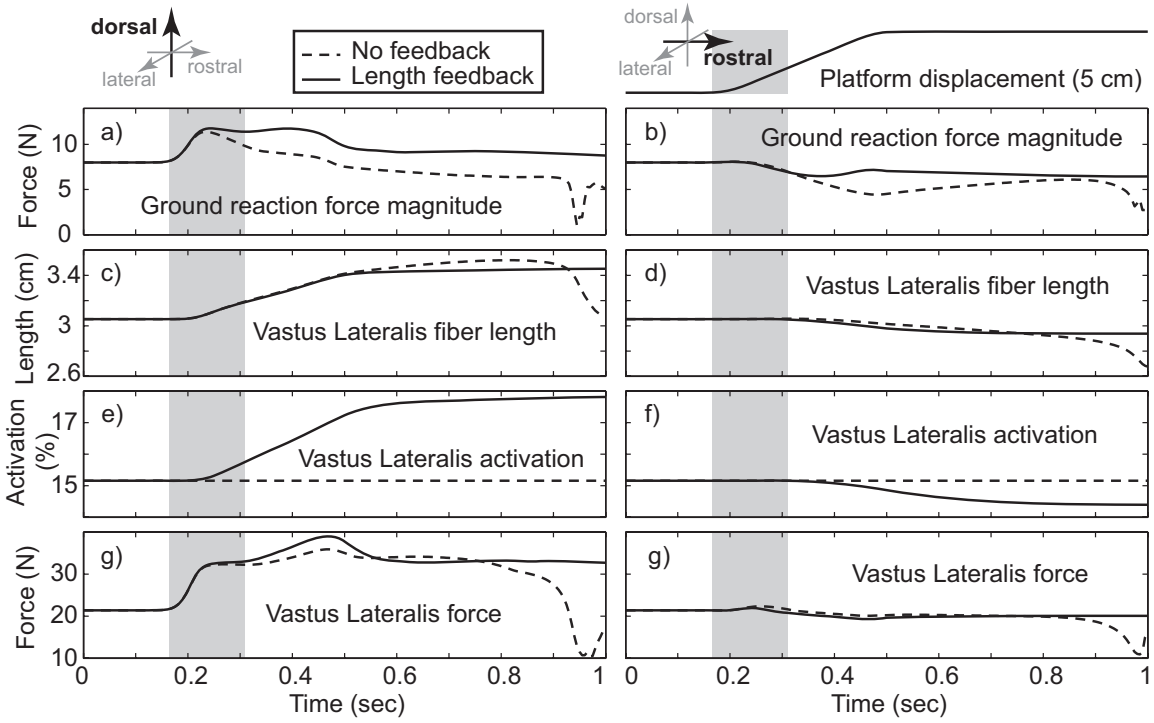

Figure 4.4: Forward simulations of the model with fiber length feedback (solid) and without feedback (dashed) for different endpoint perturbation directions. a-b) The magnitude of the ground reaction force varies with feedback and with perturbation direction. Vertical limb perturbation results in an increase in ground reaction force (a) while a perturbation in the rostral direction results in a decrease in total endpoint force (b). The addition of length feedback decreases the change in GRF as the limb is perturbed vertically and increases the GRF response to rostral perturbation. c-d) Vastus Lateralis (VL) is typical of all muscles in that its length change depends on the direction of perturbation. A vertical perturbation results in substantially stretching VL (c) and a rostral perturbation slightly shortens VL (d). The amount of length change depends on whether fiber length feedback is present or not (c,d). e-f) With length feedback, length change in VL results in a proportional change in the activation of VL. g-h) The force in the muscle depends on both the stretch of the muscle and the activation.

Exemplary forward simulation results are shown in Figure 4.4. When the endpoint was displaced vertically (Figure 4.4a, c, e, g) or rostrally (Figure 4.4b, d, f, h), the simulation produced a complex endpoint force response (Figure 4.4a-b). The immediate response is dominated by acceleration and inertia, reflected in the rapid force rise in response to vertical perturbation (Figure 4.4a), which requires substantial acceleration of the femur segment. The rostral perturbation induces acceleration of the less massive foot segment, and a smaller acceleration dependent rise in force. In each direction, muscle lengths change proportionally with endpoint position (Figure 4.4c-d), and for simulations including length feedback, activation changes accordingly (Figure 4.4e-f). Resultant muscle force reflects the combined effects of changing activation, tendon elasticity, and muscle force-velocity or viscosity. This is most apparent in VL during vertical perturbation (Figure 4.4g), in which VL force rises rapidly, then yields as the tendon strain equilibrates with muscle viscosity. The instability of the model without feedback is evident in the continued drift of forces and muscle length change after the completion of perturbation, leading in both perturbation directions to catastrophic collapse around 0.95s. In contrast, muscle length remains nearly constant in the model with length feedback.

Full forward dynamic simulations of endpoint perturbations of the limb also demonstrated direction dependence of muscle lengthening. Vastus Lateralis (VL) fiber length change was greater when the limb was perturbed in the vertical direction (Figure 4.4c) than in the rostral direction (Figure 4.4d). This greater change in VL fiber length when the limb is perturbed vertically resulted in a greater change in VL activation when fiber length feedback was included in the model (compare black solid line Figure 4.4e to black solid line Figure 4.4f). The change in activation for the model with fiber length feedback results in changes to the VL force (Figure 4.4g, Figure 4.4h) and the aggregate changes in all muscles result in a ground reaction force which remains closer to the

baseline across the entire perturbation (compare black solid line to gray dash line Figure 4.4a, Figure 4.4b). The magnitude of the ground reaction force increases for an upward perturbation of the limb (Figure 4.4a) and decreases slightly for a forward perturbation (Figure 4.4b) for the model with and without length feedback.

The average change in activation over the first 150 ms of the perturbation (forward dynamic simulations of the nonlinear model) was directionally tuned with the lengthening direction (obtained from the linearized approximations) for most muscles On average the angular difference between the lengthening direction and the 3-dimensional direction of maximum activation response in the simulations was 27° (Table 4.1). Vastus Intermedius is typical with the direction of maximum lengthening (Figure 4.5a, arrow) 14 degrees from the perturbation direction which elicited the maximum excitatory response. The projection of the lengthening direction into the horizontal plane was also compared with the maximum activation response direction for simulated perturbations in the horizontal plane (Table 4.1, Figure 4.5b-g). On average these were also reasonably aligned with a mean for all muscles of 33° (Table 4.1), and alignment in 3-D did not always correlate with alignment of the horizontal plane projections. The maximum responses of Gluteus Medius (GMED), Sartorius (SART), and Gracilis (GRAC) were 7°, 26°, and 9° away from the maximum lengthening direction in 3-D, and the maximum activation due to horizontal perturbations was shifted 21°, 10° and 18° from the projection of the lengthening direction in the horizontal plane. On the other hand, the maximum responses of Rectus Femoris (RF), and Vastus Intermedius (VI) were rotated by 42° and 127° from the lengthening direction, respectively, in the horizontal plane compared with rotations of 20°, and 14° three-dimensionally (compare Figure 4.5a and Figure 4.5g). Iliopsoas (ILPS) aligned poorly both in the horizontal plane (155°) and three-dimensionally (70°) (Figure 4.5e).

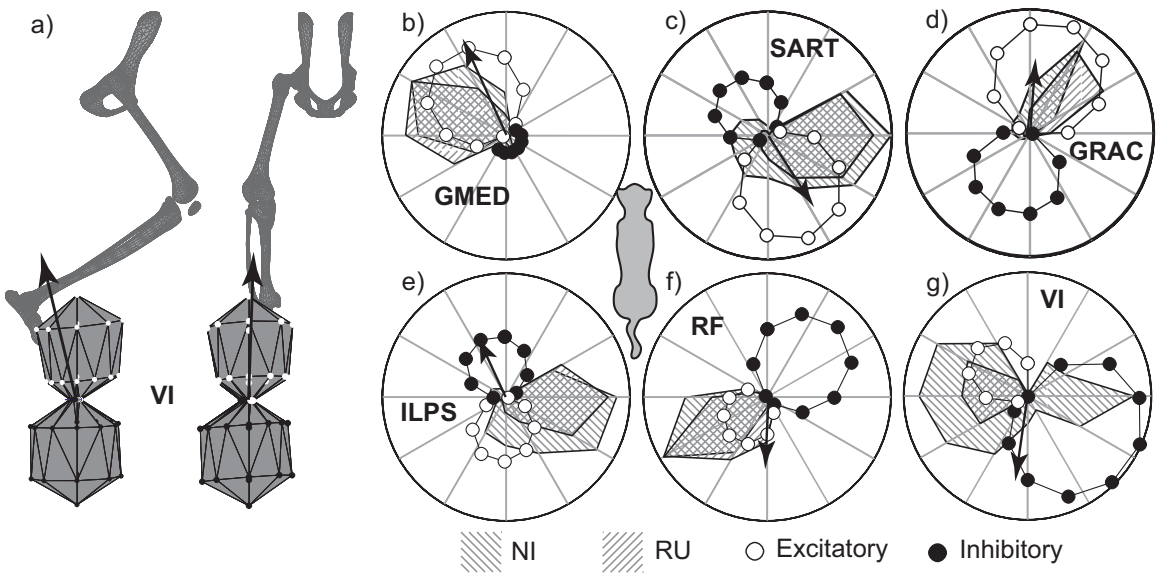

Figure 4.5: The lengthening directions (linearized approximations) are not always aligned with the direction of maximum activation response (from nonlinear simulations). a) The lengthening direction (arrow) of Vastus Intermedius (VI) is compared with the magnitude (circles) of the average change in muscle activation over the first 150 ms of the perturbation for 58 directions in three dimensions. Increases in activation (excitation: white circles) are differentiated from decreases in activation (inhibition: black circles). Vastus Intermedius lengthening direction is near vertical and the perturbation direction that results in the greatest increase in muscle activation in the forward simulations is vertical. Perturbations in the horizontal plane result in small changes in activation. b-g) The horizontal projections of the lengthening direction (arrow) are compared with the change in activation (filled and open circles) and experimental muscle tuning curves from two cats (hatched regions) for six muscles Gluteus Medius (GMED)(b), Sartorius (SART)(c), Gracilis (GRAC)(d), Iliopsoas (ILPS)(e), Rectus Femoris (RF)(f), and Vastus Intermedius (VI).

Changes in activation were not symmetric in lengthening and shortening. The increase in activation for muscles GMED, SART, and GRAC (white circles Figures 5b,c,d) due to muscle lengthening was stronger than the decrease in activation due to muscle shortening (black circles Figure 4.5b,c,d). Since the gain is constant for these simulations this can only be due to non-linearities in muscle strain. On the other hand, both RF and VI are asymmetric with the shortening response being larger than the lengthening response (Figure 4.5f,g). The response of ILPS is symmetric (Figure 4.5e).

The muscle tuning from the simulations was also compared with data from the postural response for six muscles in the right hindlimb of two intact cats (Macpherson and Fung 1999). GMED was tuned in both cats to respond to forward-left perturbations. Both SART and ILPS responded to right perturbations. GRAC responded to forward

right perturbations. Both VI and RF responded to left perturbations in cat RU but in cat NI VI responded to both left and right perturbations. The tuning of GMED, RF, and GRAC in the simulations were aligned closely with the tuning curves of cats RU and NI from the experiments. The simulated tuning of VI was closely matched to experiments for cat RU and for one of the lobes of cat NI. The simulated tuning of ILPS and SART were shifted by greater than 60° from both cats. The shape of the experimental tuning curves varied between muscles; GMED, RF, and GRAC were fairly narrow in tuning while VI, SART and ILPS had a broader response.

At the time of peak acceleration, where displacements are small, the effect of stiffness on the limb was minimal, and limb inertia and muscle viscosity dominated (Figure 4.6a,b). The change in ground reaction force in the horizontal plane for horizontal plane perturbations were the same with and without fiber length feedback (Figure 4.6b). Also at this early time the change in ground reaction force is biased to the rostral-caudal direction and is stronger for rostral-caudal perturbations (Figure 4.6b), but all endpoint forces are restorative. As the displacement of the limb increased the force response of the limb with length feedback began to deviate from the force response of the limb without feedback (Figure 4.6a). At peak velocity (t = 0.25), (the endpoint of the limb has only moved 9 mm) the restoring force in the horizontal plane for the fiber length feedback model was substantially different than the response for the no feedback model (Figure 4.6c). Without length feedback, restorative forces are generated only for displacements within 25° of rostral. Length feedback expanded the restorative range to 45° around rostral and 25° around caudal. In addition, the response to rostral directed perturbations became larger than the response to caudal directed perturbations (Figure 4.6c). This is primarily due to the asymmetric stretching of several hip muscles including GMED (Figure 4.4b). The change in endpoint force for the model without feedback during the hold phase of the ramp-and-hold perturbations was directed away from the initial posture for most directions (Figure 4.5d). The addition of length feedback

increased the magnitude of restoring forces when the limb was subject to rostral perturbations and decreased the magnitude of non-restoring forces.

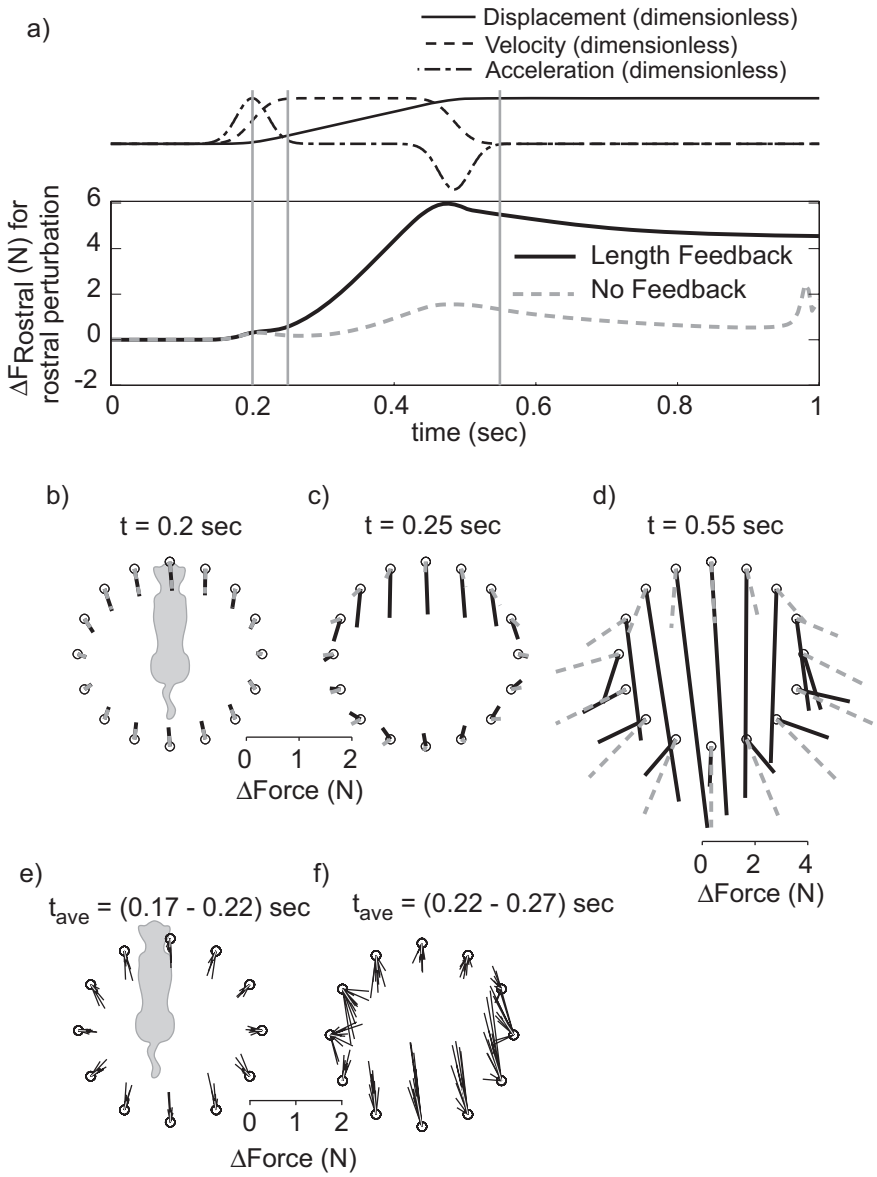

Figure 4.6: The force response varies across the timecourse of the perturbation for the model with and without fiber length feedback. a) Normalized endpoint acceleration, velocity, and position during the simulation. Peak acceleration is at 0.2s and velocity is maximal between 0.25 and 0.45s. The rostral component of the change in endpoint force is shown for a rostral perturbation and is the same for the model with and without length feedback. By the time peak velocity is reached the forces for the two conditions have begun to deviate and by the time the endpoint stops moving the forces are dramatically different. b-d) The endpoint force components in the horizontal plane for all horizontal plane perturbations for the model with (solid lines) and without (dashed lines) length feedback at peak acceleration (b), velocity (c) and displacement (d). e-f) Experimental force data for several trials averaged over 50ms windows corresponding to peak acceleration and velocity. Center of mass position changes substantially during the perturbation, so there is no experimental equivalent to the maximum displacement condition.

The simulated forces were compared to forces from the postural response of two intact cats (Macpherson and Fung 1999). The earliest neural response to perturbation occurs at a latency exceeding 50 ms, so the response over t-0.17-0.22 reflects purely passive contributions and directly oppose the perturbation (Figure 4.6e). For the first time window, when viscosity and inertia dominated, the simulated force responses were similar with a stronger rostral-caudal component than medial-lateral component (Figure 4.5b and Figure 4.5e). In addition, the magnitude of the force response was similar for the experimental and simulated data (Figure 4.5b and Figure 4.5e). For the second time window, the range of force magnitudes in the horizontal plane was similar but where the force response was greater to rostral directed perturbations in the simulated data (Figure 4.5c), the force response to caudal directed perturbations was greater in the experimental data (Figure 4.5f).

Discussion

The principle results of this study are that length feedback is sufficient to stabilize a linearized model of the cat hindlimb, to provide directional tuning of muscle activation in response to perturbations, and to increase the resistance of the nonlinear model to perturbation. These results indicate that direct fiber length feedback is sufficient to stabilize the limb against small perturbations from the equilibrium posture. Without length feedback the largest real component of the Eigen-values was greater than zero for all 10,000 activation patterns. However, the relative instability of these patterns varied dramatically with perturbation doubling times ranging from 100 ms to 5 s. With the addition of length feedback these activation patterns became stable and the perturbation halving time ranged from 100 to 400 ms. In either case, these time constants are substantially greater than the stretch reflex latency, and support the omission of feedback delays. Since data was not available to estimate the length feedback of all muscles we deemed it important to determine how sensitive the stability of the limb is to changes in

the length feedback gains. We found that a gain value of 0.5; equivalent to a 5% increase in activation level for a 10% change in fiber length (muscle would increase by 5% points e.g. from 15% activity level to 20% activity level, or from 90% to 95%) resulted in a stable limb for 98% of the activation patterns tested. Gains observed during ramp-and-hold experiments in decerebrate cats ranged between 0.16 (TA) and 12 (soleus), suggesting that the stabilizing gain is well within the physiological range. The variation in observed gains seems to favor antigravity (vasti, soleus, gastrocnemius) and so-called stabilizing muscles (TP, PB), which may reflect a strategy of reflex recruitment of muscles that contribute to normal stance. Although the limb stability would be dependent on reflex delays it may be that the short latency reflex pathways such as the monosynaptic stretch reflex provide stability for an individual limb rather than for balance.

Complex models such as the one used in this study are prone to criticism because of the large number of parameters that must be measured, approximated, or guessed. The response of the model is sensitive to these parameters to varying degrees just as the real limb is. All muscle parameters were either taken from the literature or approximated based on muscles of similar function. Therefore none of the current results are due to fitting of model parameters. The stability of the limb is not sharply sensitive to changes in the length feedback gains and was quantified across a large set of activation patterns. The sensitivity of these results to posture has yet to be determined.

Most of the maximal lengthening directions were substantially elevated from the horizontal plane, suggesting that horizontal plane perturbations may be relatively insensitive to proprioceptive responses. Both simulated and experimental turning curves were highly variable, highlighting the inadequacy of horizontal plane perturbations in characterizing limb response. Nearly half (14 of 31) of the muscles had lengthening directions that were less than 30° from vertical. The tuning of these muscles in the horizontal plane is more likely to be sensitive to changes in posture highlighting the need

for perturbations in three dimensions. Experimental interventions intended to test proprioceptive feedback should include vertical components.

Asymmetries were seen both in the change in muscle activation due to lengthening versus shortening and in the endpoint forces produced at the ground. Since the activation changes are proportional to length changes, asymmetries in the muscle activations may be due to asymmetries in muscle length changes and therefore asymmetries in joint kinematics or moment-arm relationships. Alternatively, the fact that many of the muscles barely active (19 of 31 muscles are at less than 1%) would mean that while lengthening could substantially activate the muscle, shortening could not substantially decrease the muscle activation. The asymmetries in ground reaction forces may be attributable either to these asymmetries or some other non-linear property of the muscle force generation or moment-arms. One such non-linear property is the passive force length property which does not influence force generation for these muscles (at 95% optimal fiber length) in shortening.

Direct fiber length feedback results in directional tuning of the individual muscle activations and these overlapped with the experimental tuning curves for four (GMED, RF, VI, GRAC) of the six muscles compared. This suggests that individual muscle lengthening may be a strong signal in determining the directionality of the postural response. The linearized prediction of directional tuning was consistent across a large family of stance-like muscle activation patterns, suggesting that this tuning is a feature of mechanical connectivity, segmental inertia, and joint torques required for weight support and relatively independent of the force generated by specific muscles.. However, five (GMED, RF, VI, GRAC, and ILPS) of the six muscles produced tuning curves that aligned more closely with the experimental data than with the linearized predictions, suggesting that the required assumptions for deriving the lengthening direction bias the result. This is most likely due to the same muscle strain nonlinearities that produce the asymmetry in the activation and force response.

The change in ground reaction force early in the perturbation indicates that a stronger rostral-caudal component is intrinsic to the limb and independent of neural control. Early in the response, before any neural control and even before stiffness begins to play a role (Figure 4.6b), the simulated force is stronger in the rostral-caudal direction. This preferred direction persists throughout the perturbation but its presence early indicates it is independent of a neural response. The simulated force response is asymmetric later in the perturbation (Figure 4.6c, d) with a stronger restoring force to rostral perturbations than to caudal perturbation. This asymmetry is also seen experimentally although in the opposite direction (Figure 4.6f) and is attributable to a strong non-linearity due to the low baseline activation levels. Extensors at the hip which are lengthened by rostral perturbations increase force without limit; while shortening by caudal perturbations result in only a small decrease in activation until the muscle is off. One problem with comparing with the experimental force and EMG responses is that the simulated limb had a fixed pelvis. Center of mass motion in the intact cat would result in smaller total joint angle and muscle length changes. This would reduce the magnitude of the endpoint force response which would be particularly noticeable later in the perturbation (Figure 4.6d).

Acknowledgements

This work was supported by NIH grant HD032571

CHAPTER 5

ENDPOINT PERTURBATION RESPONSE OF THE HINDLIMB OF A DECEREBRATE CAT AND HINDLIMB MODEL

Introduction

Previous work has shown that an appropriate pattern of length and velocity feedback, which could only result from neural control, produces a more stable and more energetically efficient control system for a kinematically redundant limb than does intrinsic mechanics alone. Limb stability may or may not be achieved using an appropriate activation pattern depending on where the muscles are operating on the length tension curve. In addition limb stability can be provided by the known patterns of length feedback. Length feedback alone is sufficient to produce directional tuning of postural responses, although that tuning matches experiments for 4 of the 6 muscles tested. In freely standing cats the mechanical effect of length feedback in terms of endpoint force production is radically different than the experimental observations. The question arises, why there are such large differences between the simulated data and the experimental results. Potential explanations include the structure of model, initial activation patterns, muscle operating length, artifacts in the experimental data, or that the perturbation poorly represents the perturbation of a free standing cat. One potential dramatic difference that results is that the change in joint angles and muscle lengths may be exaggerated in the simulations since the CoM is not allowed to move with the endpoint. It is unclear what if any would be the difference between perturbations applied to a constrained individual limb versus the entire support surface of a balancing cat. Identifying the source of the discrepancy requires a closer look at the responses and the closest biological equivalent of the model perturbations are single limb displacements of a decerebrate cat.

Previously, the outputs that have been compared between the model and experiments are endpoint force and EMG responses, which neglect the kinematics of the postural response. While endpoint force is useful in determining the endpoint impedance of the limb, the joint impedance can only be determined from experimental data with a combination of kinematics and endpoint force. Previously in the thesis no comparison has been made between modeled and experimental joint kinematics.

The goal of this work was to quantify the limb response experimentally at the joint level and not just at the endpoint level, and to quantify the limb response when the center of mass does not move, to identify potential sources of disagreement between modeled and experimental results.

Methods

Summary

Ramp and hold perturbations were applied to the toe of the right hindlimb of a decerebrate cat to determine the endpoint force and kinematic response of the limb in a reduced preparation. The posture and endpoint force at the beginning of the perturbation were used to initialize forward dynamic simulations of a cat hindlimb model. The simulated and experimental results were compared.

Animal

The experiment was performed on an animal that was being used for another experiment. The Emory University Institutional Animal Care and Use Committee approved the procedures in this experiment. The cat was anesthetized with isofluorane and placed in a stereotaxic frame. An intercollicular decerebration was performed and all brain matter rostral to the transection was removed. The body was supported with a sling under the abdomen and a clamp on the tail. The body and head were positioned at a natural stance. Each foot was placed on a six-degree-of-freedom force transducer which

was attached to a movable platform. The platform had the capability of moving any combination of the four transducers. Six kinematic markers were placed on the right hindlimb using bony landmarks as guides. The markers were placed at the iliac crest (IC), greater trochanter (GT), upper ankle (UA), lateral malleolus (LM), lateral metatarsophalangeal joint (MTP), and toe.

Experimental Protocol

The experiment included three protocols to determine the limb response of the decerebrate cat. The first set of perturbations were applied while the cat was under anesthesia (passive), the second set after anesthesia had been removed (unstimulated), and the third set with a background activation in the ipsilateral limb elicited by stimulating the contralateral tibial nerve at two times threshold (crossed-extension). Only the results from unstimulated and crossed-extension are shown since the passive data was nearly identical to the unstimulated data.

The perturbations for all three protocols were ramp and hold displacements of the right hindlimb and were applied in 16 directions in the horizontal plane (Figure 5.1). The perturbations had a peak velocity of 10 cm/s and the total displacement was 4 cm.

Anatomical Model

The model has been described previously (Burkholder and Nichols 2004). Briefly the model had seven kinematic degrees of freedom consisting of hip flexion (HF), hip adduction (HA), hip external rotation (HR), knee extension (KE), knee adduction (KA), ankle extension (AE), and ankle adduction (AA). The pelvis was welded to ground (zero degrees of freedom) and the motion of the foot was constrained under motion control. The equations of motion for the system were expressed in the generalized coordinate system, $\vec{\theta} = [\theta_{HF}, \theta_{HA}, \theta_{HR}, \theta_{KE}, \theta_{KA}, \theta_{AE}, \theta_{AA}]^T$, where the subscripts denote the positive direction of joint movement. Limb motion was described by the vector equation,

$$\ddot{\vec{\theta}} = \vec{f}_{\ddot{\theta}} = \mathbf{M}(\vec{\theta})^{-1}\left[-\vec{v}(\vec{\theta},\dot{\vec{\theta}}) - \vec{G}(\vec{\theta}) + \mathbf{R}(\vec{\theta})\vec{F}_M(\vec{\theta}, L_F, a) - \mathbf{J}(\vec{\theta})^T \vec{F}_{END}(\vec{\theta}, L_F, a)\right]. \quad (1)$$

where **M** is the inertia matrix, $\vec{v}$ is the centrifugal and Coriolis torques, $\vec{G}$ is the gravitational torques, **R** is the moment arm matrix, **J** is the Jacobian mapping joint velocities to the translational velocity of the MTP, $\vec{F}_M$ is the vector of muscle forces, $\vec{F}_{END}$ is the resultant force at the MTP joint. For clarity, the state dependence of the variables is omitted in future references. 31 muscles were modeled using a Zajac adaptation of the Hill muscle model (Zajac 1989). The tendon lengths were adjusted so that each muscle fiber was at 95% of optimal fiber length in the initial posture for each simulation.

Data Collection

Force data were collected from six-degree-of-freedom transducers at 2 kHz 1 second before perturbation until after the end of the perturbation. The data were low-pass filtered using a 3rd order butterworth filter at 40 Hz. Kinematic data were captured at 250 Hz using two cameras and PEAK data acquisition software. Custom MatLab software (Mathworks, Natick, MA) was used to calculate model joint angles from the images at each time point. First, 3 dimensional coordinates of each of the six kinematic markers were triangulated from the two camera images, and low-pass filtered using a 3rd order butterworth filter at 37.5 Hz. The UA and LM markers were used to compute the location of a virtual knee (VK) joint. We solved for values of θ_{HF} and θ_{HA} that aligned the vector from GT to VK in the model with the same vector computed from the images. Likewise, θ_{KE}, θ_{KA}, θ_{AE}, and θ_{AA} were computed by aligning the VK – LM and LM – MTP vectors. The hip rotation angle θ_{HR} could not be computed from the limited kinematic data and was set to be constant for each perturbation. This constant angle was chosen for each perturbation to be the value that minimized the non-sagittal values of the distal joints θ_{KE} θ_{AE} in the first frame.

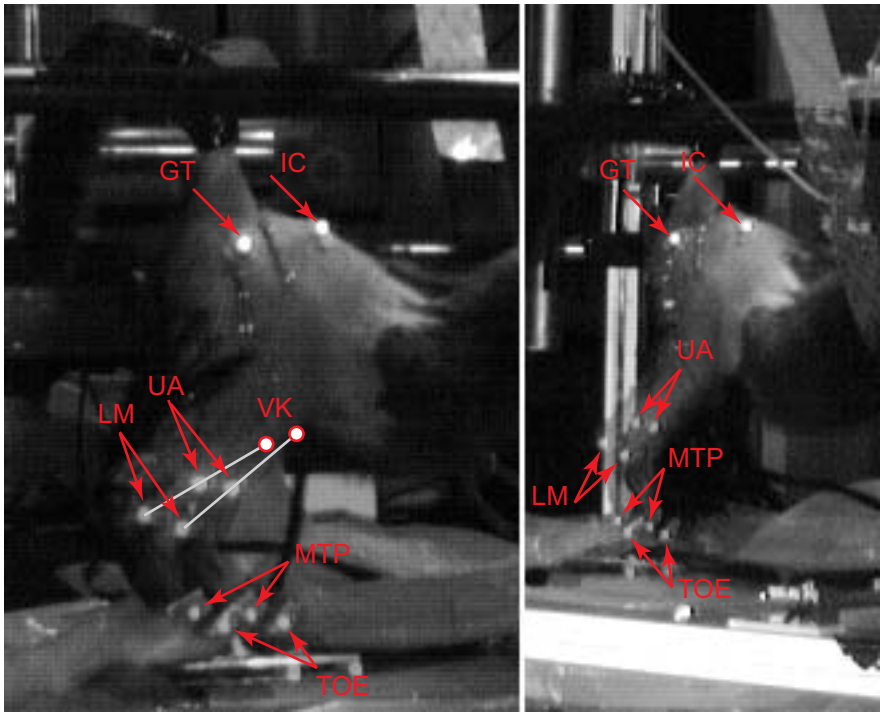

Figure 5.1: Sample images showing two frames at the initial state and at peak displacement. Six kinematic markers were placed on the right hindlimb at the iliac crest (IC), greater trochanter (GT), lateral malleolus (LM), upper ankle (UA),lateral metatarsophalangeal joint (MTP), and toe (TOE). Two markers (LM and UA) were used to calculate the position of the knee (VK).

Simulations

Forward dynamic perturbation simulations were performed on the mathematical model for 2 conditions: *unstimulated* and *crossed-extension* for the same directions applied to the experiments. The *unstimulated* simulations were performed with the limb in the posture and with ground reaction force ($\bar{F}_{END}^{active}$) calculated from the kinematic and force data at the beginning of the unstimulated trials. The *crossed-extension* simulations were performed with the limb posture and ground reaction force ($\bar{F}_{END}^{x-ext}$) calculated from the beginning of the crossed-extension trials. The simulations were performed with the muscle forces calculated by quadratic programming with cost function

$$c = \bar{F}_M{}^T \bar{F}_M \,, \tag{8}$$

and constraints,

$$\mathbf{R}\vec{F}_M = \vec{G} + \mathbf{J}^T \vec{F}^i_{MTP}, \tag{9}$$

$$\vec{F}_{M,l} \le \vec{F}_M \le \vec{F}_{M,u}. \tag{10}$$

To allow changes in activation without saturation, an upper ($\vec{F}_{M,u}$) and lower ($\vec{F}_{M,l}$) bound to the muscle force vector was chosen so that $\vec{F}_{M,u}$ was 5% below the largest force and $\vec{F}_{M,l}$ was 1% greater than the minimum force that could be generated by the muscles at a particular posture. The activation patterns for the unstimulated and crossed-extensions are shown in Table 5.1.

Perturbations were applied by constraining endpoint acceleration to be,

$$\ddot{\vec{x}} = 4\left(e^{-0.5\left(\frac{t-0.2}{0.01}\right)^2} - e^{-0.5\left(\frac{t-0.6}{0.01}\right)^2} \right) \vec{x}_{dir} \frac{m}{\sec^2} \tag{17}$$

which resulted in a endpoint displacement similar to that of the experiments (Figure 5.1). The directions of perturbations ($\vec{x}_{dir}$) were spaced evenly in 16 directions in the horizontal plane as were the experiments.

Data Analysis

The endpoint forces were averaged at three different time windows to observe the force response to mostly acceleration (t1 = 0.2 – 0.25 sec), velocity and displacement (t2 = 0.3 – 0.5 sec) and pure displacement (t3 = 0.7 – 1.2 sec) portions of the postural perturbations (Figure 5.2a,d 2nd, 3rd, and 4th grayed regions). The background force is quantified as the the average force from 0.15 sec before the onset to the onset of the perturbation (Figure 5.2a,d 1st grayed region). The background forces were subtracted from the averaged forces for each of the three time periods and this change in force magnitude (ΔF) is reported for the three time periods. In addition the angular deviation is defined as the included angle between the background force vector and the average force

vector for each time period. These analytical methods were applied to both experimental and simulated data.

Table 5.1: Activation patterns and baseline forces for the unstimulated and crossed-extension simulations. 0 is no activation and 1 is maximally active

	Unstimulated	Crossed-extension
SART	0.51	0.78
ILPS	0.02	0.03
GMIN	0.95	0.95
GMED	0.01	0.10
GMAX	0.03	0.36
PYR	0.44	0.84
QF	0.01	0.01
PEC	0.01	0.01
ADL	0.01	0.01
ADF	0.01	0.01
BFA	0.01	0.01
BFP	0.02	0.05
GRAC	0.01	0.01
ST	0.01	0.01
SM	0.01	0.01
RF	0.01	0.01
VM	0.01	0.01
VI	0.08	0.32
VL	0.08	0.30
EDL	0.01	0.01
LG	0.01	0.01
PLAN	0.01	0.01
MG	0.01	0.05
SOL	0.01	0.74
FHL	0.01	0.04
FDL	0.01	0.01
TP	0.02	0.02
PB	0.02	0.16
PT	0.18	0.21
PL	0.31	0.49
TA	0.11	0.01
$F_{Rostral}$	-0.22	-1.13
F_{Dorsal}	-0.73	-7.70
$F_{Lateral}$	0.03	1.12

The joint angles calculated from the kinematic markers were averaged over a 0.4 sec period 0.5 sec after the ramp portion of the perturbation (Figure 5.2b,c,e,f, second grayed region). The joint angles averaged over the first 0.3 seconds of video (before the perturbations, Figure 5.2b,e, first grayed region) were subtracted from the displaced postures to get the directional tuning of the joint responses.

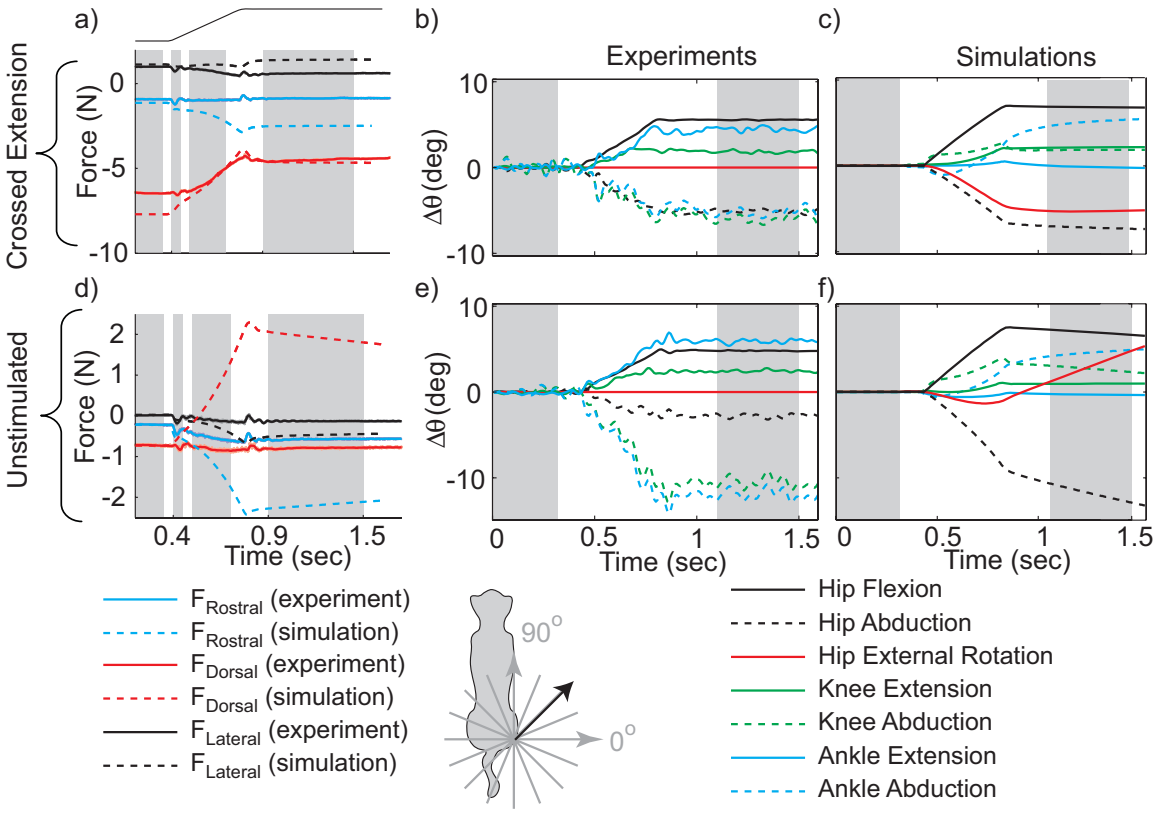

Figure 5.2: The ground reaction forces and kinematics are shown for a forward-right perturbation of the limb in the decerebrate cat and the simulated hindlimb model for the unstimulated and crossed-extension conditions. In both crossed-extension (a-c) and unstimulated (d-f) trials the endpoint force (a,d) was initially similar for the experimental (solid lines) and simulated (dashed lines) trials and force varied proportionally with endpoint displacement. The kinematics also varied proportionally with the perturbation for both experiments (b,e) and simulations (c,f).

Results

A typical response of the endpoint force and kinematics demonstrates differences between simulations and experiments and the crossed-extension state and unstimulated

state (Figure 5.2). A small burst in force is seen at motion onset and termination (t = 0.4, 0.8) in the experiments but not in the simulations (Figure 5.2a,d). It is likely that this is an artifact of the transducer. In all cases, endpoint force increases monotonically with endpoint displacement and settles to a new equilibrium force at the displaced position (Figure 5.2a,d). The joint angle displacements are proportional to the endpoint displacement (Figure 5.2b,c,e,f). All the experimental, but not all simulated, joint angles reached a displaced equilibrium posture. A small amount of ringing in the force response was seen in the experiments but not in the simulations (Figure 5.2a,d). Pixel resolution issues in the acquisition of the kinematic data resulted in the variability of the joint angles (Figure 5.2b,e).

The joint angle changes in the experiment were, for the most part, consistent between the unstimulated and crossed-extension trials (Figure 5.3). The hip flexed for forward perturbations and extended for backward perturbations in both the unstimulated and crossed-extension state (Figure 5.3a) and the hip adducted for leftward perturbations and abducted for rightward perturbations (Figure 5.3g). Both degrees of freedom at the hip experienced greater motion while the cat was in the crossed-extension state than in the unstimulated state (Figure 5.3a,g). The knee extended for forward perturbations, flexed for backward perturbations while the cat was in the unstimulated state (Figure 5.3c). The knee extensions and flexions in the unstimulated state were less than 3 degrees at the greatest. In the crossed-extension state the sagittal plane knee motion was further reduced to approximately 2 degrees in extension for most perturbation directions. The knee adducted for leftward perturbations, and abducted for rightward perturbations for both the unstimulated and crossed-extension states but this motion was stronger in the unstimulated state (Figure 5.3i). Ankle sagittal plane motion was asymmetric favoring extension when the toe was perturbed backward and leftward over flexion when the toe was perturbed forward and rightward (Figure 5.3e). The degree of extension was nearly identical for the unstimulated and crossed-extension states but the amount of flexion was

greater in the crossed-extension state. The ankle adducted for leftward perturbations and abducted for rightward perturbations and these responses were stronger in the unstimulated state than in the crossed-extension state (Figure 5.3k).

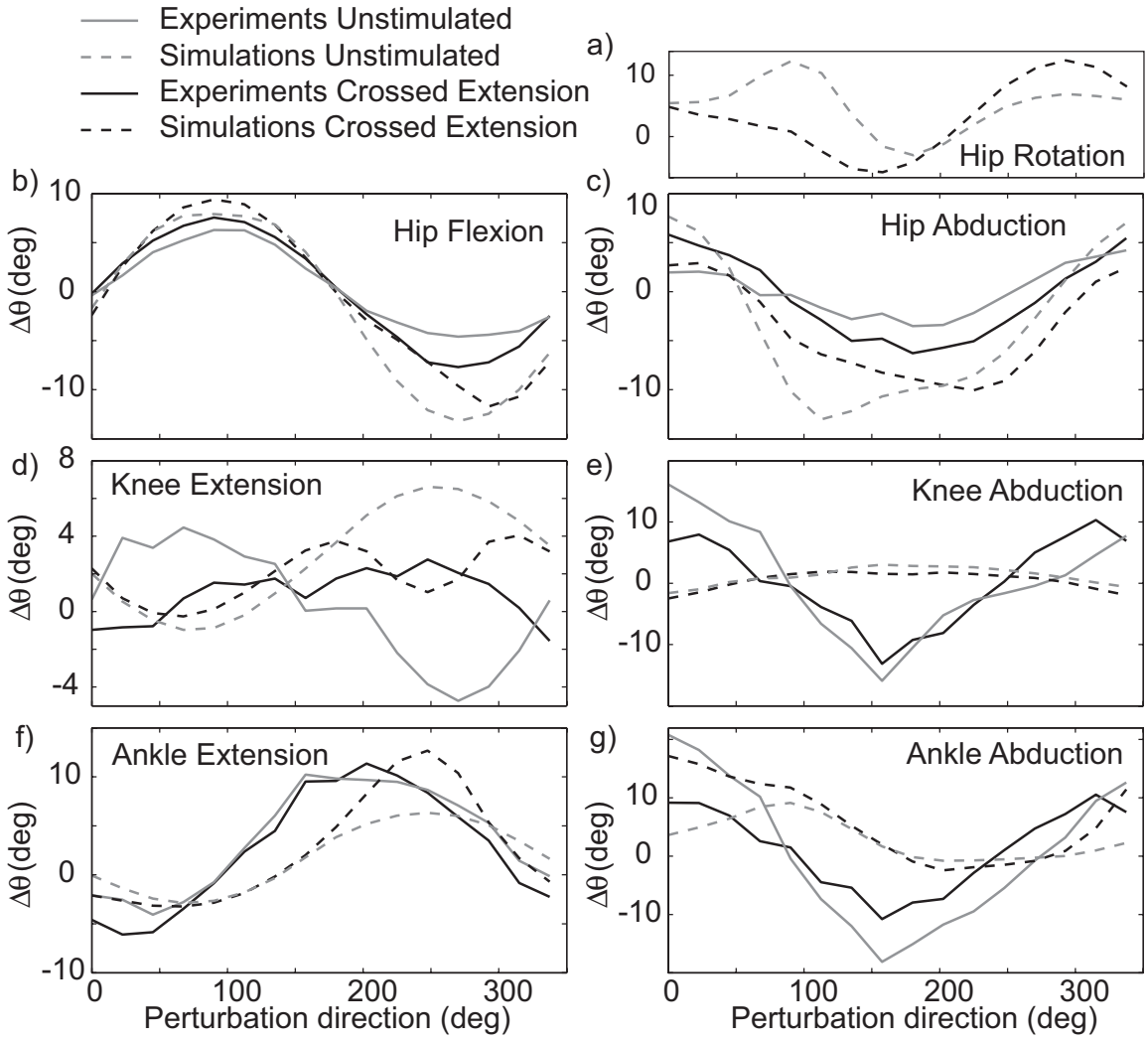

Figure 5.3: The joint angle changes at maximum displacement vary with perturbation direction and these variations are similar in unstimulated and crossed-extension trials. Since only two points on the femur were used to calculate joint angles hip rotation (a) was reported for simulations but not for experiments. Hip flexion (b), and hip adduction (c) vary sinusoidally with perturbation direction. Knee extension (d) is small for both experiments and simulations. Knee abduction (e) motion is dramatically larger in experiments than simulations. Peak knee abduction occurs for rightward perturbations in the simulations and for leftward perturbations in the experiments. Ankle extension (f) and abduction (g) vary sinusoidally with perturbation direction.

The hip flexes for forward perturbations and extends for backward perturbations for both the unstimulated and crossed-extension states similar to the experiments (Figure 5.3b). Also, the hip adducted for leftward perturbations and abducted for rightward perturbations (Figure 5.3h). While these motions were stronger in the crossed-extension state than unstimulated state in the experiments they were generally stronger (with the exception of hip flexion) in the unstimulated state than in the crossed-extension state (Figure 5.3b,h). The ab/adduction response at the hip was asymmetric in the simulations, favoring adduction (Figure 5.3h). The knee extended or did not move for nearly all perturbation directions in the unstimulated and crossed-extension states and this motion was stronger in the unstimulated than the crossed-extension states (Figure 5.3d). The knee non-sagittal motion in the simulations was opposite the knee motion in the experiments; the knee adducted for leftward perturbations and abducted for rightward perturbations (Figure 5.3j). However this motion was small, less than 3 degrees. At the ankle the sagittal plane motion was similar to experiments with the ankle extending for backward and leftward perturbations and flexing for forward and rightward perturbations (Figure 5.3f). While in the experiments the ankle response was greater in flexion for the crossed-extension than the unstimulated and the same in extension (Figure 5.3e), in the simulations the ankle response was greater in extension for the crossed-extension than the unstimulated state and the same in flexion (Figure 5.3f). Ankle non-sagittal motion was also strongly asymmetric with abduction dominating in the rightward and forward perturbation directions (Figure 5.3l). By comparison with the experimental results, the simulated joint angle changes were generally more asymmetric (Figure 5.3).

The angular deviation at t1 and t2 in the unstimulated simulations (Figure 5.4a) match the experiments (Figure 5.4b) for backward perturbations (180° – 360°) but not forward perturbations (0° – 180°). Both experiment and model deviate by approximately 20° from stance force, and that deviation varies smoothly over 180° – 360°. At t3 the angular deviation in the simulations does not match the angular deviation of the

experiments for all perturbation directions. The change in force in the unstimulated simulation (Figure 5.4e) matches the experimental data (Figure 5.4f) for t1 and t2 across all perturbation directions and matches at t3 over the range (180° – 360°).

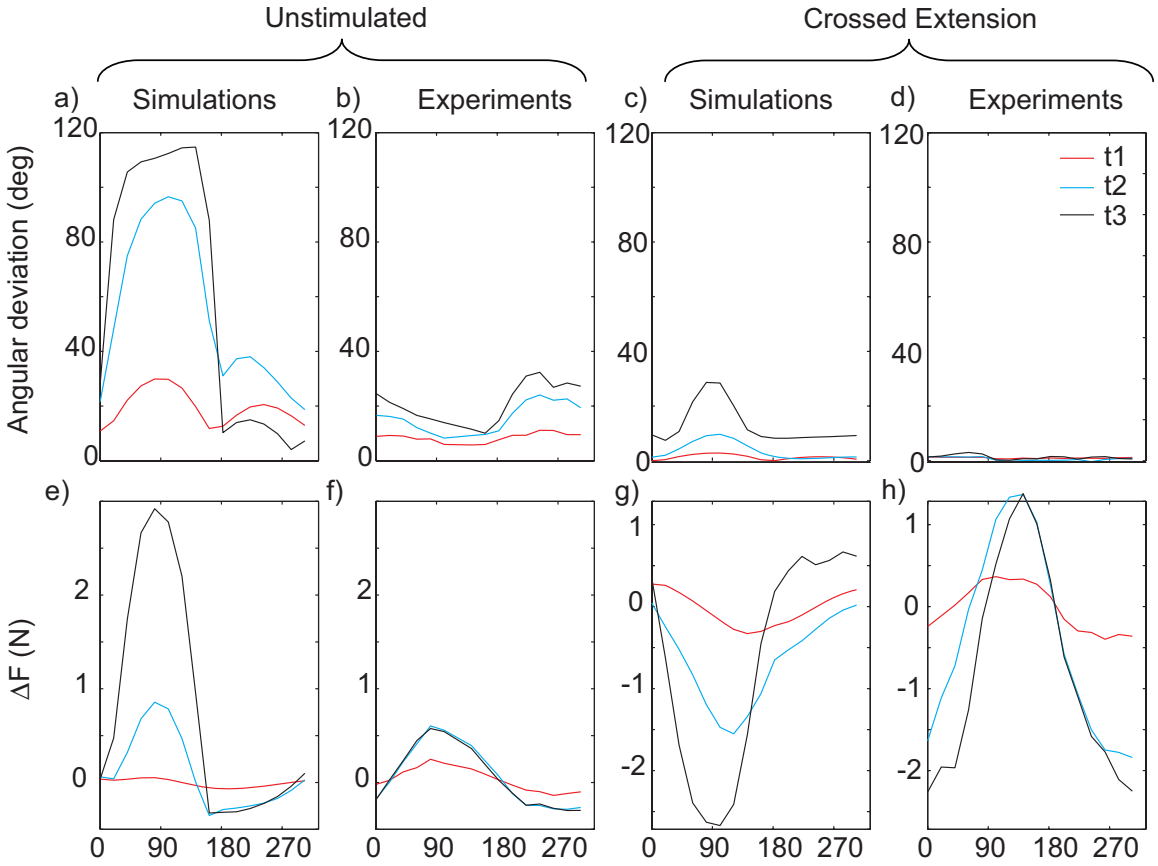

Figure 5.4: Angular deviation and change in ground reaction force in the experimental and simulated limb responses to endpoint position perturbation quantified at three time periods after perturbation onset (peak acceleration: t1 red, peak velocity: t2 blue, and peak displacement: t3 black). a-d) The angular deviation of the unstimulated trials is much larger for forward (0° – 180°) perturbations in the simulations (a) than in the experiments (b). For crossed-extension trials the angular deviation is substantial for forward perturbations in the simulations (c) and is negligible for all perturbation directions in the experiments (d). e-h) The change in force for unstimulated trials is similar in simulated (e) and experimental (f) responses at t1 and t2. For crossed-extension trials the change in force of the simulations (g) is out of phase with the experiments (h).

In the crossed-extension experiments (Figure 5.4d), the force direction of the response did not deviate from the background force. In the simulations (Figure 5.4c) the force also did not deviate from the background force for t1 and t2 across the range 180° –

360° and deviated by approximately 10° at the later time (t3) across this range. In the crossed-extension experiments (Figure 5.4h) the change in force varied sinusoidally across perturbation direction with an increase in amplitude for t2 and t3. The change in force of the crossed-extension simulations (Figure 5.4g) also varied sinusoidally but was out of phase with the experiments.

The length change for posterior Biceps Femoris and Semitendinosis is sinusoidal across perturbation directions for time period t3 of the unstimulated simulations (Figure 5.5) but force generation is asymmetric. For forward perturbations both muscles are lengthened beyond optimal fiber length and so experience an increase in passive force in these directions. Since the activation of the muscles is small (ST = 1%, BFP = 2%, Table 5.1) the asymmetric passive force dominates. Similar asymmetries were seen in hip flexors for backward perturbations but with much smaller magnitudes (data not shown).

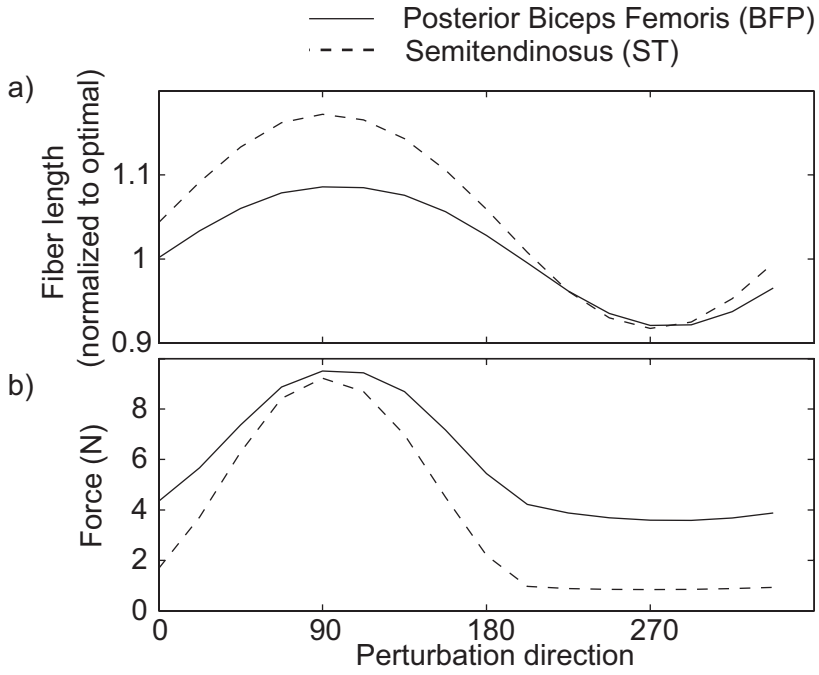

Figure 5.5: Muscle force and fiber length averaged over t3 for the unstimulated simulations for the bi-articular hamstrings posterior Biceps Femoris (BFP) and Semitendinosus (ST). These muscles experience a sinusoidal fiber length changes (a) and asymmetric force generation (b).

Discussion

The endpoint force response of the model compared favorably with the experimental results for perturbations in the forward direction but not in the backward direction. This asymmetry is attributable to non-linear properties of the muscle model, particularly the passive tension of muscles that cross the hip. The model compared well with the sagittal plane kinematics but not the non-sagittal kinematics. These differences may be due to the limited data available to resolve hip motion. The differences in the kinematics of the unstimulated and crossed-extension experiments were small.

The fact that the force magnitude in the decerebrate cat varies with perturbation direction even in the earliest time window (t1) before any reflex response is possible demonstrates that neither reflexive mechanisms nor interlimb coordination are required for a direction specific response such as the force constraint strategy. At later time periods the force was strongly asymmetric in the simulations but not in the experiments. This asymmetry can be attributed to the passive forces generated in the muscles.

Experimental evidence suggests that muscles operate near optimal fiber length in a variety of species (Burkholder and Lieber 2001). Accordingly the muscles were set to operate at 95% of their optimal fiber length. In the muscle model, passive force begins when the muscle is stretched past optimal fiber length and the passive force is not scaled by muscle activation. The change in force in muscles that have low activation levels would therefore be dominated by the passive forces rather than the active forces. For the hamstrings which have large moment arms in the cat this effect is amplified and asymmetries in muscle force are translated to asymmetries in joint torques and endpoint forces. In future work it may be important to determine the onset of passive forces for each muscle. Future work will also test the sensitivity of these results to activation pattern, model sensitivities (e.g. posture, muscle and joint parameters), reflex connectivity. In addition the force and kinematic data from these experiments will be combined so that endpoint impedances can be transformed to impedances at the joints.

This will allow us to identify if there are key joints that modulate endpoint response of the limb or what combinations of joints regulate this response. From that point we can use the model to determine intermuscular feedback that will accomplish this observed force and kinematic responses.

If the increase in stiffness were the same between all joints the same endpoint perturbation would result in the same displacements for all the joints. This was not observed however in the kinematics of the experiments. Hip motion in both the sagittal and non-sagittal planes increased and knee motion decreased in both planes. The ankle motion decreased in the non-sagittal plane but increased in the sagittal plane for forward-right perturbations and was unchanged in backward left perturbations. The result then seemed to be that stiffness at the knee was increased relative to stiffness at the hip and stiffness at the ankle increased relative to hip stiffness in the non-sagittal plane but not in the sagittal plane. This strategy of stiffening the distal joints in the non-sagittal plane would better preserve the limb configuration at the perturbed stance. In the sagittal plane it is more difficult to come to this conclusion because of the ambiguity in the ankle motion. Most of these differences between unstimulated and crossed-extension states were not observed in the simulations. This may be taken as evidence that the difference between the two states is not simply a change in activation pattern. To determine whether other influences such as the excitability of the spinal reflex pathways is important is a future direction of the work.

Despite the fact that the simulations did not reproduce the differences between the states, they were in general successful at predicting sagittal plane kinematics of the limb response. In particular the relative magnitude of hip, knee, and ankle motion were accurate with larger hip and smaller knee motion. The non-intuitive rotation of the preferred direction of ankle motion to forward and right perturbations was also accurately reproduced in the simulations as was the asymmetry of ankle motion, with much larger extensions to backward left perturbations than flexions to forward right perturbations.

The simulations performed poorly at reproducing the non-sagittal displacements observed in the experiments, with different directions and large asymmetries. One reason that the model may reproduce sagittal plane motion well and not non-sagittal motion is that three degrees of freedom at the hip cannot be resolved with only two known locations (GT and VK).

CHAPTER 6

CONCLUSIONS

In addition to its intrinsic importance during quiet standing, posture also serves as the background for a wide variety of other critical motor tasks. The hierarchical nature of the motor control system suggests that the different layers (intrinsic musculoskeletal, reflexive, voluntary) may be responsible for different aspects of a postural task (e.g. joint stability, limb stability, center of mass balance). The role of spinal reflexes in postural control has been debated primarily in the context of balancing the CoM (Lyalka et al. 2005, Macpherson and Fung 1999). Since stability and coordination of the constituents (muscles, joints, and limbs) is necessary to balance the CoM it is conceivable that the responsibility for stabilizing the constituents is provided by the lower levels of the motor control hierarchy including intrinsic muscle properties and spinal reflex pathways. In particular muscle stiffness and length feedback both provide a positional sensor for the configuration of the limb and could be used to stabilize at the level of muscle, joint, and limb. I hypothesized that the spinal reflexes are organized according to optimal principles of stability, control accuracy, and energy at the whole limb level. I hypothesized that the lowest levels of the motor control system, the intrinsic properties of muscles are insufficient to stabilize a whole cat hindlimb and that muscle length feedback provided by spinal reflex mechanisms is sufficient to stabilize the cat hindlimb. In addition, I hypothesized that the observed postural response in terms of tuned muscle activation and constrained ground reaction forces would be observed in the limb stabilized by length feedback.

The role of direct length and velocity feedback in the postural response has remained elusive largely due to the inherent difficulty of separating the effects of the various levels of the motor control hierarchy. This thesis has been directed by the idea that with a mathematical representation of the biological system, the different levels of

intrinsic muscle and nervous control can be independently and systematically applied and the effect of each of these levels on the postural response evaluated. In addition the mathematical approach allows a rigorous determination of the stability of the limb subject to the different levels of control, and the application of optimal control theory to predict and test strategies of neural control.

The first goal was to determine whether the length and velocity feedback of the limb were organized to provide optimal control of the limb. Previous work has shown that asymmetric heterogenic feedback contributes to the postural response of biological systems. A satisfactory functional explanation for this feedback has not been put forth. The hypothesis tested in the first study was that asymmetric multi-joint control strategy would confer an energetic and stability advantage in maintaining endpoint position of a kinematically redundant system. The hypothesis was tested by determining optimal control models incorporating symmetric or asymmetric feedback with the goal of maintaining endpoint location of a kinematically redundant, planar limb. Asymmetric feedback improved endpoint control performance of the limb by 16%, reduced energetic cost by 21% and increased interjoint coordination by 40% compared to the symmetric feedback system. The increases in efficiency and control associated with the asymmetry were unique to the kinematically redundant system; when the same criteria and tasks were applied to a non-redundant two-link model the optimal asymmetric controllers were only slightly better than the symmetric controllers (energetic improvement: 5%, control accuracy improvement: 4%). Functionally, the overall effect of the asymmetry was that torque generation at distal joints were more sensitive to motion of proximal joints than vice versa. This organization is consistent with heterogenic stretch reflex gains measured experimentally. Likewise, the magnitude of asymmetry for the optimal endpoint controller is also consistent with experimentally determined magnitudes. In conclusion, asymmetric feedback has a functionally relevant role in coordinating redundant degrees of freedom in maintaining the position of the endpoint of a limb.

The optimal control criteria developed in the first study were applied to the seven degree of freedom hindlimb model to determine the structure of optimal length and velocity feedback for this model. These criteria resulted in length and velocity feedback organization similar to that for the simplified model. That is, the optimal patterns of feedback emphasized torque generation at distal joints in response to motion of proximal joints. This organization would require spinal reflexes originating in the spindles of hip muscles to activate ankle muscles. Although no such connections have been observed in the spindle pathways of the cat it is possible that force feedback which has a wider limb distribution could provide this asymmetry and this idea remains to be tested.

The second hypothesis specifically tested whether the lowest levels of the motor control system, the intrinsic properties of muscles, are insufficient to stabilize a cat hindlimb. A 3-dimensional musculoskeletal model of the cat hindlimb with 31 muscles operating at near maximum stiffness (65% optimal fiber length) was used to determine the possible contributions of intrinsic muscle properties to limb stability during isometric force generation. Using dynamic stability analysis it was demonstrated that within the large set of activation patterns that satisfy the force requirement for posture, only a reduced subset produce a mechanically-stable limb configuration. If the muscles were assumed to operate at lengths closer to optimal (95% of optimal fiber length) there were no globally stable muscle activation patterns, suggesting that the intrinsic viscoelastic properties of muscle are insufficient to provide limb stability. However, even when the limb was unstable, the time-constants of instability were sufficiently great to allow long-latency neural feedback mechanisms to intervene, which may be preferential for movements requiring maneuverability versus stability.

The results highlighted that in addition to co-contraction and reflexive action, stiffness of the limb may be achieved by biasing the selection of muscle activation patterns to locally stiff muscles. The overall local stiffness of the muscles was influenced to a large extent by the moment-arm/joint angle relationship of the muscle as well as the

intrinsic stiffness of the fibers. While activation of locally stabilizing muscles did not guarantee whole-limb stability in our analysis, it was possible to increase probability of whole limb stability by preferentially selecting muscles with greater local joint stiffness. This strategy could be a useful criterion in the force-sharing problem.

Finally, since the model could not be stabilized by intrinsic muscle stiffness when the muscles operated at near optimal fiber lengths, the hypothesis was tested that the known patterns of homonymous fiber length feedback were sufficient to provide limb stability. Also this study tested whether known features of the postural response, including the tuning of EMG activation during horizontal perturbations and the force constraint strategy could be attributed to spinal reflex mechanisms. The 3-dimensional musculoskeletal model was enhanced with a tendon model and fiber length feedback. The principle results of this study are that length feedback is sufficient to stabilize a linearized model of the cat hindlimb and to provide directional tuning of muscle activation in response to perturbations. These results indicate that direct fiber length feedback is sufficient to stabilize the limb against small perturbations from the equilibrium posture. Without length feedback the limb was unstable for all activation patterns and with the addition of length feedback these activation patterns became stable. In either case, these time constants are substantially greater than the stretch reflex latency, and support the omission of feedback delays.

Direct fiber length feedback results in directional tuning of the individual muscle activations and these overlapped with the experimental tuning curves for four of the six muscles compared, suggesting that individual muscle lengthening may be a strong signal in determining the directionality of the postural response. Preferred directions in the ground reaction force early in the perturbation indicate that at least a component of the experimentally observed directionality is independent of a neural response.

Finally, the fourth study compared kinematics and kinetics of the hindlimb model without reflex control and a decerebrate cat as horizontal ramp and hold perturbations

were applied to the toe. The important differences in force production were the direction and symmetry. The early force response of the cat was directly in opposition to the perturbation direction while in the simulations the force response was directionally constrained. At later time periods the force was strongly asymmetric in the simulations but not in the experiments. The asymmetry was found to be due to the passive tension of the muscle model.

The kinematics of the decerebrate cat seemed to indicate a strategy of stiffening the distal joints in the non-sagittal plane to preserve the limb configuration at the perturbed stance. In the sagittal plane hip and ankle motion were of comparable magnitude and knee motion was reduced. The simulations predicted this sagittal plane coordination and also predicted an experimentally observed rotation of the preferred direction and asymmetry of ankle motion. However, the simulations performed poorly at reproducing the non-sagittal displacements observed in the experiments, with different directions and large asymmetries.

Taken together these results provide evidence that direct length feedback in the spinal reflex pathways provide limb stability, and may account for the directional tuning of muscle EMG to horizontal plane perturbations. Likewise the preferred direction of the restoring ground reaction forces may be due to the intrinsic viscoelasticity of the limb.

Future efforts will be concentrated in three areas. First the sensitivity of the results to modeling assumptions needs to be thoroughly quantified. Fortunately the stability can be determined from the linearized system making forward dynamic simulations unnecessary. Thus far the results seem to be most sensitive to muscle activation levels, non-sagittal angles of the posture, joint locations and directions, and kinematic constraints such as the pinned toe. Second, a more complete picture of the reflex feedback will be implemented, including force feedback. The reflex model also needs to be modified to scale with the background activation level. Third and lastly, these analyses will be extended from limb stability to balance control of the whole body.

Ultimately the goal of the observed postural response is to stabilize the whole body and comparisons of this response with a complete four-legged cat model would be of great value.

APPENDIX A

SENSITIVITY OF THE MUSCLE ACTIVATION POPULATION TO POSTURE

The sensitivity of the percentage of stable populations to posture changes was determined. The methods of Chapter 3 were duplicated to determine the percentage of activation patterns that resulted in a stable limb (maximum real eigenvalue less than zero). Three different postures (Table A.1) were evaluated, including the posture used in Chapter 3 (Russell 1). For each posture the muscles were set to operate at 65%, 70%, or 95% of their optimal fiber length. In addition, each joint angle was varied independently by ±5°. For the 135 conditions 10,000 activation patterns were generated to produce the endpoint force used in Chapter 3.

Table A.1: Three postures were used for the sensitivity analysis

	Default	Russell 2	Russell 1
HF	-60.5	-53.8	-54.3
HA	-14.6	-2.0	7.5
HR	0.0	0.0	-10.6
KE	-82.0	-88.6	-86.4
KA	0.0	-3.3	11.1
AE	-78.0	-50.5	-43.0
AA	0.0	-0.1	-9.3

The model was originally constructed in the default posture and this is the posture that was used to validate the moment arms of the muscle (Burkholder and Nichols 2004). The Russell 1 posture was determined by the methods similar to those described in Chapter 5 from kinematic data of an intact cat (McKay et al. 2007). The Russell 2

posture used the same kinematic data and the methods described in Chapter 5. However, the location of the femoral condyles in the model were corrected and hip rotation, as a free parameter, was chosen to be zero.

Of the three postures the Default posture was the most stable with all perturbed postures greater than 98% stable at 65% optimal fiber length and greater than 65% stable at 70% optimal fiber length. The Russell1 posture was the least stable with all perturbed postures less than 55% stable at 65% optimal fiber length and less than 20% stable at 70% optimal fiber length. In addition the Default posture was the least sensitive to perturbations in the joint angles and the Russell1 posture was the most sensitive. There were no stable activation patterns found for any posture at 95% optimal fiber length.

Table A.2: Stability of the limb across postural conditions

Posture		Default			Russell 2			Russell1		
Operating Length		65%	70%	95%	65%	70%	95%	65%	70%	95%
Nominal		99.4	76.8	0.0	92.1	45.8	0.0	35.3	9.5	0.0
HF	-5°	99.1	73.2	0.0	84.7	32.8	0.0	17.2	2.2	0.0
	+5°	98.2	72.2	0.0	96.0	47.9	0.0	51.6	17.2	0.0
HA	-5°	99.9	85.3	0.0	85.0	35.3	0.0	30.9	6.8	0.0
	+5°	99.1	73.8	0.0	96.8	56.8	0.0	40.1	12.3	0.0
HR	-5°	99.8	82.3	0.0	86.3	38.3	0.0	37.6	9.3	0.0
	+5°	98.6	70.9	0.0	96.3	51.7	0.0	31.9	8.0	0.0
KE	-5°	98.7	71.7	0.0	85.7	33.4	0.0	18.4	3.2	0.0
	+5°	99.6	79.3	0.0	95.7	54.7	0.0	52.9	19.5	0.0
KA	-5°	99.6	80.3	0.0	96.2	54.5	0.0	52.5	17.9	0.0
	+5°	99.4	74.5	0.0	85.2	32.9	0.0	0.0	0.0	0.0
AE	-5°	99.9	82.3	0.0	94.8	53.4	0.0	53.6	18.4	0.0
	+5°	97.9	68.3	0.0	84.9	27.5	0.0	17.1	1.9	0.0
AA	-5°	99.9	87.2	0.0	83.4	39.1	0.0	38.3	10.5	0.0
	+5°	98.9	68.6	0.0	96.2	47.2	0.0	34.1	6.0	0.0

APPENDIX B

OPTIMAL CONTROL OF THE THREE DIMENSIONAL MODEL

The cost functions used in Chapter 2 were applied to the model of Chapters 3-5 to determine optimal joint and endpoint controllers for the extended 3 dimensional 7-DoF model. The results of the optimization are similar to and confirm the results of Aim 1; the joint controller is more compliant in endpoint space, and the joints are coordinated in the endpoint controller so that endpoint displacement is minimized (data not shown). The stiffness structures of these controllers (Figure B.1) were also similar to those of the simplified model in Chapter 2 in that the joint controller (Figure B.1a) had only diagonal stiffness terms and the endpoint controller (Figure B.1b) was asymmetric with the ankle torques being enhanced by proximal joint motion. These patterns are compared with the joint stiffness due to the intrinsic musculoskeletal properties of the limb (Figure B.1c) for a typical activation pattern from Chapter 3 and to the joint stiffness provided by autogenic and heterogenic reflexes (Figure B.1d, Figure B.2). The asymmetries required for optimal endpoint control cannot be provided by the autogenic and heterogenic patterns used. Indeed, any reflex pattern that does not contain asymmetric hip muscle / ankle muscle reflex gains cannot provide this structure.

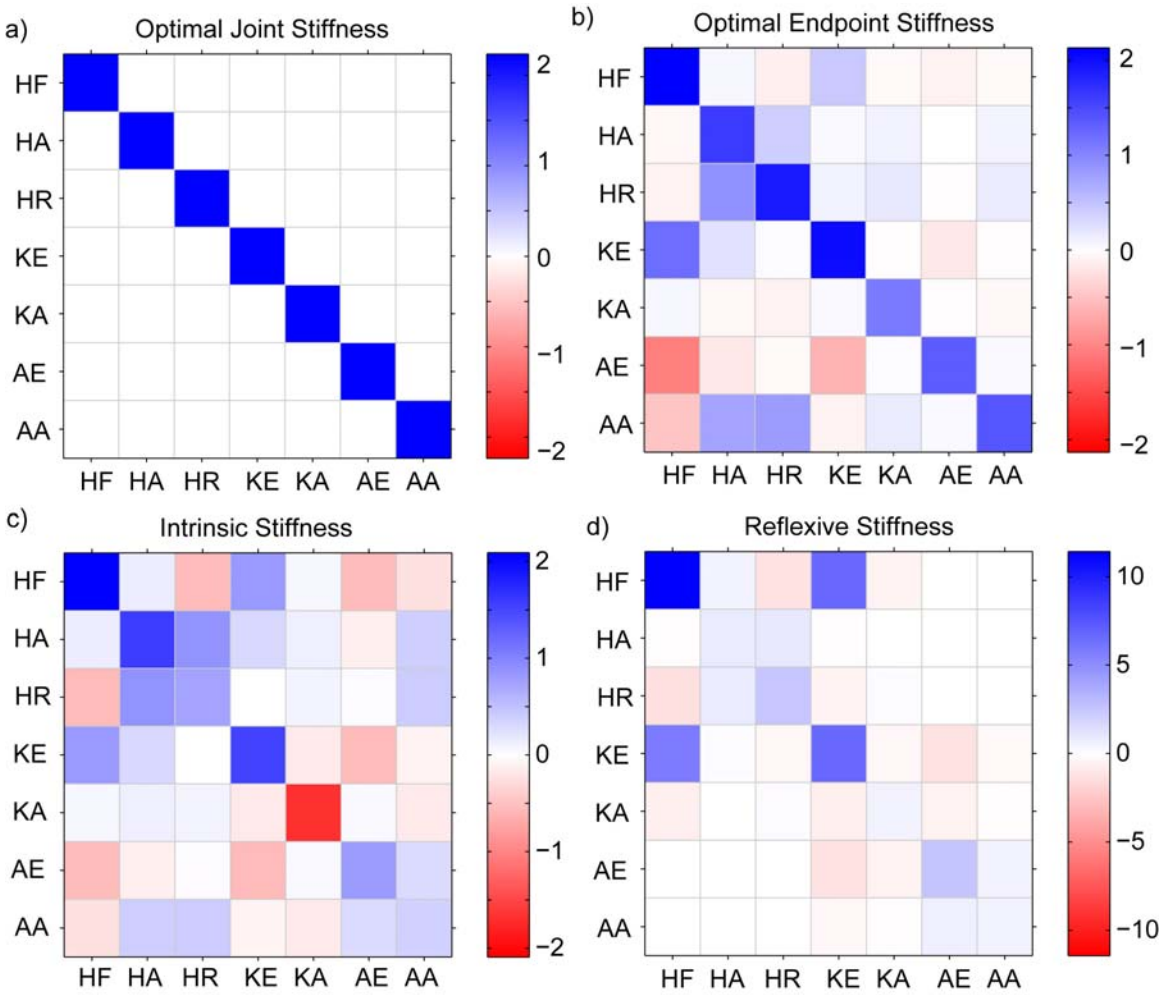

Figure B.1: Joint stiffness of the model. The shade of the grid indicates the contribution of joint displacement (columns) to torque production at a joint (rows). A linear quadratic regulator tasked to control for joint position (a) predicts a diagonal stiffness matrix. A linear quadratic regulator tasked to control for endpoint position (b) predicts an asymmetric joint stiffness matrix with stronger hip-motion-to-ankle-torque contributions (lower left elements of b) than ankle-motion-to-hip-torques (upper right elements of b). The intrinsic properties of muscle (c) provide a symmetric joint stiffness. The approximate contributions of the reflex feedback to joint stiffness (d) are nearly symmetric as well.

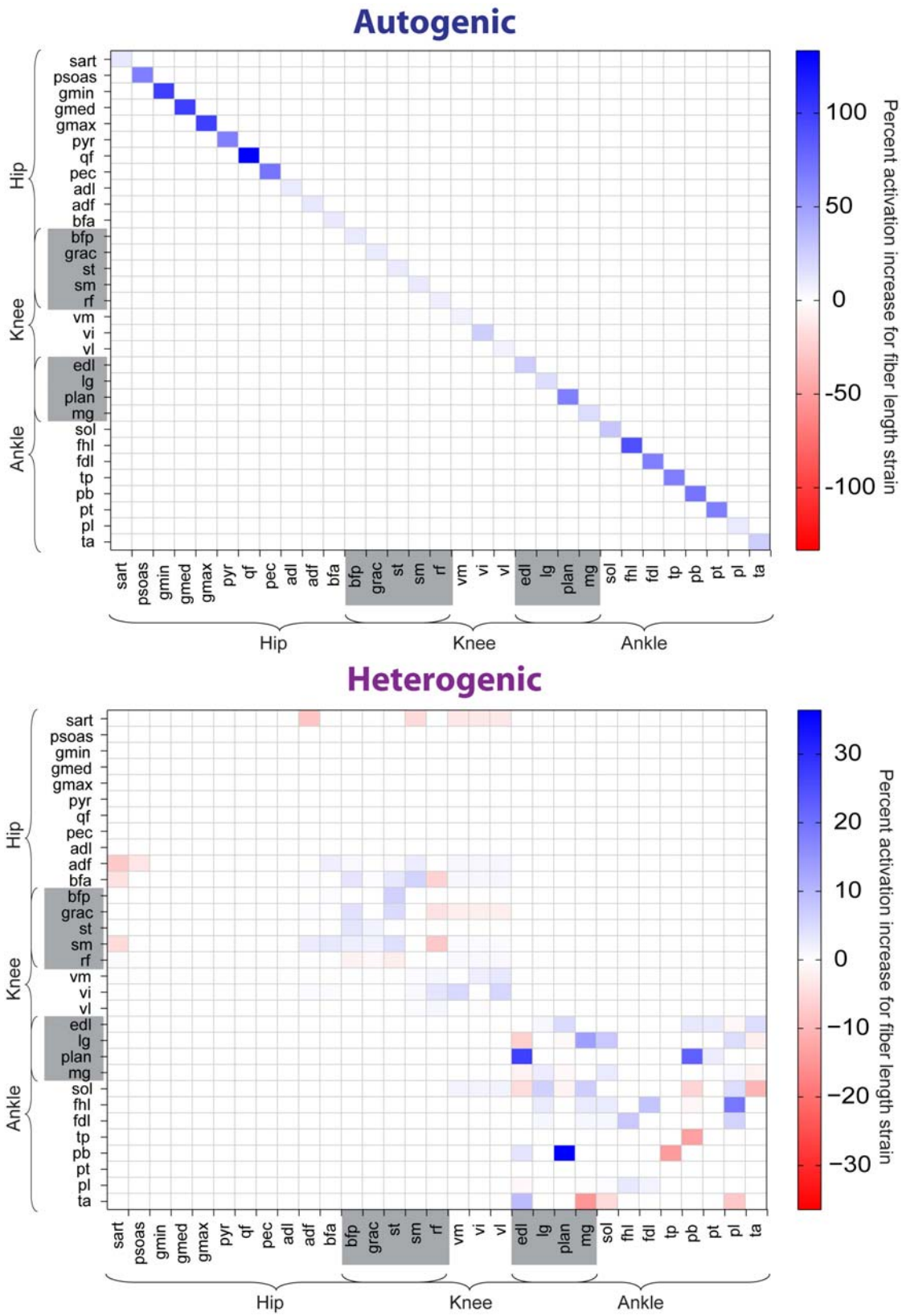

Figure B.2: Reflex feedback pathways. The connections between each of the 31 modeled muscles are represented in the boxes. The shade corresponds to a percent increase in activation of the recipient muscle (row) for a stretch of the donor muscle (column) in length units normalized to optimal fiber length.

REFERENCES

Alexandrov, A.V., Frolov, A.A., Horak, F.B., Carlson-Kuhta, P., Park, S., 2005. Feedback equilibrium control during human standing. Biol Cybern:1-14.

Bard, P., Macht, M.B. (1958) The behavior of chronically decerebrate cat. Churchill, London.

Barin, K., 1989. Evaluation of a Generalized-Model of Human Postural Dynamics and Control in the Sagittal Plane. Biological Cybernetics 61(1):37-50.

Beloozerova, I.N., Sirota, M.G., Orlovsky, G.N., Deliagina, T.G., 2005. Activity of pyramidal tract neurons in the cat during postural corrections. J Neurophysiol 93(4):1831-44.

Bernstein, N. (1967) The Coordination and Regulation of Movements. Pergamon Press, New York.

Bonasera, S.J., Nichols, T.R., 1994. Mechanical actions of heterogenic reflexes linking long toe flexors with ankle and knee extensors of the cat hindlimb. J Neurophysiol 71(3):1096-110.

Bonasera, S.J., Nichols, T.R., 1996. Mechanical actions of heterogenic reflexes among ankle stabilizers and their interactions with plantarflexors of the cat hindlimb. J Neurophysiol 75(5):2050-70.

Bosco, G., Poppele, R.E., 1997. Representation of multiple kinematic parameters of the cat hindlimb in spinocerebellar activity. J Neurophysiol 78(3):1421-32.

Bosco, G., Poppele, R.E., Eian, J., 2000. Reference frames for spinal proprioception: limb endpoint based or joint-level based? J Neurophysiol 83(5):2931-45.

Bryson, A.E., Ho, Y.-C. (1975) Applied optimal control : optimization, estimation, and control. Hemisphere Pub. Corp., New York.

Bunderson, N.E., Ting, L.H., Burkholder, T.J., 2007. Asymmetric interjoint feedback contributes to postural control of redundant multi-link systems. Journal of Neural Engineering 4(3):234-245.

Bunderson, N.E., Burkholder, T.J., Ting, L.H., 2008. Reduction of neuromuscular redundancy for postural force generation using an intrinsic stability criterion. J Biomech doi:10.1016/j.jbiomech.2008.02.2004.

Burkholder, T.J., Nichols, T.R., 2000. The mechanical action of proprioceptive length feedback in a model of cat hindlimb. Motor Control 4(2):201-20.

Burkholder, T.J., Lieber, R.L., 2001. Sarcomere length operating range of vertebrate muscles during movement. J Exp Biol 204(Pt 9):1529-36.

Burkholder, T.J., Nichols, T.R., 2004. Three-dimensional model of the feline hindlimb. Journal of Morphology 261(1):118-129.

Campbell, K.S., Lakie, M., 1998. A cross-bridge mechanism can explain the thixotropic short-range elastic component of relaxed frog skeletal muscle. J Physiol 510 (Pt 3):941-62.

Close, R.I., 1972. Dynamic properties of mammalian skeletal muscles. Physiol Rev 52(1):129-97.

Crago, P.E., Houk, J.C., Hasan, Z., 1976. Regulatory Actions of Human Stretch Reflex. Journal of Neurophysiology 39(5):925-935.

Crago, P.E., Houk, J.C., Rymer, W.Z., 1982. Sampling of total muscle force by tendon organs. J Neurophysiol 47(6):1069-83.

Crowninshield, R.D., Brand, R.A., 1981. A physiologically based criterion of muscle force prediction in locomotion. Journal of Biomechanics 14(11):793-801.

Daley, M.A., Felix, G., Biewener, A.A., 2007. Running stability is enhanced by a proximo-distal gradient in joint neuromechanical control. J Exp Biol 210(Pt 3):383-94.

De Leon, R.D., Hodgson, J.A., Roy, R.R., Edgerton, V.R., 1998. Full weight-bearing hindlimb standing following stand training in the adult spinal cat. J Neurophysiol 80(1):83-91.

Deliagina, T.G., Orlovsky, G.N., Zelenin, P.V., Beloozerova, I.N., 2006. Neural bases of postural control. Physiology (Bethesda) 21:216-25.

Deliagina, T.G., Sirota, M.G., Zelenin, P.V., Orlovsky, G.N., Beloozerova, I.N., 2006. Interlimb postural coordination in the standing cat. J Physiol 573(Pt 1):211-24.

Deliagina, T.G., Beloozerova, I.N., Zelenin, P.V., Orlovsky, G.N., 2008. Spinal and supraspinal postural networks. Brain Res Rev 57(1):212-21.

Eccles, J.C., 1956. Excitatory and Inhibitory Synaptic Action. Harvey Lectures(51):1-24.

Eccles, J.C., Eccles, R.M., Lundberg, A., 1957. The convergence of monosynaptic excitatory afferents on to many different species of alpha motoneurones. Journal of Physiology 137(1):22-50.

Eccles, J.C., Eccles, R.M., Lundberg, A., 1957. Synaptic Actions on Motoneurones in Relation to the 2 Components of the Group-I Muscle Afferent Volley. Journal of Physiology-London 136(3):527-546.

Eccles, R.M., Lundberg, A., 1958. Significance of Supraspinal Control of Reflex Actions by Impulses in Muscle Afferents. Experientia 14(6):197-199.

Edwards, W.T., 2007. Effect of joint stiffness on standing stability. Gait Posture 25(3):432-9.

Epstein, M., Herzog, W. (1998) Theoretical models of skeletal muscle. Wiley, Chichester; New York.

Epstein, M., Herzog, W., 2003. Aspects of skeletal muscle modelling. Philos Trans R Soc Lond B Biol Sci 358(1437):1445-52.

Fagg, A.H., Shah, A., Barto, A.G., 2002. A Computational Model of Muscle Recruitment for Wrist Movements. J Neurophysiol 88(6):3348-3358.

Fregly, B.J., Zajac, F.E., 1996. A state-space analysis of mechanical energy generation, absorption, and transfer during pedaling. J Biomech 29(1):81-90.

Fung, J., Macpherson, J.M., 1999. Attributes of quiet stance in the chronic spinal cat. Journal of Neurophysiology 82(6):3056-3065.

Gasser, H.S., Hill, A.V., 1924. The dynamics of muscular contraction. Proceedings of the Royal Society of London. Series B: Biological Sciences 96(678):398-437.

Getz, E.B., Cooke, R., Lehman, S.L., 1998. Phase transition in force during ramp stretches of skeletal muscle. Biophys J 75(6):2971-83.

Gordon, A.M., Huxley, A.F., Julian, F.J., 1966. The variation in isometric tension with sarcomere length in vertebrate muscle fibres. J Physiol 184(1):170-92.

Gordon, A.M., Huxley, A.F., Julian, F.J., 1966. The variation in isometric tension with sarcomere length in vertebrate muscle fibres. Journal of Physiology 184(1):170-92.

Gurfinkel, V., Cacciatore, T.W., Cordo, P., Horak, F., Nutt, J., Skoss, R., 2006. Postural muscle tone in the body axis of healthy humans. J Neurophysiol 96(5):2678-87.

Hamill, J., Knutzen, K. (2003) Biomechanical basis of human movement. Lippincott Williams & Wilkins, Philadelphia.

Hasan, Z., 2005. The human motor control system's response to mechanical perturbation: should it, can it, and does it ensure stability? J Mot Behav 37(6):484-93.

He, J.P., Levine, W.S., Loeb, G.E., 1991. Feedback gains for correcting small perturbations to standing posture. IEEE Trans Autom Control 36:322-32.

Henry, S.M., Fung, J., Horak, F.B., 2001. Effect of stance width on multidirectional postural responses. J Neurophysiol 85(2):559-70.

Hiebert, G.W., Whelan, P.J., Prochazka, A., Pearson, K.G., 1996. Contribution of hind limb flexor muscle afferents to the timing of phase transitions in the cat step cycle. J Neurophysiol 75(3):1126-37.

Higginson, J.S., Zajac, F.E., Neptune, R.R., Kautz, S.A., Delp, S.L., 2006. Muscle contributions to support during gait in an individual with post-stroke hemiparesis. J Biomech 39(10):1769-77.

Hill, A.V., 1938. The Heat of Shortening and the Dynamic Constants of Muscle. Proccedings of the Royal Society of London 126, B(843):136-95.

Hoffer, J.A., Leonard, T.R., Cleland, C.L., Sinkjaer, T., 1990. Segmental reflex action in normal and decerebrate cats. J Neurophysiol 64(5):1611-24.

Hogan, N., 1985. The mechanics of multi-joint posture and movement control. 52(5):315-31.

Holmes, P., Full, R., Koditschek, D.E., Guckenheimer, J., 2006. The dynamics of legged locomotion: models, analyses, and challenges. SIAM Review 48(2):207-304.

Horak, F.B., Macpherson, J.M. (1996) Postural orientation and equilibrium. In: Rowell, L.B.,Shepherd, J.T. Handbook of Physiology, Section 12. American Physiological Society, New York, 255-92.

Houk, J.C., Rymer, W.Z., Crago, P.E., 1981. Dependence of dynamic response of spindle receptors on muscle length and velocity. J Neurophysiol 46(1):143-66.

Hulliger, M., Durmuller, N., Prochazka, A., Trend, P., 1989. Flexible fusimotor control of muscle spindle feedback during a variety of natural movements. Prog Brain Res 80:87-101; discussion 57-60.

Huxley, A.F., 1957. Muscle structure and theories of contraction. Progress in Biophysics and Biophysical Chemistry 7:255-318.

Huxley, A.F., Simmons, R.M., 1971. Mechanical properties of the cross-bridges of frog striated muscle. J Physiol 218(1):59P-60P.

Huyghues-Despointes, C.M., Cope, T.C., Nichols, T.R., 2003. Intrinsic properties and reflex compensation in reinnervated triceps surae muscles of the cat: effect of movement history. J Neurophysiol 90(3):1547-55.

Inglis, J.T., Macpherson, J.M., 1995. Bilateral labyrinthectomy in the cat: effects on the postural response to translation. J Neurophysiol 73(3):1181-91.

Jami, L., 1992. Golgi tendon organs in mammalian skeletal muscle: functional properties and central actions. Physiol Rev 72(3):623-66.

Jankowska, E., 1992. Interneuronal relay in spinal pathways from proprioceptors. Prog Neurobiol 38(4):335-78.

Karayannidou, A., Deliagina, T.G., Tamarova, Z.A., Sirota, M.G., Zelenin, P.V., Orlovsky, G.N., Beloozerova, I.N., 2008. Influences of sensory input from the limbs on feline corticospinal neurons during postural responses. J Physiol 586(Pt 1):247-63.

Kargo, W.J., Giszter, S.F., 2000. Afferent roles in hindlimb wipe-reflex trajectories: free-limb kinematics and motor patterns. J Neurophysiol 83(3):1480-501.

Kirkwood, P.A., Sears, T.A., 1975. Monosynaptic excitation of motoneurones from muscle spindle secondary endings of intercostal and triceps surae muscles in the cat. J Physiol 245(2):64P-66P.

Kuo, A.D., 1995. An optimal control model for analyzing human postural balance. IEEE Trans Biomed Eng 42(1):87-101.

Kuo, A.D., 2005. An optimal state estimation model of sensory integration in human postural balance. J Neural Eng 2(3):S235-49.

Kurtzer, I., Pruszynski, J.A., Herter, T.M., Scott, S.H., 2006. Primate upper limb muscles exhibit activity patterns that differ from their anatomical action during a postural task. J Neurophysiol 95(1):493-504.

Lacquaniti, F., Soechting, J.F., 1986. EMG responses to load perturbations of the upper limb: effect of dynamic coupling between shoulder and elbow motion. Exp Brain Res 61(3):482-96.

Lacquaniti, F., Maioli, C., 1994. Independent control of limb position and contact forces in cat posture. J Neurophysiol 72(4):1476-95.

Lacquaniti, F., Maioli, C., 1994. Coordinate transformations in the control of cat posture. J Neurophysiol 72(4):1496-515.

Liddell, E.G.T., Sherrington, C., 1924. Reflexes in response to stretch (myotatic reflexes). Proceedings of the Royal Society of London. Series B: Biological Sciences 96(675):212-242.

Liddell, E.G.T., Sherrington, C., 1925. Further observations on myotatic reflexes. Proceedings of the Royal Society of London Series B-Containing Papers of a Biological Character 97(683):267-283.

Liu, D., Todorov, E., 2007. Evidence for the flexible sensorimotor strategies predicted by optimal feedback control. J Neurosci 27(35):9354-68.

Lloyd, D.P.C., 1946. Integrative pattern of excitation and inhibition in two-neuron reflex arcs. Journal of Neurophysiology 9(6):439-444.

Lloyd, D.P.C., 1946. Facilitation and Inhibition of Spinal Motoneurons. Journal of Neurophysiology 9(6):421-438.

Loeb, G.E., Duysens, J., 1979. Activity patterns in individual hindlimb primary and secondary muscle spindle afferents during normal movements in unrestrained cats. J Neurophysiol 42(2):420-40.

Lyalka, V.F., Zelenin, P.V., Karayannidou, A., Orlovsky, G.N., Grillner, S., Deliagina, T.G., 2005. Impairment and recovery of postural control in rabbits with spinal cord lesions. J Neurophysiol 94(6):3677-90.

Macpherson, J.M., 1988. Strategies that simplify the control of quadrupedal stance. I. Forces at the ground. J Neurophysiol 60(1):204-17.

Macpherson, J.M., 1988. Strategies that simplify the control of quadrupedal stance. II. Electromyographic activity. J Neurophysiol 60(1):218-31.

Macpherson, J.M., 1994. Changes in a postural strategy with inter-paw distance. J Neurophysiol 71(3):931-40.

Macpherson, J.M., Fung, J., Jacobs, R., 1997. Postural orientation, equilibrium, and the spinal cord. Adv Neurol 72:227-32.

Macpherson, J.M., Fung, J., 1999. Weight support and balance during perturbed stance in the chronic spinal cat. Journal of Neurophysiology 82(6):3066-3081.

Matthews, P.B., 1963. The Response of De-Efferented Muscle Spindle Receptors to Stretching at Different Velocities. J Physiol 168:660-78.

Matthews, P.B., Stein, R.B., 1969. The regularity of primary and secondary muscle spindle afferent discharges. J Physiol 202(1):59-82.

McKay, J.L., Burkholder, T.J., Ting, L.H., 2007. Biomechanical capabilities influence postural control strategies in the cat hindlimb. J Biomech 40(10):2254-60.

Merton, P.A., 1953. Slowly Conducting Muscle Spindle Afferents. Acta Physiologica Scandinavica 29(1):87-88.

Miller, J.F., Paul, K.D., Lee, R.H., Rymer, W.Z., Heckman, C.J., 1996. Restoration of extensor excitability in the acute spinal cat by the 5-HT2 agonist DOI. J Neurophysiol 75(2):620-8.

Morasso, P.G., Schieppati, M., 1999. Can muscle stiffness alone stabilize upright standing? J Neurophysiol 82(3):1622-6.

Morasso, P.G., Sanguineti, V., 2002. Ankle muscle stiffness alone cannot stabilize balance during quiet standing. J Neurophysiol 88(4):2157-62.

Mussa-Ivaldi, F.A., Hogan, N., Bizzi, E., 1985. Neural, Mechanical, and Geometric Factors Subserving Arm Posture in Humans. Journal of Neuroscience 5(10):2732-2743.

Neptune, R.R., Kautz, S.A., Zajac, F.E., 2001. Contributions of the individual ankle plantar flexors to support, forward progression and swing initiation during walking. J Biomech 34(11):1387-98.

Nichols, T.R., Houk, J.C., 1976. Improvement in linearity and regulation of stiffness that results from actions of stretch reflex. J Neurophysiol 39(1):119-42.

Nichols, T.R., 1989. The organization of heterogenic reflexes among muscles crossing the ankle joint in the decerebrate cat. J Physiol 410:463-77.

Nichols, T.R., Cope, T.C., Abelew, T.A., 1999. Rapid spinal mechanisms of motor coordination. Exerc Sport Sci Rev 27:255-84.

Nichols, T.R., Cope, T.C., 2004. Cross-bridge mechanisms underlying the history-dependent properties of muscle spindles and stretch reflexes. Can J Physiol Pharmacol 82(8-9):569-76.

Osu, R., Franklin, D.W., Kato, H., Gomi, H., Domen, K., Yoshioka, T., Kawato, M., 2002. Short- and long-term changes in joint co-contraction associated with motor learning as revealed from surface EMG. J Neurophysiol 88(2):991-1004.

Park, S., Horak, F.B., Kuo, A.D., 2004. Postural feedback responses scale with biomechanical constraints in human standing. Exp Brain Res 154(4):417-27.

Patel, R.V., Shadpey, F., 2005. Control of Redundant Robot Manipulators - Theory and Experiments. Control of Redundant Robot Manipulators: Theory and Experiments 316:Vii-+.

Perreault, E.J., Kirsch, R.F., Crago, P.E., 2004. Multijoint dynamics and postural stability of the human arm. 157(4):507-17.

Peterka, R.J., 2002. Sensorimotor integration in human postural control. J Neurophysiol 88(3):1097-118.

Powers, R.K., Binder, M.D., 1985. Distribution of oligosynaptic group I input to the cat medial gastrocnemius motoneuron pool. J Neurophysiol 53(2):497-517.

Pratt, C.A., Fung, J., Macpherson, J.M., 1994. Stance Control in the Chronic Spinal Cat. Journal of Neurophysiology 71(5):1981-1985.

Pratt, C.A., 1995. Evidence of positive force feedback among hindlimb extensors in the intact standing cat. J Neurophysiol 73(6):2578-83.

Prochazka, A., 1989. Sensorimotor gain control: a basic strategy of motor systems? Prog Neurobiol 33(4):281-307.

Rack, P.M., Westbury, D.R., 1969. The effects of length and stimulus rate on tension in the isometric cat soleus muscle. J Physiol 204(2):443-60.

Rack, P.M., Westbury, D.R., 1974. The short range stiffness of active mammalian muscle and its effect on mechanical properties. J Physiol 240(2):331-50.

Ramsay, J.O., Silverman, B.W. (2005) Functional data analysis. Springer, New York ; Berlin.

Richardson, A.G., Slotine, J.J., Bizzi, E., Tresch, M.C., 2005. Intrinsic musculoskeletal properties stabilize wiping movements in the spinalized frog. J Neurosci 25(12):3181-91.

Roy, R.R., Kim, J.A., Monti, R.J., Zhong, H., Edgerton, V.R., 1997. Architectural and histochemical properties of cat hip 'cuff' muscles. Acta Anat (Basel) 159(2-3):136-46.

Sacks, R.D., Roy, R.R., 1982. Architecture of the hind limb muscles of cats: functional significance. J Morphol 173(2):185-95.

Sage, H.G., De Mathelin, M.F., Ostertag, E., 1999. Robust control of robot manipulators: a survey. International Journal of Control 72(16):1498-1522.

Schepens, B., Drew, T., 2004. Independent and convergent signals from the pontomedullary reticular formation contribute to the control of posture and movement during reaching in the cat. J Neurophysiol 92(4):2217-38.

Schilling, N., 2005. Ontogenetic development of locomotion in small mammals--a kinematic study. J Exp Biol 208(Pt 21):4013-34.

Scholz, J.P., Schoner, G., 1999. The uncontrolled manifold concept: identifying control variables for a functional task. Exp Brain Res 126(3):289-306.

Schouten, A.C., De Vlugt, E., Van Hilten, J.J.B., Van der Helm, F.C.T., 2008. Quantifying proprioceptive reflexes during position control of the human arm. Ieee Transactions on Biomedical Engineering 55(1):311-321.

Sherrington, C.S., 1898. Experiments in examination of the peripheral distribution of the fibers of the posterior roots of some spinal nerves. Part II. Philosophical Transactions of the Royal Society of London. Series B: Biological Sciences 190:45-86.

Sherrington, C.S., 1910. Flexion-reflex of the limb, crossed extension-reflex, and reflex stepping and standing. J Physiol 40(1-2):28-121.

Sinkjaer, T., Hoffer, J.A., 1990. Factors determining segmental reflex action in normal and decerebrate cats. J Neurophysiol 64(5):1625-35.

Sinkjaer, T., 1997. Muscle, reflex and central components in the control of the ankle joint in healthy and spastic man. Acta Neurol Scand Suppl 170:1-28.

Stephens, J.A., Reinking, R.M., Stuart, D.G., 1975. Tendon organs of cat medial gastrocnemius: responses to active and passive forces as a function of muscle length. J Neurophysiol 38(5):1217-31.

Stroeve, S., 1999. Analysis of the role of proprioceptive information during arm movements using a model of the human arm. Motor Control 3(2):158-185.

Szidarovszky, F., Bahill, T. (1992) Linear systems theory. CRC Press, Boca Raton.

Taube, W., Schubert, M., Gruber, M., Beck, S., Faist, M., Gollhofer, A., 2006. Direct corticospinal pathways contribute to neuromuscular control of perturbed stance. Journal of Applied Physiology 101(2):420-9

Ting, L.H., Kautz, S.A., Brown, D.A., Zajac, F.E., 1999. Phase reversal of biomechanical functions and muscle activity in backward pedaling. J Neurophysiol 81(2):544-51.

Ting, L.H., McKay, J.L., 2008. Neuromechanics of muscle synergies for posture and movement. Curr Opin Neurobiol 17(6):622-8.

Todorov, E., Jordan, M.I., 2002. Optimal feedback control as a theory of motor coordination. Nature Neuroscience 5(11):1226-1235.

Todorov, E., 2004. Optimality principles in sensorimotor control. Nature Neuroscience 7(9):907-915.

Torres-Oviedo, G., Macpherson, J.M., Ting, L.H., 2006. Muscle synergy organization is robust across a variety of postural perturbations. J Neurophysiol 96(3):1530-46.

Torres-Oviedo, G., Ting, L.H., 2007. Muscle Synergies Characterizing Human Postural Responses. J Neurophysiol 98(4):2144-2156.

Valero-Cuevas, F.J., Johanson, M.E., Towles, J.D., 2003. Towards a realistic biomechanical model of the thumb: the choice of kinematic description may be more critical than the solution method or the variability/uncertainty of musculoskeletal parameters. J Biomech 36(7):1019-30.

van Antwerp, K.W., Burkholder, T.J., Ting, L.H., 2007. Inter-joint coupling effects on muscle contributions to endpoint force and acceleration in a musculoskeletal model of the cat hindlimb. J Biomech 40(16):3570-9.

Welch, T.D., Ting, L.H., 2008. A feedback model reproduces muscle activity during human postural responses to support-surface translations. J Neurophysiol 99(2):1032-8.

Wilmink, R.J., Nichols, T.R., 2003. Distribution of heterogenic reflexes among the quadriceps and triceps surae muscles of the cat hind limb. 90(4):2310-24.

Windhorst, U., 2007. Muscle proprioceptive feedback and spinal networks. Brain Res Bull 73(4-6):155-202.

Winter, D.A., Patla, A.E., Prince, F., Ishac, M., Gielo-Perczak, K., 1998. Stiffness control of balance in quiet standing. J Neurophysiol 80(3):1211-21.

Winter, D.A., Patla, A.E., Rietdyk, S., Ishac, M.G., 2001. Ankle muscle stiffness in the control of balance during quiet standing. J Neurophysiol 85(6):2630-3.

Young, R.P., Scott, S.H., Loeb, G.E., 1992. An intrinsic mechanism to stabilize posture--joint-angle-dependent moment arms of the feline ankle muscles. Neurosci Lett 145(2):137-40.

Zajac, F.E., 1989. Muscle and tendon: properties, models, scaling, and application to biomechanics and motor control. Crit Rev Biomed Eng 17(4):359-411.

Zajac, F.E., 2002. Understanding muscle coordination of the human leg with dynamical simulations. J Biomech 35(8):1011-8.

VITA

NATHAN ERIC BUNDERSON

Nate grew up in Emery County, Utah where he graduated from Emery High School. He received a B.S. and M.S. in Mechanical Engineering from Utah State University, Logan, Utah in 2004 (and considers himself an aggie for life) before coming to Georgia Tech to pursue a doctorate in Bioengineering. He loves his wife and family and misses the mountains and deserts.